Mon. Not. R. Astron. Soc. **311**, 456–484 (2000)

The *ROSAT* International X-ray/Optical Survey (RIXOS): source catalogue

K. O. Mason,[1] F. J. Carrera,[1,2] G. Hasinger,[3] H. Andernach,[4] A. Aragon-Salamanca,[5] X. Barcons,[2] R. Bower,[6] W. N. Brandt,[7] G. Branduardi-Raymont,[1] J. Burgos-Martín,[8] F. Cabrera-Guerra,[8] R. Carballo,[2,9] F. Castander,[5] R. S. Ellis,[5] J. I. González-Serrano,[2] E. Martínez-González,[2] J. M. Martín-Mirones,[9] R. G. McMahon,[5] J. P. D. Mittaz,[1] K. L. Nicholson,[1] M. J. Page,[1] I. Pérez-Fournon,[8] E. M. Puchnarewicz,[1] E. Romero-Colmenero,[1] A. D. Schwope,[3] B. Vila,[8] M. G. Watson[10] and D. Wonnacott[1]

[1]*Mullard Space Science Laboratory, University College London, Holmbury St. Mary, Dorking, Surrey RH5 6NT*
[2]*Instituto de Física de Cantabria, Consejo Superior de Investigaciones Científicas-Universidad de Cantabria, Santander, Spain*
[3]*Astrophysikalisches Institut Potsdam, An der Sternwarte 16, 14482 Potsdam, Germany*
[4]*Depto. de Astronomía, IFUG, Guanajuato, Mexico*
[5]*Institute of Astronomy, Madingley Road, Cambridge CB3 OHA*
[6]*Physics Dept., University of Durham, Durham DH1 3LE*
[7]*Astronomy Dept., Pennsylvania State University, 525 Davey Lab, University Park, PA 16802, USA*
[8]*Instituto de Astrofísica de Canarias, La Laguna, Tenerife, Spain*
[9]*Dpto. de Fisica Moderna, Universidad de Cantabria, Santander, Spain*
[10]*Department of Physics and Astronomy, University of Leicester, Leicester LE1 7RH*

Accepted 1999 July 20. Received 1999 July 20; in original form 1998 August 6

ABSTRACT

We describe the *ROSAT* International X-ray/Optical Survey (RIXOS), a medium-sensitivity survey and optical identification of X-ray sources discovered in *ROSAT* high Galactic latitude fields ($|b| > 28°$) and observed with the Position Sensitive Proportional Counter (PSPC) detector. The survey made use of the central 17 arcmin of each *ROSAT* field. A flux limit of 3×10^{-14} erg cm^{-2} s^{-1} (0.5–2 keV) was adopted for the survey, and a minimum exposure time of 8000 s was required for qualifying *ROSAT* observations. X-ray sources in the survey are therefore substantially above the detection threshold of each field used, and many contain enough counts to allow the X-ray spectral slope to be estimated.

Spectroscopic observations of potential counterparts were obtained of all sources down to the survey limit in 64 fields, totalling a sky area of 15.77 deg^2. Positive optical identifications are made for 94 per cent of the 296 sources thus examined. A further 18 fields (4.44 deg^2), containing 105 sources above the 3×10^{-14} erg cm^{-2} s^{-1} survey limit, are completely optically identified to a higher flux of 8×10^{-14} erg cm^{-2} s^{-1} (0.5–2 keV). Optical spectroscopic data are supplemented by deep CCD imaging of many sources to reveal the morphology of the optical counterparts, and objects too faint to register on Sky Survey plates. The faintest optical counterparts have $R \sim 22$.

This paper describes the survey method, and presents a catalogue of the RIXOS sources and their optical identifications. Finding charts based on Sky Survey data are given for each source, supplemented by CCD imaging where necessary.

Key words: surveys – stars: late-type – galaxies: active – galaxies: clusters: general – quasars: general – X-rays: general.

© 2000 RAS

Downloaded from https://academic.oup.com/mnras/article-abstract/311/3/456/1016504 by Estación Experimental del Zaidín user on 25 September 2018

Table 1. *ROSAT* fields used in the RIXOS survey.

Fid	ROR	N_H 10^{20} H atoms cm^{-2}	Exp Time (s)	Spec Time (s)	RA (2000)	Dec (2000)	Radius (')	Total	ID	P	Target
(1)	(2)	(3)	(4)	(5)	(6)	(7)	(8)	(9)	(10)	(11)	(12)
*281	P701092	5.76	9117	8442	00 10 29	10 58 12	2.67	3	3	0	[HB89] 0007 + 106
*262	P701048	3.37	13894	12819	01 24 34	03 47 60	2.67	5	5	0	NGC 520
292	P200468	3.48	8663	7095	01 43 22	04 19 48	2.67	5	3	1	GJ 70
246	P300003	6.19	25174	22472	02 06 53	15 18 00	4.00	8	2	3	TT Ari
*245	P700099	8.81	25727	23607	03 28 27	02 48 00	0.00	3	2	1	[HB89] 0323 + 022
279	P700531	4.28	9547	7636	03 53 48	−10 25 12	0.00	7	3	1	BR 0351 − 1034
270	P700271	3.57	10879	8081	04 05 34	−13 08 24	2.67	6	3	2	[HB89] 0403 − 132
*283	P701055	10.46	9043	6147	04 16 53	01 05 24	4.00	8	4	3	[HB89] 0414 + 009
*211	P700210	3.95	21043	14298	07 21 53	71 20 24	2.67	7	6	1	[HB89] 0716 + 714
*234	P700112	4.05	19844	15658	07 42 41	65 10 48	1.33	3	3	0	Mrk 78
*255	P700315	5.07	15992	7361	07 58 29	37 47 24	4.00	7	4	3	NGC 2484
*213	P700258	4.35	8354	6269	08 04 31	65 00 00	0.00	7	6	1	[HB89] 0759 + 651
*293	P200473	4.59	8954	7098	08 19 48	37 31 12	0.00	7	6	1	GD 90
*206	P200453	3.65	15927	13559	08 26 53	26 37 48	4.00	5	5	0	DX Cnc
*228	P400020	3.66	10978	9297	08 38 48	36 31 12	2.67	5	3	2	GBS0839 + 37
*221	P700546	2.90	12391	9932	08 48 19	37 40 12	2.67	6	5	1	[HB89] 0845 + 378
304	P700887	3.56	18552	17732	08 53 10	13 52 48	2.67	9	4	3	[HB89] 0850 + 140
250	P700436	3.52	21565	19372	08 58 41	14 08 60	2.67	7	1	2	[HB89] 0855 + 143
*257	P700326	2.18	14511	11469	09 05 31	34 07 48	0.00	6	5	0	B2 0902 + 343
*248	P700329	1.50	23561	19550	09 09 34	42 54 00	2.67	4	2	0	[HB89] 0906 + 430
*216	P700211	3.54	19495	14701	09 21 36	62 15 36	2.67	5	4	1	87GB 091738.6 + 622823
299	P700262	1.56	10298	8011	09 25 12	52 17 24	2.67	2	1	0	Mrk 110
*290	P700389	1.46	8158	6669	09 39 53	35 54 00	2.67	2	2	0	3C 223.0
*253	P700387	1.59	17193	14814	09 41 05	38 54 00	2.67	2	2	0	[HB89] 0937 + 391
*285	P400141	3.43	8957	8190	09 43 43	16 31 12	0.00	4	2	1	PSR 0940 + 16
*305	P701214	2.25	12532	8353	09 49 46	73 14 24	2.67	6	3	2	87GB 094429.5 + 732721
*218	P400059	3.01	9038	5371	09 53 10	07 55 48	2.67	6	6	0	PSR 0950 + 08
*252	P700319	0.78	19006	11893	10 01 58	55 40 48	5.33	7	7	0	NGC 3079
*286	P700774	2.33	8868	7406	10 04 19	05 13 12	0.00	3	2	1	[HB89] 1001 + 054
*232	P900214	0.84	15911	11651	10 10 12	50 45 00	0.00	3	2	1	UKMS Field, no target
230	P700265	0.79	23995	18778	10 10 14	51 45 00	0.00	3	0	0	UKMS Field, no target
229	P700263	0.79	14616	12287	10 10 14	52 45 00	0.00	5	4	0	UKMS Field, no target
*208	P700264	0.73	17331	15224	10 10 17	53 45 00	0.00	5	3	1	UKMS Field, no target
231	P900213	0.73	16813	10890	10 10 17	54 45 00	0.00	7	4	2	UKMS Field, no target
*115	P000049	2.50	38910	–[a]	10 11 00	28 15 00	0.00	2	1	0	Nowhere, no target
*225	P200076	2.19	26522	18123	10 19 38	19 52 12	2.67	1	1	0	AD Leo
*302	P700540	1.23	19359	10041	10 24 34	47 09 00	0.00	3	2	1	IRAS 10214 + 4724
*273	P700384	2.81	10209	5172	10 42 46	12 03 36	2.67	7	6	0	[HB89] 1040 + 123
*260	P300158	0.93	14008	9962	10 47 14	54 18 36	0.00	4	4	0	EK UMa
*133	P300137	1.19	9400	6167	10 56 55	49 42 00	2.67	4	4	0	CY UMa
*291	P200127	2.02	16670	–[c]	11 03 24	36 02 24	2.67	0	0	0	HD 95735
303	P700872	3.55	13081	9962	11 06 47	72 34 12	2.67	6	4	0	NGC 3516
*258	P700358	3.36	14425	13035	11 18 17	07 46 12	1.47	6	6	0	[HB89] 1115 + 080
*123	P700228	1.22	24950	19887	11 19 05	21 18 36	4.00	11	10	0	PG 1116 + 215
*259	P700010	1.96	14061	10545	11 20 17	13 35 24	4.00	5	4	1	NGC 3628
*271	P700510	2.07	10676	5785	11 24 43	38 45 36	2.67	3	2	1	NGC 3665
*287	P700499	1.06	8827	8827	11 25 36	54 22 48	1.47	1	1	0	Mrk 40
*251	P700372	4.44	21284	–[c]	11 29 17	−04 24 00	2.67	0	0	0	Mrk 1298
*227	P200091	1.77	33886	25321	11 36 34	29 47 60	0.00	4	3	1	GD 140
*240	P700055	1.22	58534	50084	11 57 56	55 27 14	5.33	4	4	0	NGC 3998
222	P701202	2.43	13563	12885	12 01 14	−03 40 48	2.67	5	2	1	Mrk 1310
*116	P000054	1.22	30590	–[a]	12 03 60	56 10 12	0.00	3	3	0	Nowhere, no target
124	P700232	1.64	17400	13651	12 04 41	27 53 60	2.67	5	2	0	[HB89] 1202 + 281
127	P700221	1.71	22400	20207	12 17 55	30 06 36	2.67	11	4	2	[HB89] 1215 + 303
*126	P700223	1.95	10400	10795	12 21 34	28 13 48	2.67	3	2	1	ON 231
288	P700506	1.43	8820	6773	12 28 24	31 28 48	2.67	5	1	0	[HB89] 1225 + 317
266	P700435	2.05	12299	8351	12 32 02	20 09 36	2.67	6	4	1	Mrk 771
*219	P700208	1.29	24340	20172	12 56 14	56 52 12	2.67	6	4	2	UGC 8058, Mrk 231
*226	P700073	1.19	48051	38128	12 56 58	47 20 24	1.07	6	4	2	3C 280
*265	P700216	1.10	13034	12024	13 10 29	32 20 60	2.67	6	5	0	[HB89] 1308 + 326
*224	P100308	1.01	34943	19366[b]	13 16 24	29 06 00	2.67	3	2	1	HZ43
*278	P701034	1.94	9611	9023	13 32 24	11 06 36	2.67	4	3	1	Mrk 789
277	P700473	1.74	9918	8995	13 38 17	48 16 48	2.67	9	5	1	NGC 5256
*254	P700391	1.05	17116	9076	13 44 43	55 53 24	1.07	5	5	0	Mrk 273
*268	P700392	2.08	11553	10090	13 56 02	18 22 12	2.67	4	2	2	Mrk 463
*274	P700227	2.16	10141	4581	14 06 22	22 23 60	2.67	1	1	0	PG 1404 + 226
*249	P700117	1.20	22692	–[c]	14 06 43	34 11 23	2.67	0	0	0	C 294
*217	P700248	1.13	25319	21739	14 13 48	44 00 00	2.67	7	7	0	PG 1411 + 442

Downloaded from https://academic.oup.com/mnras/article-abstract/311/3/456/1016504 by Estación Experimental del Zaidín user on 25 September 2018

Table 1 – *continued*

Fid	ROR	N_H 10^{20} H atoms cm^{-2}	Exp Time (s)	Spec Time (s)	RA (2000)	Dec (2000)	Radius (')	Total	ID	P	Target
(1)	(2)	(3)	(4)	(5)	(6)	(7)	(8)	(9)	(10)	(11)	(12)
*215	P150046	1.18	11516	8434	14 19 46	54 23 24	2.67	4	3	1	[HB89] 1418 + 546
*110	P200329	1.07	18250	23688	14 28 43	33 10 45	0.00	5	5	0	LHS2924
*261	P201103	3.31	13937	12855	15 34 41	26 43 12	2.67	2	0	2	HR 5793
237	P700230	2.95	8442	6370	16 13 58	65 43 12	2.67	2	1	0	[HB89] 1613 + 658
*122	P170174	4.12	38450	30325[b]	16 29 24	78 04 48	4.00	8	7	1	2RE J162911.2 + 780443
*212	P700255	1.19	8933	6878	16 30 19	37 19 12	0.00	5	5	0	[HB89] 1628 + 374
*223	P200721	1.84	47467	37173	16 34 24	57 09 00	2.67	5	3	1	CM Dra
*238	P700246	4.08	9357	7654	16 34 29	70 31 48	2.67	6	2	1	[HB89] 1634 + 706
*236	P700123	2.55	8196	4946	17 01 24	51 49 12	0.00	4	3	0	[HB89] 1700 + 518
*220	P701200	3.94	10578	6364	17 26 12	74 31 12	2.67	8	8	0	RX J1726.2 + 7431
*272	P700489	4.67	10461	7378	18 06 50	69 49 12	2.67	9	7	2	[HB89] 1807 + 698
*205	P100578	4.31	10313	9624	23 12 22	10 46 48	4.00	6	5	0	BPM 97859
*294	P200474	4.25	9488	9227	23 18 46	12 36 00	0.00	3	3	0	KUV 23162 + 1220
*125	P200322	5.04	26300	22513	23 25 19	23 24 36	4.00	3	2	1	HR 8905

Column 1: RIXOS field ID (Fid). Fields marked with a '*' constitute the RIXOS3 sample (see Section 4). **Column 2:** *ROSAT* observation request number. **Column 3:** Galactic absorbing column in the direction of the field centre derived from Stark et al. (1992). **Column 4:** Total *ROSAT* exposure time used for the detection. **Column 5:** *ROSAT* exposure time used for the spectral analysis. **Columns 6** and **7:** J2000 coordinates of field centre. **Column 8:** Excluded radius around the target. **Columns 9–11:** Respectively, the total number of RIXOS sources in the field, the number of secure identifications, and the number of probable identifications. **Column 12:** Name of the *ROSAT* target.
[a]: No *ROSAT* public data available at the time of the spectral analysis.
[b]: Detection image co-added from several individual images. The ROR number given corresponds to the single longest exposure, which was also used for the spectral analysis.
[c]: No spectral analysis performed, because no sources were detected in this field above the survey flux limit.

1 INTRODUCTION

Since its launch in 1990, the *ROSAT* satellite (Trümper 1983) has proved to be of major value in studying faint X-ray source populations. With its good imaging quality and low instrumental background the X-ray telescope on *ROSAT* has amply fulfilled its promise as a survey instrument, delivering images of the X-ray sky which have unprecedented sensitivity. *ROSAT* conducted a scanning survey of the entire sky, mostly during the first six months of its operation, and has completed many thousand pointed observations since. The all-sky survey reached a depth of better than about 5×10^{-13} erg cm^{-2} s^{-1} in the 0.5–2.0 keV band (Voges et al. 1999), while the deepest pointed observations detect sources down to $\sim 2 \times 10^{-15}$ erg cm^{-2} s^{-1} (Hasinger et al. 1998; McHardy et al. 1998). Such observations provide a census of X-ray sources and population types. Among other things, they can be used to investigate the evolution of extragalactic sources, and to form statistical samples of objects for studying the physics of their emission processes.

At the deepest flux levels that *ROSAT* can reach, source densities on the high Galactic latitude sky are about 500 per square degree, but this drops to only 0.5 per square degree at a flux of 5×10^{-13} erg cm^{-2} s^{-1} (0.5–2 keV). Thus, in order to register significant numbers of sources with intermediate fluxes, data from several *ROSAT* fields are required. The RIXOS survey, described in this paper, addresses this intermediate-flux regime by assembling a sample of almost 300 sources brighter than 3×10^{-14} erg cm^{-2} s^{-1} (0.5–2 keV) taken from 64 *ROSAT* pointed observations. Optical identifications (IDs) for this sample, which is referred to as RIXOS3 and covers in total 15.77 square degrees of sky, are 94 per cent complete. We also include data on a further 4.44 square degrees of sky which is completely optically identified to a flux level of 8×10^{-14} erg cm^{-2} s^{-1} and referred to as RIXOS8.

In addition to the deep surveys noted above, other surveys of *ROSAT* sources in the literature include the QSF survey (Shanks et al. 1991), the Cambridge-Cambridge *ROSAT* Serendipitous Survey (Boyle et al. 1995) and the UK Medium Survey (Carballo et al. 1995). These extend to fainter flux limits than RIXOS, at various levels of completeness, but cover a smaller sky area.

The nearest precedent to RIXOS is the *Einstein* Extended Medium Sensitivity Survey (Stocke et al. 1991) that included $\sim$800 sources over $\sim$800 deg^2, with very different flux limits, ranging from 3×10^{-12} to 5×10^{-14} erg cm^{-2} s^{-1} in the 0.3–3.5 keV band.

2 SURVEY METHOD

To assemble the sample of X-ray sources used in RIXOS, we chose *ROSAT* PSPC fields which had exposure times of at least 8000 s. This ensures that sources at our intended survey flux limit of 3×10^{-14} erg cm^{-2} s^{-1} (0.5–2.0 keV) lie significantly above the sensitivity threshold of every field. We also limit the choice of fields to those which have Galactic latitudes greater than 28° in either hemisphere, since RIXOS is primarily intended for extragalactic source studies. Though not a formal selection criterion, the Galactic absorbing column density in RIXOS fields (see Table 1) is generally no more than a few times 10^{20} H atom cm^{-2} based on the data of Stark et al. (1992), so attenuation of the source signal above 0.5 keV is never severe.

We eliminate from consideration fields which have bright and/or extended targets which might increase the overall background level against which to search for field sources. Only data within 17 arcmin of the field centre are used, to ensure the best X-ray image quality and the most accurate source positions. The target of the observation (where there was one) was excluded from the survey together with any area around it that was contaminated by its point spread function (typically 2–3 arcmin radius, see Table 1). In a number of fields either there was no target, the target was further than 20 arcmin off-axis, or the target was not detected. In these cases we did not exclude any part of the central area from our analysis.

Downloaded from https://academic.oup.com/mnras/article-abstract/311/3/456/1016504 by Estación Experimental del Zaidín user on 25 September 2018

© 2000 RAS, MNRAS **311**, 456–484

https://academic.oup.com/mnras/article-abstract/311/3/456/1016504 by Estación Experimental del Zaidín user on 25 September 2018

Table 2. RIXOS Source Catalogue.

Source Name (1)	Err (2)	RA(J2000) (3)	Dec(J2000) (4)	F_X (5)	c/ks (6)	MLC (7)	α_X (8)	Mag (9)	α_{opt} (10)	ID (11)	Type (12)	z (13)	Em lines (14)	W (15)	Note (16)	Fid_Sid (17)
RX J000923.4+105038	14	00 09 22.90	+10 50 37.3	8.8/8.5	6.1 ± 1.1	51	−0.7 ± 0.5	E18.71	0.4	AGN		0.349	Hα,[O III],Hβ,Mg II	3		281_21
RX J001002.5+110837	0	00 10 02.09	+11 08 35.9	319.9/264.5	213.4 ± 5.1	1971	−0.2 ± 0.0	C10.0		Star	G5Ve				NC	281_1
RX J001033.9+105227	10	00 10 33.51	+10 52 31.3	3.1/2.4	1.8 ± 0.5	19	−1.2 ± 0.7	S20.3	−0.2	AGN		2.918	C III],C IV,Lyα	11	I	281_11
RX J012412.4+033723	6	01 24 12.43	+03 37 20.6	5.6/4.9	3.9 ± 0.6	57	−1.3 ± 0.2	E19.71	−1.2	AGN		0.924	[O II],Hβ,Mg II,C III]	6		262_12
RX J012433.2+034334	3	01 24 33.18	+03 43 34.4	22.4/21.8	17.1 ± 1.2	236	−1.3 ± 0.1	E18.29		AGN		0.336			C	262_10
RX J012454.3+035815	12	01 24 54.52	+03 58 10.0	3.5/2.9	2.2 ± 0.5	34	−1.5 ± 0.3	E19.90	−1.5	AGN		0.882	Mg II	5		262_1
RX J012457.3+035347	6	01 24 57.57	+03 53 47.5	4.8/4.3	3.4 ± 0.6	34	−1.2 ± 0.3	E17.70		AGN		1.202			C	262_2
RX J012515.2+033904	8	01 25 15.43	+03 39 09.0	9.3/9.4	7.5 ± 0.9	91	−1.5 ± 0.1	E18.91	−1.2	AGN		0.312	Hα,[O III],Hβ,Mg II	4		262_34
RX J014250.2+041358	10	01 42 50.59	+04 14 00.1	3.6/4.4	3.4 ± 0.8	23	−0.7 ± 0.6	S21.4	−1.0	AGN	:	1.2	Mg II	15	N	292_19
RX J014300.9+042202	11	01 43 00.98	+04 22 09.6	4.5/4.3	3.3 ± 0.8	29	−0.4 ± 0.6			:Gal		0.135			NI	292_17
RX J014338.9+043517	24	01 43 39.67	+04 35 26.5	4.4/4.1	2.9 ± 0.8	26	−1.5 ± 0.4	S20.8	0.0	AGN		0.594	[O III],Hβ,Mg II	2	I	292_8
RX J014358.0+042243	11	01 43 58.00	+04 22 43.0	3.3/2.6	2.3 ± 0.7	21	−0.7 ± 0.7								I	292_12
RX J014400.7+042559	16	01 44 00.47	+04 26 03.3	3.4/4.7	3.3 ± 0.8	21	−1.1 ± 0.5	S20.6	−1.2	AGN		0.655	Mg II	:3	I	292_11
RX J020608.5+151235	6	02 06 08.66	+15 12 33.8	8.0/8.9	6.4 ± 0.6	134	−1.4 ± 0.2	O12.58		:Gal		0.043			C	246_20
RX J020619.1+150341	8	02 06 18.94	+15 03 41.0	9.0/7.3	6.2 ± 0.6	143	0.1 ± 0.1	E10.96		:Star	G0				C	246_35
RX J020621.2+151107	158	02 06 21.20	+15 11 07.0	6.9/3.2	2.3 ± 0.4	117	−1.3 ± 0.5	E18.0		Clus(2)		0.251			I	246_508
RX J020624.6+152905	7	02 06 24.60	+15 29 05.0	5.0/5.2	3.6 ± 0.5	82	−1.3 ± 0.5								I	246_14
RX J020701.9+151502	7	02 07 01.90	+15 15 02.0	3.5/3.9	2.8 ± 0.4	60	−1.6 ± 0.4								NI	246_44
RX J020706.8+150455	9	02 07 06.80	+15 04 55.0	4.9/4.6	3.5 ± 0.5	79	−1.2 ± 0.4								NI	246_37
RX J020707.2+153055	12	02 07 07.20	+15 30 55.0	3.3/3.1	2.2 ± 0.4	54	−1.6 ± 0.5	s16.3		:Star						246_10
RX J020721.9+150940	5	02 07 22.03	+15 09 37.4	5.9/6.2	4.3 ± 0.5	98	−0.5 ± 0.5	E17.94		AGN	Sy1.9	0.148	Hα,[O III],Hβ	:2		246_40
RX J032734.0+025502	16	03 27 34.87	+02 54 50.6	3.5/3.8	1.6 ± 0.3	171	−1.9 ± 0.6	S21.0	−0.9	AGN	:	0.712	Mg II	9	I	245_4
RX J032754.0+023344	158	03 27 54.10	+02 33 41.4	63.5/37.4	15.5 ± 0.8	941	−1.6 ± 0.2	E12.10		ELG	Sy/Lnr	0.034			C	245_543
RX J032817.1+025114	4	03 28 16.92	+02 51 11.5	8.8/6.4	3.9 ± 0.4	141	0.5 ± 0.2	E11.97		:Star	G5					245_6
RX J035318.6−101706	9	03 53 18.93	−10 17 03.7	5.3/7.5	5.2 ± 0.9	36	−2.2 ± 0.2	S18.1	0.0	AGN		1.146	Mg II,C III]	5		279_1
RX J035321.3−100934	30	03 53 20.53	−10 09 30.1	3.1/3.2	2.7 ± 0.8	36	−2.0 ± 0.5	S18.8	−0.6	AGN		0.626	Mg II	5		279_27
RX J035322.3−102509	5	03 53 22.43	−10 25 12.3	11.1/11.5	8.5 ± 1.1	77	−1.2 ± 0.3	S17.8	−2.5	AGN	Sy1.9	0.184	Hα,[O III],Hβ,[O II]	6		279_6
RX J035348.5−102010	6	03 53 48.50	−10 20 10.0	7.3/6.7	4.7 ± 0.9	51	−1.6 ± 0.3									279_4
RX J035414.3−102351	10	03 54 14.53	−10 23 50.6	3.4/3.8	3.1 ± 0.7	23	−0.2 ± 0.3	s10.8		:Star	K5					279_12
RX J035422.0−103823	14	03 54 22.00	−10 38 23.0	7.2/7.1	4.6±0.9	46	−2.4 ± 0.2									279_19
RX J035439.7−103352	17	03 54 39.70	−10 33 52.0	5.5/5.5	3.9 ± 0.9	35	−0.9 ± 0.6									279_18
RX J040523.4−125936	9	04 05 23.33	−12 59 36.5	4.0/3.9	3.6 ± 0.8	32	−0.5 ± 0.2	C 9.95		:Star	F3V				C	270_13
RX J040534.9−125842	3	04 05 34.94	−12 58 39.4	24.3/24.8	19.4 ± 1.6	195	−1.3 ± 0.1	C18.2		AGN		0.121			C	270_14
RX J040536.0−131258	8	04 05 36.24	−13 12 56.8	4.9/5.5	4.2 ± 0.9	40	−1.1 ± 0.4	s18.2	−1.9	AGN		0.226	Hα,[O III],Hβ	:3		270_3
RX J040546.8−131110	9	04 05 46.90	−13 11 09.8	3.7/3.4	2.3 ± 0.7	30	−1.9 ± 0.3	s18.4	−0.4	:AGN					N	270_4
RX J040621.3−130340	16	04 06 21.30	−13 03 40.0	3.1/2.6	1.1 ± 0.6	24	1.8 ± 1.9								N	270_17
RX J040628.5−125757	27	04 06 28.66	−12 58 06.0	4.9/2.6	3.9 ± 1.0	36	−0.4 ± 1.3	s19.3	−1.1	AGN		0.258	Hα,[O III]	4		270_18
RX J041602.3−005456	16	04 16 02.48	+00 54 56.0	5.9/4.7	3.4 ± 0.9	28	0.4 ± 0.6	s19.2	−1.2	AGN		0.724	[O III],Hβ,Mg II	6	I	283_21
RX J041612.1+011432	16	04 16 13.49	+01 14 26.9	3.7/2.8	2.4 ± 0.7	18	0.5 ± 0.6	C9.5		:Star	G5				NC	283_5
RX J041617.7+011014	13	04 16 17.70	+01 10 14.0	3.3/8.5	2.0 ± 0.7	17	1.2 ± 1.3			:Clus(1)		0.164			I	283_4
RX J041630.3+011503	5	04 16 30.09	+01 15 02.5	18.0/16.3	12.1 ± 1.5	94	0.7 ± 0.3	E16.57	−1.0	AGN		1.219	Mg II,C III]	5		283_6
RX J041704.5+011347	15	04 17 04.50	+01 13 47.0	5.0/4.3	3.6 ± 0.9	17	0.5 ± 0.5			:Clus(2)		0.32			I	283_8
RX J041722.4−005514	13	04 17 22.66	+00 55 12.0	6.7/5.2	4.0 ± 0.9	33	0.0 ± 0.3	E17.69	0.0	AGN		0.284	Hα,[O III],Hβ	3		283_14
RX J041739.2−005645	17	04 17 39.20	−00 56 45.0	7.4/4.6	3.8 ± 1.0	36	−0.1 ± 0.3								I	283_13
RX J041750.9+010846	16	04 17 51.36	+01 08 43.4	8.9/4.5	3.7 ± 1.0	43	0.7 ± 0.7	E16.90	−1.5	AGN		0.272	Hα,[O III],Hβ	5		283_11
RX J071858.8+712432	8	07 18 59.11	+71 24 19.5	6.6/6.3	4.9 ± 0.7	96	−1.0 ± 0.3	E17.70	−1.2	AGN		1.397	Mg II,C III]	2	C	211_30
RX J072001.6+711524	4	07 20 00.91	+71 15 18.4	7.5/6.7	6.0 ± 0.7	113	−0.4 ± 0.1	C9.0		:Star	F8				C	211_34
RX J072014.5+713228	96	07 20 14.50	+71 32 28.0	11.0/2.3	1.9 ± 0.8	38	−1.0 ± 1.0			Clus(1)		0.268			C	211_526
RX J072016.4+711417	6	07 20 16.70	+71 14 08.0	4.2/3.8	2.9 ± 0.5	64	−1.1 ± 0.4	R20.30	−0.2	AGN		0.465	[O III],Hβ,Mg II	5		211_35
RX J072047.8+710945	158	07 20 38.98	+71 10 09.5	26.0/5.5	4.6 ± 0.6	64	0.4 ± 0.2	E12.42		Star	F5e				N	211_539
		07 20 47.80	+71 09 45.0					E15.9		Clus(3)		0.23			N	
RX J072135.2+711334	4	07 21 36.00	+71 13 22.0	7.3/7.3	5.5 ± 0.7	113	−1.5 ± 0.2	E17.74	−0.1	AGN		0.232	Hα,[O III],Hβ	2		211_42

Table 2 – *continued*

Source Name (1)	Err (2)	RA(J2000) (3)	Dec(J2000) (4)	F_X (5)	c/ks (6)	MLC (7)	α_X (8)	Mag (9)	α_{opt} (10)	ID (11)	Type (12)	z (13)	Em lines (14)	W (15)	Note (16)	Fid_Sid (17)
RX J074142.4+652500	9	07 41 42.31	+65 25 03.7	7.9/9.0	6.9 ± 0.8	107	−1.5 ± 0.2	E17.38	−1.0	AGN		1.666	Mg II,C III],C IV	6		234_1
RX J074205.7+645813	12	07 42 04.99	+64 58 12.7	3.3/4.2	2.8 ± 0.5	46	−1.9 ± 0.2	E18.82	−1.9	AGN		1.019	Mg II,C III]	7		234_33
RX J074234.7+651720	158	07 42 34.70	+65 17 20.0	7.0/4.2	1.9 ± 0.4	107	0.9 ± 1.6	E14.6		Clus(4)		0.167				234_505
RX J075726.7+375507	14	07 57 27.22	+37 55 07.3	4.4/3.5	2.7 ± 0.7	47	−1.0 ± 0.7	S21.0	−2.2	AGN		: 0.75	Mg II	14	I	255_23
RX J075806.4+375443	8	07 58 05.15	+37 54 41.5	3.1/3.1	2.1 ± 0.6	34	3.6 ± 1.3	S15.3		:Star	K2				I	255_20
RX J075820.4+373331	15	07 58 20.88	+37 33 15.1	3.0/2.3	1.3 ± 0.6	32	2.0 ± 1.7	E13.30		:Star	K2					255_32
RX J075821.1+375536	7	07 58 20.95	+37 55 32.9	4.1/3.1	2.2 ± 0.6	45	−2.2 ± 0.4	E19.22	−1.5	AGN		0.864	Hγ,Mg II	5		255_19
RX J075830.7+373205	24	07 58 30.86	+37 32 05.3	3.5/4.4	3.1 ± 0.8	37	0.9 ± 0.7	E13.72		:Star	G8					255_33
RX J075907.1+373259	23	07 59 06.74	+37 32 35.9	3.3/3.7	2.9 ± 0.9	34	−1.2 ± 0.8	E17.11	0.6	AGN		0.260	Hα,[O III],Hβ	2		255_7
RX J075918.4+374906	8	07 59 19.24	+37 49 04.6	4.1/2.9	2.4 ± 0.7	45	−1.6 ± 0.5	S20.5	−1.9	AGN		0.582	Mg II	4	I	255_13
RX J080232.5+645144	158	08 02 32.50	+64 51 44.0	11.0/4.5	3.2 ± 0.9	26	−0.9 ± 0.9	E16.2		Clus(3)		0.16				213_522
RX J080309.3+650808	6	08 03 09.58	+65 08 10.0	16.4/14.1	12.6 ± 1.5	96	−0.2 ± 0.1	C8.3		:Star	G2				C	213_1
RX J080312.3+644744	14	08 03 10.80	+64 47 53.9	7.6/7.6	6.1 ± 1.2	42	−1.0 ± 0.4	E17.58	−1.5	AGN		0.664	O III],Hβ,Mg II	4		213_20
RX J080425.3+644735	11	08 04 25.44	+64 47 30.1	7.9/7.6	6.0 ± 1.1	45	−1.4 ± 0.3	E18.87	−0.9	AGN		0.467	O III],Hβ,Mg II	3		213_19
RX J080432.4+645652	11	08 04 33.12	+64 56 49.1	3.2/3.6	2.4 ± 0.8	19	0.5 ± 1.4	S20.8	−2.1	AGN		1.550	Mg II,C III],C IV	7	I	213_11
RX J080443.4+650630	8	08 04 43.07	+65 06 28.7	6.6/5.8	4.6 ± 1.0	40	−0.7 ± 0.5	S20.6	−1.0	AGN		0.542	O III],Hβ,Mg II	3	I	213_7
RX J080645.0+651106	18	08 06 46.97	+65 11 02.9	8.7/6.5	5.9 ± 1.3	48	−1.4 ± 0.4	S20.0	−1.7	AGN		0.438	O III],Hβ,Mg II	4	I	213_17
RX J081845.6+372403	8	08 18 45.55	+37 24 02.9	16.4/16.6	12.7 ± 1.5	99	−1.2 ± 0.2	E18.70	−1.7	AGN		0.760	Mg II	3		293_10
RX J081914.8+373946	9	08 19 15.05	+37 39 52.9	6.4/5.8	4.3 ± 0.9	40	−0.8 ± 0.6	S20.3	−2.8	AGN		0.824	Mg II	3	I	293_1
RX J081931.0+372600	9	08 19 30.82	+37 25 57.7	4.6/3.6	3.2 ± 0.7	29	−0.3 ± 0.2	E8.68		:Star	G5					293_8
RX J082007.6+372840	4	08 20 07.70	+37 28 39.4	14.7/15.1	11.4 ± 1.3	96	−1.3 ± 0.2	E11.82	0.9	AGN		0.082	Hα,[O III],Hβ	2	C	293_6
RX J082012.7+373501	7	08 20 12.69	+37 35 02.8	6.6/8.0	5.6 ± 1.0	42	−0.3 ± 0.7	E19.18	0.6	AGN		0.189	Hα,[O III],Hβ	1		293_13
RX J082030.5+372034	13	08 20 29.59	+37 20 40.0	4.5/4.1	2.9 ± 0.7	27	−0.7 ± 0.9	S19.5	−1.6	AGN		0.922	Mg II,C III]	2	I	293_12
RX J082101.7+374046	18	08 21 01.70	+37 40 46.0	6.2/8.8	6.9 ± 1.2	36	−0.7 ± 0.4	E14.4		Clus(2)		0.082				293_15
RX J082605.8+262740	158	08 26 05.83	+26 27 42.1	5.0/2.5	2.0 ± 0.5	26	0.0 ± 0.3	E15.34		Star	M5.0e					206_517
RX J082615.1+264239	96	08 26 15.85	+26 42 12.0	9.0/3.9	3.1 ± 0.5	21	−1.4 ± 0.3	S20.1	−2.0	AGN		0.740	MG II	2	I	206_522
RX J082721.2+263649	64	08 27 22.22	+26 36 35.3	6.0/3.4	2.5 ± 0.5	18	−1.0 ± 0.4	S21.0	1.9	AGN		0.484	O III],Hβ,Mg II	4	I	206_507
RX J082729.4+263410	6	08 27 29.31	+26 34 08.8	5.8/6.1	4.4 ± 0.6	68	−0.5 ± 0.4	S20.8	−1.2	AGN		0.805	Mg II	2	I	206_9
RX J082733.7+263716	6	08 27 33.67	+26 37 16.0	5.4/6.2	4.5 ± 0.6	24	−0.7 ± 0.3	E19.23	−1.3	AGN		0.690	[O III],Hβ,[O II],Mg II	3	C	206_6
RX J083731.4+363201	9	08 37 31.68	+36 32 01.0	9.5/10.1	7.3 ± 1.0	72	−0.3 ± 0.4	E17.78	−0.3	AGN		1.726	Mg II,C III],C IV	10		228_1
RX J083918.7+361855	4	08 39 18.70	+36 18 55.0	34.6/32.7	25.4 ± 1.8	270	−1.4 ± 0.1	E15.3		Clus(2)		0.335				228_18
RX J083949.0+362948	13	08 39 49.49	+36 29 49.2	3.5/2.3	1.7 ± 0.5	28	−0.8 ± 0.2	E14.84		Star	M4.5e					228_14
RX J083949.2+362530	5	08 39 49.03	+36 25 32.2	16.8/14.7	12.9 ± 1.3	130	−0.4 ± 0.1	S10.3		:Star	K0					228_15
RX J083958.9+363929	27	08 40 00.55	+36 39 29.5	3.6/3.4	2.5 ± 0.7	27	−0.3 ± 0.3	E11.68		:Star	K2					228_11
RX J084715.7+373214	3	08 47 16.10	+37 32 17.0	52.3/55.1	46.1 ± 2.4	466	−1.0 ± 0.1	E17.16	−2.1	AGN		0.451	Hα,[O III],Hβ,Mg II	2	C	221_35
RX J084822.0+373554	6	08 48 22.20	+37 35 50.8	6.6/5.4	4.3 ± 0.7	63	−1.7 ± 0.2	S19.1	−0.6	AGN		0.184	Hα,[O III],Hβ	1	I	221_16
RX J084836.2+374254	8	08 48 36.33	+37 42 54.0	3.9/4.0	2.9 ± 0.6	21	−0.9 ± 0.4	S19.5	−1.6	AGN		0.900	O III],Hβ,Mg II	2	I	221_2
RX J084906.8+373708	5	08 49 07.27	+37 37 07.3	9.0/8.0	7.2 ± 0.9	84	−0.3 ± 0.1	E13.82		Star	M4.5e					221_9
RX J084907.0+373158	158	08 49 07.00	+37 31 58.0	15.0/5.2	3.9 ± 0.7	26	−0.3 ± 0.6			:Clus(0)		0.218			C	221_511
RX J084910.1+374146	3	08 49 10.20	+37 41 46.3	24.8/26.5	20.4 ± 1.5	230	−1.0 ± 0.1	E17.50	−0.3	AGN		0.292	[O III],Hβ	2		221_7
RX J085202.8+135823	17	08 52 03.24	+13 58 18.8	3.7/4.1	3.1 ± 0.5	47	−0.7 ± 0.4	E17.73		:ELG		0.088	Hα			304_50
RX J085231.8+133632	17	08 52 32.28	+13 36 49.3	3.5/4.7	4.5 ± 0.8	134	−1.1 ± 0.3	E11.87		:Star						304_23
RX J085233.6+134930	8	08 52 33.60	+13 49 30.0	3.2/3.3	2.5 ± 0.4	14	−0.6 ± 0.4									304_26
RX J085240.2+134653	6	08 52 40.20	+13 46 53.0	7.2/8.1	6.3 ± 0.6	24	−0.1 ± 0.3									304_25
RX J085253.1+134601	6	08 52 53.30	+13 46 06.2	6.6/7.4	5.7 ± 0.6	91	−1.5 ± 0.1	E18.25	−0.3	AGN		1.497	Mg II,C III],C IV	2		304_29
RX J085310.2+134543	6	08 53 10.13	+13 45 41.4	3.9/4.2	3.4 ± 0.5	56	−1.4 ± 0.2	E19.05	−0.8	AGN		0.682	[O II],Mg II	1		304_30
RX J085312.4+135857	6	08 53 12.26	+13 58 55.9	5.1/5.1	4.0 ± 0.5	70	−1.1 ± 0.2	E19.22	−1.2	AGN		1.163	Mg II,C III]	6		304_48
RX J085340.3+134927	3	08 53 40.39	+13 49 04.8	11.0/12.0	9.3 ± 0.8	56	0.0 ± 0.3	E17.25		ELG	Sy2	0.194	[S II],[N II],Hα,[O II]	0	NC	304_10
RX J085345.5+134948	8	08 53 45.96	+13 49 47.3	3.1/3.0	2.5 ± 0.4	113	−1.9 ± 0.2	C7.3		:Star	A3				NC	304_7
RX J085748.0+140957	7	08 57 47.86	+14 09 58.7	5.2/6.0	4.5 ± 0.6	81	−0.9 ± 0.3	E16.92	−1.9	AGN	Sy1.9	0.178	Hα,[O III]	:2		250_14
RX J085752.5+141051	7	08 57 52.63	+14 10 58.1	5.5/5.6	4.6 ± 0.5	86	0.4 ± 0.2	E13.53		:Star	F8					250_13
RX J085825.9+135724	12	08 58 25.90	+13 57 24.0	3.0/3.0	2.3 ± 0.5	47	−0.6 ± 0.5								NI	250_57

© 2000 RAS, MNRAS **311**, 456–484

https://academic.oup.com/mnras/article-abstract/311/3/456/1004 by Estación Experimental Zaidin user on 25 September 2018

https://academic.oup.com/mnras/article-abstract/311/3/456/1016504 by Estación Experimental del Zaidin user on 25 September 2018

Table 2 – *continued*

Source Name (1)	Err (2)	RA(J2000) (3)	Dec(J2000) (4)	F_X (5)	c/ks (6)	MLC (7)	α_X (8)	Mag (9)	α_{opt} (10)	ID (11)	Type (12)	z (13)	Em lines (14)	W (15)	Note (16)	Fid_Sid (17)
RX J085834.9+142411	10	08 58 34.90	+14 24 11.0	4.1/4.7	3.7 ± 0.5	20	−0.4 ± 0.4									250_5
RX J085841.2+140540	5	08 58 41.18	+14 05 38.4	4.7/4.2	3.5 ± 0.5	76	0.5 ± 0.2	E14.90		:Star	K2					250_35
RX J085851.2+141149	6	08 58 51.20	+14 11 49.0	3.0/3.9	2.4 ± 0.4	49	1.7 ± 1.0								I	250_40
RX J085934.3+141500	7	08 59 34.30	+14 15 00.0	6.8/7.9	5.5 ± 0.6	104	0.9 ± 0.5									250_47
RX J090429.2+340545	11	09 04 29.35	+34 05 44.9	3.4/3.0	2.5 ± 0.6	37	−1.0 ± 0.3	E18.50	−1.7	AGN		1.304	Mg II,C III]	5		257_20
RX J090505.5+341352	3	09 05 05.50	+34 13 51.6	16.6/16.1	13.5 ± 1.1	185	−1.2 ± 0.1	E17.95	−1.8	AGN		1.021	Mg II,C III]	14		257_1
RX J090515.3+342208	14	09 05 15.65	+34 22 14.9	4.8/5.2	4.5 ± 0.7	49	−0.8 ± 0.3	E19.23	−1.0	AGN		1.099	Mg II,C III]	2		257_14
RX J090517.8+335004	16	09 05 17.80	+33 50 04.0	5.0/8.2	4.7 ± 0.8	52	2.2 ± 1.4								NI	257_28
RX J090634.3+340053	17	09 06 34.04	+34 00 44.7	3.3/2.6	2.2 ± 0.5	34	−1.0 ± 0.3	s21.6	−1.0	AGN		0.328	[O III],Hβ	0	I	257_37
RX J090642.5+335940	19	09 06 43.58	+33 59 21.1	4.3/4.7	3.4 ± 0.7	45	−1.0 ± 0.3	E17.93	−2.0	AGN		1.260	Mg II,C III]	4		257_38
RX J090900.2+424327	7	09 09 00.20	+42 43 27.0	4.4/4.1	3.3 ± 0.5	79	−0.3 ± 0.3								I	248_56
RX J090926.5+424228	3	09 09 26.52	+42 42 28.1	13.7/14.6	11.6 ± 0.8	250	−1.5 ± 0.1	E18.05	100.0	AGN	Sy1	0.242	Hα, [O III],Hβ	3	C	248_51
RX J090943.6+430255	4	09 09 43.56	+43 02 54.6	7.8/8.5	6.8 ± 0.6	39	−0.8 ± 0.1	E19.10	0.4	AGN		0.274	Hα,[O III],Hβ	2		248_2
RX J091049.4+430407	12	09 10 49.40	+43 04 07.0	5.5/5.4	4.3 ± 0.6	95	0.1 ± 0.3								NIC	248_42
RX J091950.0+622710	12	09 19 49.75	+62 27 05.8	7.5/7.9	6.9 ± 0.8	22	−0.6 ± 0.1	E14.38		Star	M1e					216_21
RX J092043.9+621719	6	09 20 43.40	+62 17 22.0	4.1/4.5	3.4 ± 0.5	59	−0.8 ± 0.3	R19.82	−2.9	AGN		0.804	Mg II	5		216_7
RX J092244.1+621243	6	09 22 43.50	+62 12 40.0	3.5/3.5	2.9 ± 0.5	51	0.5 ± 0.3	R14.21		:Star	G2					216_28
RX J092252.4+620211	16	09 22 52.78	+62 02 10.0	3.5/4.0	3.1 ± 0.6	46	−1.0 ± 0.4	E18.75	−1.6	AGN		0.795	Mg II	3		216_33
RX J092307.3+620823	8	09 23 07.80	+62 08 18.0	5.1/5.4	4.0 ± 0.6	71	−1.0 ± 0.3	R21.20	−0.7	AGN		0.941	Mg II	7		216_30
RX J092409.6+521729	8	09 24 09.60	+52 17 29.0	4.9/3.9	3.1 ± 0.8	39	−1.9 ± 0.2									299_105
RX J092427.6+521514	10	09 24 27.34	+52 15 10.1	3.3/2.5	2.0 ± 0.6	26	−1.9 ± 0.3	E18.98	−2.1	AGN		0.735	Mg II	2		299_106
RX J093958.2+360911	20	09 39 58.80	+36 09 21.2	3.0/4.4	3.6 ± 1.0	18	−0.8 ± 0.4	E17.58	−1.4	AGN		2.575	C III],C IV,Lyα	6		290_21
RX J094013.5+355733	9	09 40 14.47	+35 57 13.3	3.5/3.8	2.9 ± 0.7	23	−0.3 ± 0.2	E17.17		Star	M2e					290_1
RX J094120.3+390037	8	09 41 20.47	+39 00 39.6	3.0/2.6	2.5 ± 0.5	31	−1.2 ± 0.2	E18.96	−1.5	AGN		1.211	Mg II,C III]	6		253_5
RX J094148.7+383907	14	09 41 48.43	+38 39 01.8	4.3/4.6	3.8 ± 0.6	53	−1.4 ± 0.2	E19.14	−1.8	AGN	Sy1.9	0.237	Hα	:3		253_32
RX J094330.7+164002	115	09 43 30.70	+16 40 02.0	15.0/7.9	6.0 ± 0.9	100	−0.8 ± 0.3			Clus(2)		0.255			I	285_514
RX J094344.9+164448	115	09 43 44.90	+16 44 48.0	18.3/3.6	2.6 ± 0.7	118	−1.1 ± 0.6	E16.5		:Clus(1)		0.180				285_518
RX J094405.8+162947	5	09 44 05.69	+16 29 49.2	8.4/8.1	6.5 ± 0.9	57	0.1 ± 0.2	E13.90		Star	K2e					285_4
RX J094427.0+164630	41	09 44 27.00	+16 46 30.0	3.4/2.8	2.7 ± 0.9	21	−0.5 ± 0.9								NI	285_102
RX J094614.5+732034	20	09 46 14.18	+73 20 35.5	3.3/4.0	3.3 ± 0.8	101	0.3 ± 0.4	c9.9		:Star	K2				C	305_33
RX J094641.0+731517	11	09 46 39.72	+73 15 14.8	4.7/4.9	3.6 ± 0.7	35	−0.9 ± 0.3	E19.00								305_30
RX J094725.0+731922	8	09 47 24.65	+73 19 21.4	4.8/5.4	4.4 ± 0.8	61	−1.1 ± 0.2	E19.03	−2.3	AGN		0.854	[O III],Hβ,Mg II	2		305_34
RX J095105.1+730248	7	09 51 06.17	+73 02 48.5	6.6/8.5	7.0 ± 1.0	62	−0.3 ± 0.3	E18.45	−0.9	AGN		0.387	Hα,[O III],Hβ,Mg II	3		305_18
RX J095113.8+731833	4	09 51 13.73	+73 18 34.6	10.8/11.5	9.4 ± 1.1	35	−1.5 ± 0.1	E18.07	−1.1	AGN		0.252	Hα,[O III],Hβ	3		305_11
RX J095221.3+080305	9	09 52 21.24	+08 03 13.3	13.6/12.2	9.6 ± 1.5	87	−1.1 ± 0.2	E18.18	−2.2	AGN		0.631	[O III],Hβ,Mg II	3		218_27
RX J095239.9+080714	10	09 52 39.80	+08 07 15.0	9.6/11.2	8.6 ± 1.4	61	−0.9 ± 0.3	R18.31	−2.0	AGN		0.545	[O III],Hβ,Mg II	5		218_1
RX J095250.2+075035	6	09 52 50.30	+07 50 34.6	10.4/8.4	6.4 ± 1.2	71	−1.2 ± 0.3	R19.92	−2.6	AGN		0.224	Hα,[O III],Hβ	1	I	218_14
RX J095253.8+075042	9	09 52 53.69	+07 50 39.5	3.9/3.4	2.4 ± 0.7	27	−1.0 ± 0.6	E18.42	100.0	AGN		1.450			C	218_13
RX J095327.6+075613	8	09 53 27.39	+07 56 14.6	4.3/3.0	2.5 ± 0.7	29	−1.5 ± 0.4	E19.74	−1.8	AGN		0.703	Mg II	4		218_9
RX J095340.9+074424	12	09 53 41.31	+07 44 18.8	4.3/5.5	3.9 ± 1.0	61	0.3 ± 0.8		0.1	AGN		:0.76			I	218_21
RX J100032.1 + 553630	6	10 00 31.97	+55 36 29.5	12.4/12.7	10.9 ± 1.0	184	−1.2 ± 0.1	E17.46	−1.4	ELG	Sy2	0.216	[S II],[N II],Hα	1		252_38
RX J100056.1 + 554059	4	10 00 56.28	+55 40 58.4	6.1/5.5	4.7 ± 0.7	93	−1.1 ± 0.1	E19.07	−1.3	AGN		1.037	Mg II,C III]	6		252_36
RX J100110.2 + 552835	11	10 01 10.11	+55 28 34.9	5.2/4.3	3.8 ± 0.7	75	−1.5 ± 0.1	v17.5	100.0	AGN		2.091	Mg II,C III]	15	C	252_46
RX J100119.9 + 554553	7	10 01 19.50	+55 45 57.4	3.1/3.3	2.5 ± 0.5	47	−1.0 ± 0.2	s21.0	−1.5	AGN		0.680	Mg II	5	I	252_34
RX J100120.3 + 555349	1	10 01 20.78	+55 53 53.7	64.5/64.2	53.6 ± 2.3	970	−1.1 ± 0.0	v17.00	−1.4	AGN		1.413	Mg II,C III]	3	NC	252_31
		10 01 20.95	+55 53 49.2					v17.00	−1.4	AGN		1.415	Mg II,C III]	3		
RX J100244.9 + 555756	16	10 02 44.76	+55 57 55.1	5.3/6.2	5.4 ± 0.9	74	−0.7 ± 0.2	o21.2	1.7	:AGN		:0.219	[O III]		I	252_1
RX J100309.3 + 554134	7	10 03 09.41	+55 41 33.4	3.6/3.8	3.3 ± 0.6	54	−1.2 ± 0.2	E18.53	−2.3	AGN		0.673	Hβ,Mg II	6		252_9
RX J100334.7 + 050222	21	10 03 34.68	+05 02 31.9	3.8/5.1	3.8 ± 0.8	41	−1.8 ± 0.2	E16.40	−1.5	AGN		1.498	Mg II,C III],C IV	10		286_2
RX J100447.7 + 050016	5	10 04 47.64	+05 00 16.9	28.6/27.0	23.1 ± 1.9	184	0.1 ± 0.1	c 7.7		:Star	G2				C	286_9
RX J100454.8 + 050418	19	10 04 53.98	+05 03 45.0	4.0/4.0	3.0 ± 0.7	26	−0.4 ± 0.6	E 6.68		Gal		0.013			NC	286_103
RX J100836.8 + 543733	11	10 08 36.19	+54 37 29.3	9.7/10.1	8.4 ± 1.0	122	−1.6 ± 0.1	E17.65	−0.5	AGN		0.783	Hβ,Mg II	1		231_301

© 2000 RAS, MNRAS **311**, 456–484

Table 2 – *continued*

Source Name (1)	Err (2)	RA(J2000) (3)	Dec(J2000) (4)	F_X (5)	c/ks (6)	MLC (7)	α_X (8)	Mag (9)	α_{opt} (10)	ID (11)	Type (12)	z (13)	Em lines (14)	W (15)	Note (16)	Fid_Sid (17)
RX J100851.6 + 524553	8	10 08 52.20	+52 45 52.0	5.2/4.8	4.2 ± 0.7	59	−0.1 ± 0.2	R13.1		Star	K2e				N	229_302
RX J100900.6 + 503730	16	10 08 58.82	+50 37 30.7	3.1/3.3	2.6 ± 0.6	37	−0.6 ± 0.3	R19.20	0.2	AGN		0.227	Hα,[O III],Hβ	2		232_16
RX J100913.1 + 535907	11	10 09 13.94	+53 59 07.8	7.1/7.0	7.3 ± 0.9	89	−1.5 ± 0.1	R19.1	−1.5	AGN		0.471	Hα,[O III],Hβ,Mg II	2		208_18
RX J100920.7 + 513539	9	10 09 20.70	+51 35 39.0	3.3/3.1	2.8 ± 0.4	61	−1.2 ± 0.1									230_401
RX J100922.0 + 534926	3	10 09 21.84	+53 49 25.0	11.7/11.3	10.0 ± 0.9	25	−1.3 ± 0.1	E17.92	−0.1	AGN		0.387	[O III],Hβ,Mg II	2		208_2
RX J100924.1 + 543631	7	10 09 24.10	+54 36 31.0	5.5/6.1	4.7 ± 0.7	72	−0.1 ± 0.3									231_305
RX J100926.3 + 533424	8	10 09 26.74	+53 34 23.9	5.1/5.0	4.1 ± 0.6	67	−0.8 ± 0.1	R19.40	−0.5	AGN		1.718	Mg II,C III],C IV	10		208_55
RX J100935.3 + 533307	11	10 09 35.30	+53 33 07.0	3.5/3.8	3.1 ± 0.5	45	−0.4 ± 0.2								I	208_54
RX J100945.8 + 523441	2	10 09 46.01	+52 34 40.8	38.4/37.0	30.7 ± 1.6	445	−1.4 ± 0.0	R17.60	1.6	AGN		0.175	Hα,[O III],Hβ	3		229_301
RX J100953.8 + 510049	16	10 09 53.66	+51 00 49.3	4.0/3.1	2.5 ± 0.6	47	−0.3 ± 0.3	E 7.67		:Star	G8				C	232_302
RX J101000.4 + 545851	14	10 10 01.80	+54 58 43.7	3.4/3.3	2.2 ± 0.6	44	−0.2 ± 1.3	E18.13		:ELG		0.137			I	231_307
RX J101001.3 + 503836	8	10 10 00.72	+50 38 43.1	3.7/4.7	3.8 ± 0.6	47	−1.0 ± 0.2	R18.50	−0.9	AGN		0.385	Hα,[O III],Hβ	3		232_301
RX J101008.8 + 525859	12	10 10 08.80	+52 58 59.0	3.1/2.9	2.3 ± 0.5	35	0.5 ± 0.7								I	229_310
RX J101010.4 + 515817	158	10 10 10.40	+51 58 17.0	5.0/1.2	1.0 ± 0.3	156	−0.8 ± 0.4								NI	230_501
RX J101014.2 + 542958	158	10 10 14.20	+54 29 58.0	23.0/10.5	8.4 ± 1.0	45	0.3 ± 0.2			Clus(2)		0.047			C	231_526
RX J101029.8 + 280925	1	10 10 29.86	+28 09 25.9	33.4/		1018		E17.65		AGN		0.555	[O III],Hβ,Mg II	3		115_53
RX J101037.6 + 523721	7	10 10 37.49	+52 37 22.4	4.6/4.2	3.8 ± 0.6	54	−1.3 ± 0.1	R19.30	−0.2	AGN		1.252	Mg II,C III]	7		229_40
RX J101045.5 + 543756	6	10 10 45.67	+54 37 55.6	4.9/4.9	4.6 ± 0.7	66	−1.1 ± 0.1	E16.91	−0.7	AGN		1.572	Mg II,C III],C IV	8		231_302
RX J101052.2 + 533821	6	10 10 52.61	+53 38 18.4	5.0/5.2	4.4 ± 0.6	67	−0.6 ± 0.1			:Star	K4/M				NI	208_33
RX J101125.6 + 543921	96	10 11 28.40	+54 39 09.0	13.0/8.8	7.8 ± 0.9	65	0.1 ± 0.2	R14.5		:Gal		0.044			N	231_503
RX J101134.9 + 544956	158	10 11 34.90	+54 49 56.0	8.0/2.6	2.0 ± 0.5	34	−0.1 ± 0.6	E18.0		Clus(2)		0.296				231_534
RX J101136.1 + 514714	158	10 11 36.10	+51 47 14.0	5.0/0.8	0.9 ± 0.3	45	−1.0 ± 0.4								N	230_502
RX J101154.7 + 525059	20	10 11 56.10	+52 51 20.0	3.0/4.3	3.0 ± 0.6	33	−0.9 ± 0.2	E19.35	−0.5	AGN		1.419	Mg II,C III]	5		229_11
RX J101159.6 + 281403	8	10 11 59.60	+28 14 03.0	3.1/		90										115_45
RX J101931.3 + 200121	6	10 19 31.39	+20 01 22.4	3.2/2.9	2.5 ± 0.4	64	−1.1 ± 0.2	E19.14	−0.9	AGN		0.488	[O III],Hβ,Mg II	3		225_1
RX J102331.9 + 471130	5	10 23 31.82	+47 11 25.4	6.4/8.1	6.1 ± 0.8	31	−0.7 ± 0.2	E19.82	−1.7	AGN		0.95	Mg II	3		302_18
RX J102411.3 + 471754	6	10 24 11.00	+47 17 53.2	3.5/4.3	3.6 ± 0.7	53	−1.2 ± 0.2	E19.00	−1.4	AGN		0.811	Mg II	2		302_14
RX J102442.3 + 465227	13	10 24 41.45	+46 52 33.6	5.1/5.0	4.5 ± 0.9	59	−0.2 ± 0.2	E13.36		:Star	K2				N	302_29
		10 24 42.77	+46 52 24.3					E14.77		:Star	M1					
RX J104206.7 + 115612	9	10 42 06.70	+11 56 12.0	4.4/5.2	4.2 ± 1.0	33	−1.3 ± 0.3								I	273_26
RX J104225.6 + 121238	2	10 42 25.68	+12 12 39.6	37.7/41.5	31.5 ± 2.5	289	−1.0 ± 0.1	E17.79	−1.0	AGN		0.270	Hα,[O III],Hβ	11		273_6
RX J104236.2 + 120625	7	10 42 36.12	+12 06 25.9	5.0/5.8	4.8 ± 1.1	39	−1.5 ± 0.2	E18.76	−1.3	AGN		1.046	Mg II,C III]	2		273_4
RX J104244.6 + 114639	22	10 42 44.91	+11 46 37.6	3.8/3.3	2.8 ± 1.0	27	−2.2 ± 0.3	E17.68	−1.3	AGN		1.080	Mg II,C III]	3		273_22
RX J104249.9 + 115123	13	10 42 50.30	+11 51 19.0	3.2/2.6	2.0 ± 0.8	24	−1.2 ± 0.6	S19.5	0.3	ELG		0.433	[O III]		I	273_23
RX J104313.8 + 120241	8	10 43 13.94	+12 02 41.3	4.8/2.9	2.1 ± 0.8	37	−0.1 ± 0.4	E12.04		Star	K0e					273_14
RX J104337.2 + 115625	14	10 43 37.61	+11 56 21.8	6.6/4.6	4.6 ± 1.1	48	−1.5 ± 0.3	E19.11	−1.2	AGN		0.361	[O III],Hβ,Mg II	2		273_18
RX J104551.4 + 540731	18	10 45 50.76	+54 07 23.5	3.8/5.6	3.9 ± 0.8	40	−0.4 ± 0.3	E19.40	−0.6	AGN		1.504	Mg II,C III],C IV	3		260_44
RX J104718.6 + 541919	7	10 47 18.60	+54 19 17.4	3.7/3.7	3.0 ± 0.6	42	−1.0 ± 0.2	E17.63	−0.7	AGN		1.823	Mg II,C III],C IV	7		260_8
RX J104841.0 + 541301	8	10 48 40.44	+54 13 01.6	5.8/6.8	5.0 ± 0.8	62	−0.9 ± 0.1	E15.50		ELG	LINER	0.104	[S II],Hα,[O III],Hβ,[O II]			260_28
RX J104901.4 + 542356	20	10 49 01.40	+54 23 56.0	4.0/5.1	4.1 ± 0.8	42	−0.6 ± 0.2	E16.1		Clus(1)		0.250			I	260_106
RX J105612.7 + 493306	158	10 56 12.70	+49 33 06.0	11.0/1.5	1.2 ± 0.5	144	−0.8 ± 0.7	E16.9		Clus(2)		0.21				133_501
RX J105649.6 + 493412	7	10 56 49.65	+49 34 13.1	5.9/6.6	5.1 ± 1.0	46	−0.8 ± 0.2	E17.27	−1.5	AGN		1.788	Mg II,C III],C IV	4		133_22
RX J105704.3 + 493612	9	10 57 04.81	+49 36 12.3	4.2/6.6	2.4 ± 0.7	32	0.4 ± 1.4	S21.2	−3.0	AGN		0.360	Hα		I	133_24
RX J105813.1 + 493927	15	10 58 13.05	+49 39 34.6	3.4/3.2	2.1 ± 0.7	25	0.3 ± 1.3	E17.98	−1.8	AGN		2.390			C	133_17
RX J110507.5 + 724201	7	11 05 07.50	+72 42 01.0	5.3/6.2	4.6 ± 0.8	50	−1.0 ± 0.3									303_108
RX J110525.0 + 723815	8	11 05 25.13	+72 38 16.4	3.9/3.8	2.8 ± 0.6	1919	−0.6 ± 0.6	E18.80	−0.8	AGN		1.392	Mg II,C III]	6		303_110
RX J110613.6 + 724939	18	11 06 13.60	+72 49 39.0	4.1/3.5	2.6 ± 0.7	37	−1.2 ± 0.5									303_112
RX J110616.0 + 724411	5	11 06 15.91	+72 44 12.8	8.5/8.6	6.5 ± 0.9	81	−1.6 ± 0.2	E18.32	0.2	AGN		0.680	Mg II	6		303_105
RX J110741.4 + 723235	5	11 07 41.59	+72 32 35.2	8.6/8.5	6.4 ± 0.9	84	−0.4 ± 0.4	E17.82		AGN		2.100			C	303_107
RX J110834.0 + 722607	6	11 08 33.19	+72 26 10.3	7.6/9.3	7.3 ± 1.0	72	−1.6 ± 0.2	E18.51	−0.9	AGN		0.329	Hα,Hβ	4		303_106
RX J111725.3 + 075325	12	11 17 25.39	+07 53 28.3	4.1/3.5	2.8 ± 0.6	157	−1.6 ± 0.3	E19.84	−0.8	AGN		0.812	Mg II	2		258_5
RX J111730.1 + 074618	56	11 17 29.64	+07 46 49.1	3.9/1.6	1.5 ± 0.4	41	−0.8 ± 0.6			Clus(2)		0.160			N	258_101

© 2000 RAS, MNRAS **311**, 456–484

https://academic.oup.com/mnras/article-abstract/311/3/456/1065... by Estación Experimental del Zaidín user on 12 September 2018

© 2000 RAS, MNRAS **311**, 456–484

https://academic.oup.com/mnras/article-abstract/311/3/456/1016504 by Estación Experimental del Zaidin user on 25 September 2018

Table 2 – *continued*

Source Name (1)	Err (2)	RA(J2000) (3)	Dec(J2000) (4)	F_X (5)	c/ks (6)	MLC (7)	α_X (8)	Mag (9)	α_{opt} (10)	ID (11)	Type (12)	z (13)	Em lines (14)	W (15)	Note (16)	Fid_Sid (17)
RXJ111750.5 + 075712	5	11 17 50.71	+07 57 11.9	15.1/15.8	11.6 ± 1.0	157	0.2 ± 0.3	E19.53	0.4	AGN		0.698	Hβ,Mg II	3		258_1
RXJ111806.2 + 212817	8	11 18 06.46	+21 28 15.6	9.7/8.7	6.7 ± 0.7	185	−1.9 ± 0.1	E18.42	−2.1	AGN		0.652	[O III],Hβ,Mg II	1		123_85
RXJ111809.9 + 212554	21	11 18 10.75	+21 25 32.2	3.2/2.8	2.5 ± 0.4	62	−0.5 ± 0.2								N	123_84
RXJ111822.1 + 074450	7	11 18 22.10	+07 44 48.8	3.3/3.6	2.6 ± 0.5	35	−0.8 ± 0.4	E19.21	−1.3	AGN		1.618	Mg II,C III],C IV	5		258_32
RXJ111833.0 + 074858	8	11 18 32.88	+ 7 49 02.1	3.1/2.6	2.5 ± 0.5	33	1.1 ± 1.6	S20.7	−1.1	AGN		0.847	Mg II	5	I	258_30
RXJ111840.4 + 212534	5	11 18 40.40	+21 25 30.0	4.4/4.5	3.6 ± 0.5	91	−1.0 ± 0.1	R20.25	−1.3	AGN		0.351	[O III],Hβ	2		123_27
RXJ111843.8 + 212145	5	11 18 43.80	+21 21 44.0	3.9/3.3	2.9 ± 0.4	81	−1.2 ± 0.1	R18.51	−0.3	AGN	Sy1.8	0.212	Hα,[O III],Hβ	2		123_28
RXJ111845.6 + 210255	10	11 18 45.70	+21 03 02.2	5.8/5.1	4.1 ± 0.6	112	−1.1 ± 0.1	E18.15	−0.9	AGN		0.494	[O III],Hβ,Mg II	8		123_66
RXJ111902.8 + 074931	12	11 19 02.78	+07 49 31.8	3.2/2.6	2.0 ± 0.5	33	−0.2 ± 0.2	E17.37		Star	M1e					258_20
RXJ111918.6 + 211339	5	11 19 18.70	+21 13 38.0	3.6/3.7	3.0 ± 0.4	74	−0.8 ± 0.2	R18.87	−0.3	AGN		1.818	Mg II,C III],C IV	5		123_41
RXJ111925.9 + 211414	6	11 19 25.80	+21 14 15.0	3.3/3.0	2.6 ± 0.4	68	−1.0 ± 0.2	R20.73	−1.0	AGN		0.477	[O III],Hβ,Mg II	2		123_42
RXJ111927.0 + 210651	96	11 19 27.00	+21 06 51.0	10.0/6.4	5.1 ± 0.6	86	−0.2 ± 0.2	E16.3		Clus(3)		0.176				123_560
RXJ111933.2 + 212760	2	11 19 33.20	+21 27 57.0	17.7/16.5	13.8 ± 0.9	358	−1.5 ± 0.1	R18.76	−1.0	AGN		0.282	[O III],Hβ	3		123_1
RXJ111942.3 + 211516	6	11 19 42.20	+21 15 16.0	3.7/3.4	2.7 ± 0.4	75	−0.1 ± 0.3	R19.45	−0.3	AGN		1.288	Mg II,C III]	5		123_46
RXJ111943.7 + 212643	9	11 19 43.70	+21 26 43.0	3.6/3.8	3.1 ± 0.4	72	−0.8 ± 0.2	R15.2		Clus(1)		0.061				123_5
RXJ112014.7 + 133230	9	11 20 14.74	+13 32 28.0	3.3/3.4	2.6 ± 0.5	37	−0.9 ± 0.3	S20.6	−1.8	AGN		0.995	Mg II,C III]	6		259_11
RXJ112018.4 + 135216	7	11 20 18.70	+13 52 13.3	17.8/18.7	15.8 ± 1.4	181	−0.2 ± 0.1	E13.53		:Star	M0				N	259_1
RXJ112026.3 + 134024	6	11 20 26.14	+13 40 24.6	5.6/5.8	4.5 ± 0.7	181	−1.0 ± 0.2	E18.59	−1.6	AGN		0.977	Mg II,C III]	8		259_5
RXJ112040.0 + 133609	10	11 20 39.79	+13 36 20.2	3.4/4.1	3.1 ± 0.6	37	−0.5 ± 0.4	E19.15	−0.6	AGN		0.408	[O III],Hβ,Mg II	2		259_7
RXJ112106.0 + 133825	8	11 21 06.00	+13 38 25.1	4.8/6.1	4.7 ± 0.7	51	−0.2 ± 0.4	E18.04	100.0	AGN		1.94			C	259_30
RXJ112337.1 + 384140	12	11 23 37.15	+38 41 37.7	4.0/4.0	3.7 ± 0.9	30	−0.1 ± 0.3	E 9.59		:Star	F2				C	271_27
RXJ112340.2 + 385128	9	11 23 40.20	+38 51 28.4	7.5/6.7	5.8 ± 1.1	30	−1.7 ± 0.2	E17.91	−2.6	AGN		1.039	Mg II,C III]	4		271_7
RXJ112456.2 + 384633	9	11 24 56.02	+38 46 33.3	3.6/4.4	3.3 ± 0.8	30	−2.0 ± 0.2	E19.10	−0.4	AGN		0.446	Hε,[O III],Hβ,Mg II	3		271_2
RXJ112524.9 + 542221	5	11 25 24.60	+54 22 20.3	10.4/9.1	8.0 ± 1.0	75	−0.4 ± 0.1	S14.		Star	M4e				NI	287_102
		11 25 25.18	+54 22 19.2					S14.		Star	M4e					
RXJ113612.4 + 294449	96	11 36 12.70	+29 44 46.0	6.0/7.3	5.7 ± 0.5	161	−0.9 ± 0.1	R18.97	−1.5	AGN		0.959	Mg II	3		227_513
RXJ113655.3 + 295131	5	11 36 55.00	+29 51 30.0	3.7/3.8	3.3 ± 0.4	98	−1.4 ± 0.1	R18.82	−1.0	AGN		1.861	Mg II,C III],C IV	6	C	227_19
RXJ113704.5 + 294842	4	11 37 04.40	+29 48 41.0	3.8/4.3	3.3 ± 0.4	100	−2.5 ± 0.1	R19.02	−0.3	:AGN		:0.114	Hα,[O III]			227_301
RXJ113727.8 + 293828	5	11 37 27.80	+29 38 24.0	9.7/10.8	8.8 ± 0.7	243	−1.2 ± 0.1	R17.96	−0.1	AGN		1.413	Mg II,C III]	6		227_37
RXJ115716.5 + 553756	6	11 57 16.61	+55 37 55.6	3.1/3.0	2.5 ± 0.3	143	−1.4 ± 0.1	E18.18	−1.5	AGN		1.263	Mg II,C III]	2		240_15
RXJ115847.0 + 551624	4	11 58 46.94	+55 16 23.5	4.6/4.4	3.5 ± 0.3	206	−0.7 ± 0.1	E19.44	−2.1	AGN		0.518	Hβ,Mg II	8		240_82
RXJ115908.9 + 553041	3	11 59 09.07	+55 30 40.3	4.1/4.5	3.8 ± 0.3	188	−1.2 ± 0.1	E17.98		ELG	Sy2	0.245	[Ne III],Hα,[O III],[O II]			240_60
RXJ115951.8 + 553231	102	11 59 51.80	+55 32 31.0	53.8/33.6	27.0 ± 0.9	2324	−0.2 ± 0.1	R14.0		Clus(3)		0.081			C	240_564
RXJ120045.4 − 035000	12	12 00 45.12	−03 50 02.0	3.0/3.1	2.6 ± 0.5	30	−1.4 ± 0.2	E18.88	−0.6	AGN		1.068	Mg II,C III]	3		222_20
RXJ120049.1 − 032738	158	12 00 49.10	−03 27 38.0	8.0/6.8	5.8 ± 0.8	46	−0.3 ± 0.3	E18.3		:Clus(2)		0.393			N	222_504
RXJ120108.9 − 033423	4	12 01 08.76	−03 34 21.4	10.9/10.3	9.3 ± 0.9	114	0.2 ± 0.1	E 7.79		Star	G0e				C	222_9
RXJ120110.8 − 033702	96	12 01 10.80	−03 37 02.0	6.0/6.7	5.1 ± 0.7	19	−0.8 ± 0.2								NI	222_511
RXJ120217.3 − 034756	17	12 02 17.30	−03 47 56.0	3.6/4.1	2.9 ± 0.6	34	−0.5 ± 0.6									222_33
RXJ120330.7 + 275532	9	12 03 30.91	+27 55 34.0	8.5/7.6	6.2 ± 0.8	112	−1.7 ± 0.1	E18.78		ELG	Sy2/Hii	0.342	[O III],Hβ,[O II]	0	N	124_36
RXJ120331.2 + 280057	16	12 03 31.20	+28 00 57.0	5.6/6.5	4.9 ± 0.8	72	−1.1 ± 0.2									124_38
RXJ120403.2 + 280715	158	12 04 03.20	+28 07 15.0	94.0/42.3	33.4 ± 1.8	386	−0.5 ± 0.1	E12.7		Clus(1)		0.167			IC	124_501
RXJ120416.2 + 560259	1	12 04 16.10	+56 02 57.0	35.9/		916		R16.29	−1.8	AGN		0.090	Hα,[O III],Hβ	3		116_14
RXJ120504.0 + 275510	9	12 05 04.00	+27 55 10.0	3.1/3.3	2.7 ± 0.5	44	−1.0 ± 0.2									124_16
RXJ120507.1 + 275023	8	12 05 07.10	+27 50 23.0	3.2/2.0	1.9 ± 0.5	44	−1.4 ± 0.3									124_24
RXJ120512.2 + 562340	1	12 05 12.55	+56 23 37.3	156.9/		3721		E11.20		Star	G7Ve					116_31
RXJ120544.7 + 560750	10	12 05 45.03	+56 07 53.8	3.0/		73		S20.5	0.0	AGN		0.766	Hγ,[O II],Mg II	2		116_28
RXJ121700.4 + 301845	12	12 17 00.96	+30 18 43.6	5.3/5.6	4.9 ± 0.6	88	−1.5 ± 0.1	E18.83	0.0	AGN		:0.975	Mg II	7		127_4
RXJ121714.1 + 295549	13	12 17 14.10	+29 55 49.0	3.2/2.9	2.7 ± 0.5	55	−1.4 ± 0.2									127_48
RXJ121726.9 + 301933	7	12 17 26.98	+30 19 37.9	7.6/5.8	4.8 ± 0.6	130	−1.8 ± 0.1	E18.17	−0.7	AGN		1.038	Mg II,C III]	2		127_3
RXJ121741.6 + 295422	11	12 17 41.60	+29 54 22.0	3.4/2.5	2.3 ± 0.4	58	−1.4 ± 0.2									127_62
RXJ121749.3 + 302338	14	12 17 49.30	+30 23 38.0	3.7/4.1	3.4 ± 0.6	59	−0.8 ± 0.2									127_2
RXJ121758.1 + 302004	10	12 17 58.10	+30 20 04.0	3.4/3.6	2.9 ± 0.5	59	−0.9 ± 0.2									127_1

Table 2 – *continued*

Source Name (1)	Err (2)	RA(J2000) (3)	Dec(J2000) (4)	F_X (5)	c/ks (6)	MLC (7)	α_X (8)	Mag (9)	α_{opt} (10)	ID (11)	Type (12)	z (13)	Em lines (14)	W (15)	Note (16)	Fid_Sid (17)
RX J121807.3 + 295610	4	12 18 07.06	+29 56 10.7	7.7/7.0	5.5 ± 0.6	136	−1.0 ± 0.1	E17.08		AGN	Sy1.5	0.152	Hα,[O III],Hβ	:3		127_21
RX J121828.6 + 301150	96	12 18 28.60	+30 11 50.0	6.0/3.1	2.5 ± 0.4	35	−0.6 ± 0.3	E18.5		:Clus(1)		:0.36			N	127_514
RX J121832.6 + 301443	96	12 18 31.30	+30 15 01.8	14.0/4.8	3.9 ± 0.5	60	−0.6 ± 0.1	C 6.53		:Star	A9.5iii				C	127_539
RX J121841.4 + 301519	10	12 18 41.40	+30 15 19.0	3.6/4.0	3.2 ± 0.5	63	−0.5 ± 0.3									127_38
RX J121842.7 + 300703	7	12 18 42.86	+30 07 01.2	3.4/3.5	2.8 ± 0.4	61	−1.1 ± 0.2	E19.98	−1.2	AGN		2.205	C III],C IV,Lyα	6		127_17
RX J122135.6 + 280613	4	12 21 35.60	+28 06 14.1	12.9/12.1	10.2 ± 1.1	107	−0.7 ± 0.2	R19.81	−0.7	AGN		3.305	Lyα		N	126_27
RX J122155.1 + 282923	33	12 21 54.30	+28 29 35.1	3.5/3.2	2.2 ± 0.6	73	−0.1 ± 0.5			:Star	M5				I	126_12
RX J122215.2 + 282124	7	12 22 15.31	+28 21 23.0	9.0/9.9	7.5 ± 0.9	73	−0.1 ± 0.3	E14.38	0.3	AGN	Sy1.8−1.	0.029	Hα,[O III],Hβ	5		126_1
RX J122741.4 + 312902	8	12 27 41.40	+31 29 02.0	4.7/5.4	4.3 ± 0.9	25	−1.3 ± 0.2									288_2
RX J122749.1 + 313321	9	12 27 49.10	+31 33 21.0	3.6/2.5	2.4 ± 0.7	25	−1.3 ± 0.3									288_1
RX J122853.6 + 311420	27	12 28 53.60	+31 14 20.0	3.6/3.4	3.2 ± 0.8	23	−1.3 ± 0.3									288_19
RX J122907.4 + 312329	9	12 29 07.22	+31 23 29.4	3.8/3.9	3.2 ± 0.7	26	−0.5 ± 0.2	C 8.54		Star	G2e				C	288_15
RX J122922.1 + 311732	22	12 29 22.10	+31 17 32.0	4.2/5.3	3.9 ± 0.9	27	−1.0 ± 0.3									288_16
RX J123118.4 + 201308	11	12 31 18.22	+20 13 09.5	3.1/2.7	2.6 ± 0.7	28	−1.3 ± 0.2	C 8.8		Star	G5e				C	266_12
RX J123138.1 + 202526	24	12 31 37.15	+20 25 35.0	3.5/5.0	2.6 ± 0.8	31	1.7 ± 1.8	E18.45		:Star	M5				N	266_35
RX J123154.9 + 195309	158	12 31 56.11	+19 53 28.0	18.0/13.3	10.8 ± 1.3	159	−1.3 ± 0.1	E17.45	−2.2	AGN	Sy1.9	0.142	Hα,[O III]	1	NIC	266_527
RX J123206.3 + 202521	15	12 32 06.48	+20 25 25.0	3.4/3.2	2.2 ± 0.7	31	−0.8 ± 0.8	E17.68	−0.6	AGN		2.460	C III],C IV,Lyα	7		266_32
RX J123210.0 + 200458	10	12 32 10.00	+20 04 58.0	3.1/2.7	2.2 ± 0.6	30	−1.2 ± 0.3									266_20
RX J123225.3 + 202316	6	12 32 26.09	+20 23 26.2	23.9/46.0	42.8 ± 2.5	218	−0.6 ± 0.1	E12.32		Star	M4e				C	266_1
RX J125420.3 + 565543	19	12 54 20.57	+56 55 37.2	3.1/2.9	2.5 ± 0.5	56	−1.0 ± 0.2	E19.42	−1.5	AGN		1.367	Mg II,C III],C IV	9		219_48
RX J125451.3 + 564425	7	12 54 51.60	+56 44 29.0	7.6/6.3	5.8 ± 0.6	140	−1.5 ± 0.1	R17.16		ELG	Sy2	0.124	[N II],Hα,[O III]	0		219_26
RX J125456.9 + 564941	4	12 54 56.70	+56 49 41.0	8.5/9.9	8.2 ± 0.8	161	−0.6 ± 0.1	R19.99	0.4	AGN		1.261	Mg II	6		219_45
RX J125524.8 + 565613	7	12 55 24.80	+56 56 13.0	3.1/3.5	2.7 ± 0.5	59	−1.6 ± 0.1	R19.30	0.0	AGN		1.190	Mg II	2		219_15
RX J125528.1 + 564640	7	12 55 28.35	+56 46 45.3	3.2/3.1	2.3 ± 0.4	61	−0.9 ± 0.2	R22.20		:Clus(0)					I	219_22
RX J125533.4 + 471557	7	12 55 33.36	+47 15 58.0	3.9/3.7	3.2 ± 0.4	140	−0.9 ± 0.1	R19.34		ELG	LINER	0.303	[O II],[O III],Hβ,[O II]	0		226_74
RX J125612.1 + 472113	4	12 56 12.17	+47 21 14.4	4.2/3.5	4.0 ± 0.4	163	−0.5 ± 0.1	C10.3		:Star	F5				C	226_130
RX J125639.4 + 471519	96	12 56 39.40	+47 15 19.0	5.0/3.1	2.7 ± 0.3	58	−0.4 ± 0.2	E18.5		Clus(1)		0.403			C	226_552
RX J125639.5 + 472410	2	12 56 39.60	+47 24 10.0	9.6/9.6	8.2 ± 0.5	372	−1.1 ± 0.1	R19.01	−4.6	AGN		1.315	Mg II,C III]	6		226_41
RX J125645.9 + 570726	11	12 56 46.51	+57 07 34.0	5.3/4.5	4.4 ± 0.6	95	−0.2 ± 0.2	C10.5		:Star	K5				C	219_1
RX J125738.4 + 472759	2	12 57 38.67	+47 28 01.1	9.4/9.2	8.6 ± 0.5	357	−0.5 ± 0.1	C10.6		:Star	G8				NC	226_27
		12 57 39.96	+47 27 49.3							:Star	K5					
RX J125748.8 + 470607	11	12 57 49.01	+47 06 04.0	3.7/4.8	3.7 ± 0.4	132	−0.8 ± 0.1	E19.42	−1.8	AGN		1.022	Mg II	2		226_114
RX J130921.1 + 322707	21	13 09 21.00	+32 27 06.8	3.2/3.2	2.5 ± 0.6	30	−0.4 ± 0.2	E14.88		Star	M1e					265_12
RX J131014.3 + 322424	6	13 10 14.14	+32 24 20.9	4.7/4.3	3.8 ± 0.6	49	−1.0 ± 0.2	E19.56	−1.6	AGN		0.448	[O III],Hβ,Mg II	3		265_17
RX J131047.6 + 321815	7	13 10 47.52	+32 18 16.6	4.3/3.8	3.6 ± 0.6	45	−0.4 ± 0.2	E15.24		Star	M4e					265_20
RX J131047.7 + 322955	6	13 10 47.70	+32 29 55.0	6.4/7.1	5.4 ± 0.7	65	0.6 ± 0.4								I	265_7
RX J131058.8 + 323335	9	13 10 59.30	+32 33 33.8	7.9/8.3	6.5 ± 0.8	78	−0.8 ± 0.1	E16.64	−0.5	AGN		1.65	Mg II,C IV,Lyα	:6	NC	265_1
RX J131112.2 + 322907	102	13 11 12.20	+32 29 07.0	33.5/22.7	18.0 ± 1.3	340	−0.4 ± 0.1			Clus(0)		0.245			C	265_505
RX J131616.1 + 291921	8	13 16 16.08	+29 19 25.0	3.7/5.3	3.9 ± 0.5	103	−0.7 ± 0.1	E19.04		:Gal		:0.36				224_3
RX J131634.8 + 285930	3	13 16 34.70	+28 59 29.0	9.0/9.7	7.2 ± 0.6	267	0.0 ± 0.2	R18.83	−3.0	AGN		0.277	Hα,[O III],Hβ	:4		224_26
RX J131636.9 + 290014	4	13 16 36.70	+29 00 15.0	4.4/4.0	3.4 ± 0.5	130	−1.3 ± 0.1	R19.05	0.2	AGN		1.544	Mg II,C III]	8		224_201
RX J133129.9 + 110802	10	13 31 29.59	+11 07 57.4	7.8/7.6	6.4 ± 1.0	55	−0.6 ± 0.2	B17.47		ELG	Sy2/Lnr	0.079	[S II],[N II],Hα,[O II]			278_15
RX J133146.3 + 105653	18	13 31 46.58	+10 56 55.7	3.1/2.6	2.6 ± 0.7	22	0.8 ± 0.7	s13.2		:Star	K7				N	278_26
RX J133152.2 + 111647	3	13 31 52.15	+11 16 49.8	46.5/54.5	35.8 ± 2.1	334	1.5 ± 0.3	E15.99	1.0	AGN	Sy1.9	0.090	Hα,[O III],Hβ	7		278_10
RX J133205.5 + 111619	7	13 32 05.42	+11 16 21.0	8.4/9.3	6.9 ± 1.0	61	−0.8 ± 0.2	E19.04	−2.1	AGN		0.949	[O III],Hβ,Mg II,C III]	4		278_9
RX J133740.5 + 480758	5	13 37 40.59	+48 07 54.2	14.6/15.1	12.5 ± 1.2	112	−0.7 ± 0.1			Star	M7.5e				IC	277_23
RX J133748.0 + 481547	12	13 37 48.00	+48 15 47.0	3.4/4.2	3.6 ± 0.7	26	−1.3 ± 0.2									277_25
RX J133751.1 + 480815	5	13 37 52.13	+48 08 23.3	11.6/11.5	10.1 ± 1.1	89	−0.7 ± 0.1	E10.70		Star	M0e				C	277_22
RX J133753.2 + 482720	9	13 37 53.06	+48 27 28.8	5.3/5.3	4.1 ± 0.7	40	−1.4 ± 0.2	E18.37	−0.3	AGN		0.595	[O III],Hβ,Mg II	4		277_1
RX J133821.3 + 480427	9	13 38 21.65	+48 04 23.5	5.9/6.0	5.0 ± 0.8	44	0.0 ± 0.2	E15.49		Star	K7e					277_20
RX J133821.8 + 482251	10	13 38 21.80	+48 22 51.0	3.2/3.0	2.2 ± 0.6	25	−1.0 ± 0.3									277_4
RX J133843.1 + 481809	9	13 38 41.91	+48 18 06.8	3.8/3.9	3.0 ± 0.6	29	−0.8 ± 0.3	E15.28		:Gal		0.088			I	277_8

© 2000 RAS, MNRAS **311**, 456–484

https://academic.oup.com/mnras/article-abstract/311/3/456/1016504 by Estación Experimental del Zaidin user on 25 September 2018

Table 2 – *continued*

Source Name (1)	Err (2)	RA(J2000) (3)	Dec(J2000) (4)	F_X (5)	c/ks (6)	MLC (7)	α_X (8)	Mag (9)	α_{opt} (10)	ID (11)	Type (12)	z (13)	Em lines (14)	W (15)	Note (16)	Fid_Sid (17)
RX J133908.1 + 482121	5	13 39 08.76	+48 21 32.8	9.1/8.4	7.5 ± 1.0	70	−0.2 ± 0.1	E16.55		Star	M5e					277_9
RX J133949.3 + 481657	20	13 39 49.30	+48 16 57.0	3.0/4.6	2.8 ± 0.7	22	0.9 ± 1.2									277_13
RX J134334.1 + 553644	158	13 43 34.10	+55 36 44.0	42.0/1.0	1.0 ± 0.5	540	−1.3 ± 0.4			Clus(0)		0.069			C	254_524
RX J134447.2 + 554655	3	13 44 47.47	+55 46 55.6	11.4/11.8	9.2 ± 1.0	157	−1.6 ± 0.1	E16.37	−1.4	AGN		0.936	[O III],Hβ,Mg II,C III]	2		254_10
RX J134447.3 + 555411	5	13 44 47.07	+55 54 10.1	5.6/6.2	4.8 ± 0.8	78	−0.2 ± 0.3	E19.25		ELG	Sy2	0.459	[O III],[O II]			254_6
RX J134511.9 + 554759	4	13 45 11.69	+55 47 58.6	8.8/7.9	6.3 ± 0.9	121	−1.3 ± 0.1	E17.76	−1.3	AGN		1.166	Mg II,C III]	7		254_11
RX J134605.4 + 560430	15	13 46 06.60	+56 04 28.9	4.0/3.2	3.3 ± 0.8	51	−1.3 ± 0.2	R19.14	−1.7	AGN		0.486	[O III],Hβ,Mg II	7		254_41
RX J135529.6 + 182413	8	13 55 29.42	+18 24 22.3	3.6/4.1	3.0 ± 0.6	32	0.6 ± 0.8	S21.6	−0.8	AGN		1.196	Mg II,C III]	8		268_11
RX J135608.7 + 183041	8	13 56 08.67	+18 30 40.3	4.4/3.4	2.8 ± 0.6	39	0.0 ± 0.3	E15.14		:Star	K5					268_7
RX J135630.3 + 181242	5	13 56 30.48	+18 12 41.8	15.4/15.3	12.2 ± 1.2	133	−2.1 ± 0.1	E17.46	−0.5	AGN		0.251	Hα,[O III],Hβ	3		268_24
RX J135642.6 + 182926	11	13 56 43.15	+18 29 25.4	3.2/2.8	2.3 ± 0.6	28	−0.1 ± 0.3	E15.61		:Star	M4.5					268_3
RX J140528.3 + 222331	6	14 05 28.32	+22 23 33.4	13.8/30.3	25.2 ± 2.5	104	−1.7 ± 0.1	E16.54	−0.9	AGN	Sy1	0.156	Hα,[O III],Hβ	2		274_8
RX J141221.5 + 435459	10	14 12 21.39	+43 55 01.4	5.2/6.3	5.5 ± 0.6	99	−1.1 ± 0.1	S20.9	−0.4	AGN		:0.590	Mg II	9	I	217_59
RX J141231.5 + 435539	96	14 12 31.53	+43 55 35.4	18.0/16.4	14.1 ± 0.9	279	−1.2 ± 0.1	E15.86		ELG	Sy2	0.095	[S II],[N II],Hα,[O III],Hβ,[O II]	0	NIC	217_560
RX J141320.1 + 440532	5	14 13 19.90	+44 05 34.0	4.2/4.5	3.6 ± 0.4	85	−0.7 ± 0.1	R17.68		ELG	Sy2/Lnr	0.137	[N II],Hα,[O III],[O II]	0		217_5
RX J141348.4 + 440644	5	14 13 48.30	+44 06 46.0	3.7/3.4	3.0 ± 0.4	75	−1.2 ± 0.1	R19.43	−1.6	AGN		0.989	Mg II	4		217_3
RX J141359.4 + 435208	5	14 13 59.20	+43 52 06.0	3.6/4.0	3.0 ± 0.4	73	−0.9 ± 0.2	R19.64	−0.4	AGN		0.435	[O III],Hβ,Mg II	4	I	217_35
RX J141414.1 + 435416	5	14 14 14.20	+43 54 14.0	4.6/4.4	3.8 ± 0.5	94	−1.4 ± 0.1	R19.17	−2.8	AGN		1.200	Mg II,C III]	4		217_34
RX J141513.8 + 440315	11	14 15 13.89	+44 03 17.2	3.3/4.0	3.3 ± 0.5	17	−1.3 ± 0.1		−0.7	AGN		0.562	[O III],Hβ,Mg II	5	I	217_21
RX J141916.7 + 541417	8	14 19 16.70	+54 14 17.0	4.0/4.8	3.5 ± 0.7	36	−1.0 ± 0.2	R17.5		:Clus(1)		0.230			I	215_11
RX J141954.3 + 543014	9	14 19 54.03	+54 30 14.4	3.4/4.4	3.4 ± 0.7	31	−1.0 ± 0.2	E17.45	−1.4	AGN		2.248	Mg II,C III],C IV,Lyα	3		215_1
RX J142009.3 + 542637	5	14 20 09.45	+54 26 38.0	8.9/8.3	6.9 ± 0.9	82	−1.4 ± 0.1	E18.98	−0.9	AGN		0.584	[O III],Hβ,Mg II	1		215_19
RX J142052.4 + 543538	17	14 20 52.34	+54 35 38.8	3.6/2.9	2.7 ± 0.7	31	−1.3 ± 0.2	E18.64	−1.7	AGN		0.613	[O III],Hβ,Mg II	2		215_32
RX J142746.0 + 330117	16	14 27 46.53	+33 01 17.4	3.1/2.6	2.0 ± 0.4	43	−1.7 ± 0.1	S20.9	−1.5	AGN		0.582	[O III],Hβ,Mg II	2		110_35
RX J142754.6 + 330003	14	14 27 54.98	+33 00 10.7	3.1/3.0	2.5 ± 0.4	44	0.0 ± 0.4		0.9	AGN		0.416	[O III],Hβ,Mg II		NI	110_34
RX J142811.7 + 332011	6	14 28 11.69	+33 20 09.2	6.5/6.6	5.9 ± 0.6	97	−1.7 ± 0.1	E18.70	−0.8	AGN		0.364	[O III],Hβ,Mg II	3		110_1
RX J142922.4 + 331036	6	14 29 22.66	+33 10 36.5	3.9/2.7	2.2 ± 0.3	59	−1.0 ± 0.2	S20.5	−1.8	AGN		1.340	Mg II,C III]	4		110_50
RX J142930.9 + 332417	17	14 29 30.18	+33 24 22.1	3.1/3.5	2.9 ± 0.4	43	−1.0 ± 0.2	S20.6	0.0	AGN		0.938	[O II],Mg II	8	I	110_8
RX J153350.9 + 264229	7	15 33 51.10	+26 42 31.7	6.5/6.3	5.3 ± 0.7	66	0.5 ± 0.2	C 9.80		:Star	G0				C	261_33
RX J153441.0 + 265443	7	15 34 40.66	+26 54 39.2	9.2/7.7	7.3 ± 0.8	92	−0.4 ± 0.1	C 9.7		:Star	G5				C	261_1
RX J161409.9 + 652646	18	16 14 08.70	+65 26 49.6	5.0/7.3	5.6 ± 1.1	29	−0.8 ± 0.4	S18.9		AGN	Sy	0.158	Hα,[O III],Hβ	3	I	237_15
RX J161418.8 + 654854	7	16 14 18.80	+65 48 54.0	6.0/8.2	5.8 ± 1.0	38	−0.9 ± 0.3								NI	237_2
RX J162622.9 + 781703	158	16 26 22.90	+78 17 03.0	12.0/6.4	4.3 ± 0.4	117	−0.9 ± 0.3	R20.3		:Clus(2)		:0.5			I	122_552
RX J162834.1 + 781924	8	16 28 34.29	+78 19 21.7	4.4/3.8	2.8 ± 0.4	117	−1.4 ± 0.3	E17.77	−1.6	AGN		1.134	Mg II,C III]	9		122_1
RX J162902.3 + 372434	12	16 29 02.53	+37 24 30.1	9.1/9.0	8.0 ± 1.2	60	−1.4 ± 0.1	S18.8	−2.3	AGN		0.923	Mg II	6	NI	212_32
		16 29 02.57	+37 24 34.4					S18.6	−1.6	AGN		0.923	Mg II	5		
RX J162926.5 + 372840	13	16 29 26.47	+37 28 42.2	4.8/4.9	3.6 ± 0.8	32	−0.8 ± 0.3	S19.3	−1.8	AGN		1.004	Mg II	3		212_6
RX J162944.1 + 781129	3	16 29 44.70	+78 11 27.0	7.0/5.6	4.7 ± 0.4	199	−0.1 ± 0.1	R15.51		Star	M5.5e					122_10
RX J163044.6 + 373013	10	16 30 44.70	+37 30 22.0	4.3/4.8	4.2 ± 0.9	29	−0.1 ± 0.2	R13.84		Star	M0e					212_1
RX J163054.6 + 781103	3	16 30 55.10	+78 11 02.0	8.9/9.2	6.4 ± 0.5	251	0.0 ± 0.3	R19.29	1.1	AGN		0.358	[O III],Hβ	3		122_13
RX J163057.7 + 370734	13	16 30 57.90	+37 07 33.0	5.4/5.2	4.8 ± 1.0	36	−1.4 ± 0.2	R19.61	−1.8	AGN		0.801	Mg II	6		212_25
RX J163111.1 + 703042	27	16 31 13.35	+70 30 37.4	4.2/5.3	4.4 ± 0.9	26	0.1 ± 0.3	R13.82		:Star	K2					238_16
RX J163126.9 + 371849	14	16 31 27.32	+37 18 57.2	3.5/3.8	3.3 ± 0.8	24	−1.0 ± 0.3	S20.4	−1.8	AGN		0.841	[Ne III],[O II],[Nev],Mg II	9	I	212_16
RX J163140.9 + 781238	3	16 31 40.80	+78 12 36.0	7.6/7.2	5.2 ± 0.4	214	−1.6 ± 0.1	R18.89	−1.6	AGN		0.380	[O III],Hβ,Mg II	3		122_14
RX J163216.2 + 775407	5	16 32 16.70	+77 54 10.0	7.8/7.2	6.4 ± 0.5	212	0.2 ± 0.1	R11.95		Star	K0e					122_31
RX J163239.0 + 781152	2	16 32 39.20	+78 11 52.0	20.4/20.5	15.6 ± 0.9	563	−0.7 ± 0.1	R11.23		ELG	LINER	0.005	[S II],[N II],Hα,[O I],[O III],Hβ,[O II]	0	C	122_16
RX J163305.8 + 704034	10	16 33 05.85	+70 40 31.1	4.6/4.8	3.7 ± 0.8	31	−0.3 ± 0.6	E18.47	−0.1	AGN	Sy1	0.325	[O III],Hβ	6		238_11
RX J163309.4 + 571039	2	16 33 09.60	+57 10 40.0	11.8/12.2	9.5 ± 0.5	434	−1.4 ± 0.1	R17.91	0.1	AGN		0.288	[O III],Hβ	4		223_17
RX J163331.9 + 570520	3	16 33 32.00	+57 05 19.0	4.9/4.6	3.7 ± 0.3	183	−0.6 ± 0.2	R18.74	−3.5	: AGN		0.386	[O III],[O II]			223_97
RX J163340.4 + 571410	96	16 33 40.40	+57 14 10.0	4.0/2.0	1.7 ± 0.2	23	−0.3 ± 0.3	R15.1		Clus(4)		0.244				223_572
RX J163349.8 + 701515	18	16 33 47.73	+70 15 14.0	6.6/5.2	4.8 ± 1.0	41	−0.1 ± 0.2	E13.56		Star	K2e					238_21
RX J163356.2 + 571550	3	16 33 56.60	+57 15 48.0	4.7/3.8	3.4 ± 0.3	175	−0.3 ± 0.1	R15.18		Star	Me					223_73
RX J163427.5 + 781002	6	16 34 27.80	+78 10 03.0	8.7/9.5	6.6 ± 0.5	229	−0.2 ± 0.3	R19.24	0.3	AGN		0.376	[O III],Hβ	1		122_21

© 2000 RAS, MNRAS **311**, 456–484

https://academic.oup.com/mnras/article-abstract/311/3/456/1045621 by Instituto de Astrofísica de Canarias user on 25 September 2019

Table 2 – *continued*

Source Name (1)	Err (2)	RA(J2000) (3)	Dec(J2000) (4)	F_X (5)	c/ks (6)	MLC (7)	α_X (8)	Mag (9)	α_{opt} (10)	ID (11)	Type (12)	z (13)	Em lines (14)	W (15)	Note (16)	Fid_Sid (17)
RX J163520.4 + 703023	8	16 35 20.40	+70 30 23.0	5.9/6.0	4.7 ± 0.9	40	−0.6 ± 0.5								I	238_2
RX J163522.5 + 701640	22	16 35 22.50	+70 16 40.0	3.5/3.8	2.5 ± 0.8	22	0.8 ± 1.7								I	238_22
RX J163616.7 + 570644	6	16 36 16.70	+57 06 44.0	6.3/6.4	5.5 ± 0.5	220	−0.9 ± 0.1								N	223_56
RX J163707.8 + 703640	17	16 37 07.80	+70 36 40.0	4.0/3.7	2.7 ± 0.7	26	−0.5 ± 1.0	R20.2							I	238_24
RX J170026.6 + 515908	14	17 00 27.12	+51 59 11.4	4.3/4.1	3.5 ± 1.0	26	−1.3 ± 0.3	E11.03	−0.3	AGN	Sy1.5	0.048	Hα,[O III],Hβ	3		236_22
RX J170035.8 + 514830	11	17 00 36.17	+51 48 26.6	3.3/2.2	1.8 ± 0.7	20	−1.5 ± 0.5	E18.90	−0.9	AGN		1.13	Mg II,C III]	3		236_21
RX J170131.7 + 515551	12	17 01 31.58	+51 55 51.2	3.1/2.6	2.0 ± 0.7	19	−1.4 ± 0.5	E19.68	−1.3	AGN		0.473	Hα,[O III],Hβ,Mg II	2		236_5
RX J170239.0 + 515225	16	17 02 39.00	+51 52 25.0	3.1/4.7	3.3 ± 0.9	18	0.1 ± 1.0									236_9
RX J172405.9 + 741831	17	17 24 04.38	+74 18 38.5	4.4/4.4	3.0 ± 0.8	32	−0.8 ± 0.7	R20.29	−1.4	AGN		0.442	[O III],Hβ,Mg II	10		220_18
RX J172446.6 + 744358	17	17 24 45.88	+74 44 07.5	3.5/3.9	3.4 ± 0.9	25	0.0 ± 0.3	R17.97		Star	M2e				I	220_1
RX J172455.2 + 743049	8	17 24 55.85	+74 30 51.8	4.3/3.7	2.7 ± 0.7	33	−0.5 ± 0.2	E14.48		Star	M4.5e					220_14
RX J172526.8 + 742614	9	17 25 25.92	+74 26 22.0	3.0/3.9	2.4 ± 0.7	23	0.9 ± 1.7	s19.7	−1.4	AGN		0.970	Mg II	3	I	220_13
RX J172621.6 + 744751	15	17 26 19.27	+74 48 01.9	7.0/6.6	5.1 ± 1.2	50	0.1 ± 0.9	V18.28	1.8	AGN		0.193	Hα,[O III],Hβ	2		220_23
RX J172629.0 + 742143	10	17 26 28.75	+74 21 41.4	3.9/3.7	2.9 ± 0.7	30	0.5 ± 0.5	E14.92		Star	M5.0e					220_11
RX J172649.8 + 744656	17	17 26 51.20	+74 47 03.8	5.8/6.0	4.6 ± 1.0	42	−1.9 ± 0.3	R19.61	−0.7	AGN	:Sy2	0.210	Hα,[O III],Hβ	0	I	220_25
RX J172904.4 + 742552	9	17 29 04.83	+74 25 57.6	5.8/6.8	5.7 ± 1.0	44	−0.3 ± 0.2	s15.8		Star	M9.0e				NI	220_33
		17 29 05.31	+74 25 56.5					s15.1		Star	M9.5e					
RX J180434.6 + 693742	11	18 04 34.34	+69 37 37.2	9.2/11.9	7.9 ± 1.2	65	−1.1 ± 0.4	E18.09	−1.6	AGN		0.604	[O III],Hβ,Mg II	6	C	272_18
RX J180530.7 + 694516	4	18 05 30.43	+69 45 16.6	17.2/13.3	10.9 ± 1.3	129	0.2 ± 0.1	E11.92		Star	G8e				C	272_9
RX J180534.0 + 694733	10	18 05 34.44	+69 47 43.5	3.9/3.4	2.6 ± 0.7	29	−1.5 ± 0.5	s19.8	−1.0	AGN		1.823	Mg II,C III],C IV	3		272_8
RX J180603.7 + 694024	4	18 06 03.10	+69 40 23.9	12.9/12.3	9.4 ± 1.2	96	−1.6 ± 0.2	E18.20		AGN	Sy1.9	0.321	[O III],Hβ		NC	272_10
RX J180728.9 + 700560	24	18 07 28.99	+70 06 09.0	3.5/3.1	1.9 ± 0.7	24	1.7 ± 1.3	E17.20		:Star	M0					272_31
RX J180812.8 + 694807	5	18 08 13.00	+69 48 05.8	10.2/10.2	7.6 ± 1.1	76	−1.7 ± 0.2	E16.82	0.8	AGN	Sy1.8	0.095	Hα,[O III],Hβ	2		272_23
RX J180823.7 + 694208	13	18 08 23.70	+69 42 08.0	3.2/2.0	1.5 ± 0.6	23	−0.7 ± 1.2	s19.9		:ELG		:0.17			NI	272_24
RX J180825.9 + 695624	7	18 08 26.09	+69 56 26.9	7.9/6.6	5.2 ± 0.9	57	−1.5 ± 0.3	E19.36	1.0	AGN		0.444	[O III],Hβ,Mg II	6		272_28
RX J180828.3 + 700027	19	18 08 28.99	+70 00 25.9	3.0/3.1	2.9 ± 0.8	21	0.3 ± 0.4	E13.15		Star	K2e					272_29
RX J231213.7 + 103332	21	23 12 13.23	+10 33 31.7	3.7/2.9	2.3 ± 0.6	25	−1.2 ± 0.6	s21.5	−1.1	AGN		0.754	Mg II	5	I	205_34
RX J231239.7 + 103824	6	23 12 39.60	+10 38 23.6	11.0/10.6	8.1 ± 1.0	80	−1.7 ± 0.2	E18.53	−1.6	AGN		0.445	[O III],Hβ,Mg II	5		205_22
RX J231242.9 + 104302	9	23 12 42.90	+10 43 02.0	5.0/5.5	3.8 ± 0.7	37	−0.1 ± 0.7								I	205_21
RX J231253.7 + 103803	8	23 12 53.69	+10 38 02.5	7.8/8.1	6.1 ± 0.9	56	−1.1 ± 0.3	E19.85	1.8	AGN		0.618	[O III],Hβ	1		205_23
RX J231303.7 + 104914	8	23 13 03.14	+10 49 10.6	5.1/4.9	3.7 ± 0.7	37	−1.4 ± 0.3	E18.88	−0.8	AGN		1.333	Mg II,C III]	3	N	205_1
		23 13 03.84	+10 49 15.2					E19.67	−1.4	AGN		0.715	Hγ,Mg II	2		
RX J231323.1 + 104059	15	23 13 23.09	+10 40 57.0	6.3/7.3	4.9 ± 0.8	44	−0.2 ± 0.6	E18.03		ELG	Sy2/Lnr	0.196	[S II],[N II],Hα,[O III],[O II]	0		205_25
RX J231744.5 + 124333	14	23 17 44.76	+12 43 34.0	6.4/7.0	6.2 ± 1.1	41	−1.3 ± 0.3	E17.04		ELG	H II	0.126	[N II],Hα,[O III]	0		294_6
RX J231806.0 + 123811	8	23 18 05.90	+12 38 11.8	5.3/5.8	4.5 ± 0.8	36	−1.3 ± 0.3	s19.9	−0.8	AGN		0.714	Mg II	8		294_1
RX J231934.2 + 122626	158	23 19 34.20	+12 26 26.0	24.9/16.9	12.0 ± 1.3	160	−0.6 ± 0.2			Clus(3)		0.124			I	294_519
RX J232443.6 + 231537	8	23 24 43.72	+23 15 37.1	3.8/4.1	3.0 ± 0.4	69	−1.0 ± 0.5	E18.55	−0.5	AGN		1.832	Mg II,C III],C IV	4		125_14
RX J232450.4 + 232104	4	23 24 50.45	+23 21 06.5	7.2/7.3	5.1 ± 0.5	134	−1.5 ± 0.2	E19.14	−1.4	AGN		0.449	[O III],Hβ,Mg II	2		125_17
RX J232509.8 + 233017	5	23 25 09.57	+23 30 15.5	4.5/3.5	3.4 ± 0.4	31	−0.3 ± 0.1	E10.56		:Star	F2				C	125_5

Column 1: Source designation, derived from the J2000 coordinates of the X-ray centroid. **Column 2:** X-ray 90 per cent confidence positional radius in arcsec. **Column 3,4:** J2000 coordinates of the optical counterpart if it is a single object. For clusters and unidentified sources the X-ray centroid is given. **Column 5:** X-ray flux in units of 10^{-14} erg cm^{-2} s^{-1} (0.5–2.0 keV). The first number is derived from the measured count rate assuming a spectral slope of $\alpha = -1$, and is the flux used to define membership in the catalogue. The second number is the flux derived from the best-fitting spectral slope and (with the exception of stellar IDs) after correcting for Galactic absorption. **Column 6:** X-ray count rate per 1000 s. **Column 7:** Total X-ray counts based on maximum likelihood fits. **Column 8:** X-ray spectral index defined such that $F_X \propto E^{\alpha_X}$ and derived by fitting three-colour X-ray data assuming Galactic absorption (except for stellar IDs). See Mittaz et al. (1999) for details. **Column 9:** Magnitude of the optical counterpart (or the brightest galaxy for clusters). The prefix denotes the type of magnitude. C – from other catalogues (see Table 3); E – from APM measurements of POSS-E plates; O – from APM measurements of POSS-O plates; R – from *R*-band CCD images; V – from *V*-band CCD images; S - slit magnitudes derived by folding the spectrum through the *R*-band response. The typical accuracy of the slit magnitudes is about 30 per cent (see Puchnarewicz et al. 1996a). **Column 10:** Slope of the optical continuum. Uncertainties in the slope are about 50 per cent and dominated by systematic effects. See Puchnarewicz et al. (1996). **Column 11:** Category of optical ID. A colon indicates uncertain IDs. The number in parenthesis following the category 'Clus' indicates the number of cluster galaxies whose redshifts have been measured. **Column 12:** ID subtype. **Column 13:** Redshift of extragalactic counterparts. A colon indicates an uncertain value. **Column 14:** Emission lines observed in AGN and ELG IDs. **Column 15:** FWHM of the emission line underlined in column 12 in units of 1000 km s^{-1} and rounded down to the nearest integer. Preference is given to the Hβ or Mg II lines when they are available and well defined. Otherwise the best-defined permitted line in the spectrum is used. More complete details of emission-line measurements are given in Puchnarewicz et al (1997). **Column 16:** Signifies that there is a catalogue cross-reference in Table 3 C, an additional note in Section 3.2 (N), or that there is a CCD image of the field in Fig. 4 (I). **Column 17:** RIXOS Field ID (FID) and Source ID (SID) for cross-reference to other RIXOS papers.

© 2000 RAS, MNRAS **311**, 456–484

https://academic.oup.com/mnras/article-abstract/311/3/456/1016504 by Estacion Experimental del Zaidin user on 25 September 2018

A total of 94 *ROSAT* fields (a mixture of Rev. 0 and Rev. 1 data) were selected as being suitable for RIXOS. When more than one *ROSAT* observation was available for a given field, the corresponding images were co-added prior to the source search, to maximize the sensitivity of the survey. Significant optical identification work was subsequently carried out in 82 fields (including three fields that had no sources down to our X-ray flux limit). The fields used are listed in Table 1 along with relevant ancillary information.

In applying the survey flux cut-off of 3×10^{-14} erg cm^{-2} s^{-1} (0.5–2.0 keV) we assumed a conversion from source counts to flux which was appropriate for a power-law source spectrum with an energy index, α, of -1 (defined here and throughout such that $F_\nu \propto \nu^\alpha$), and corrected for the (usually small) effects of Galactic absorption. Such a conversion factor is appropriate for quasars (Mittaz et al. 1999), but may systematically underestimate or overestimate the flux of other source classes.

Because the flux threshold for RIXOS was set at a value significantly above the sensitivity threshold of the individual fields used, many RIXOS sources have sufficient counts to allow us to measure their X-ray spectral slope individually. This work was done subsequent to the definition of the catalogue and is described by Mittaz et al. (1999). This allowed us to get (in principle) an improved estimate of the source flux based on a power-law spectral fit to the *ROSAT* PSPC data collected in three broad energy channels (the Galactic neutral hydrogen absorption has been taken into account for the fits to the extragalactic sources, but the fluxes given are what they would be before absorption by the Galaxy). In the cases in which more than one observation was used to create the image to be source searched, the longest single exposure time observation was chosen for the spectral analysis.

2.1 X-ray source detection

The RIXOS X-ray images (in PHA channels 52–201) have been analysed using an improved version of the interactive analysis system EXSAS (Zimmermann et al. 1994). The first steps of the detection procedure, i.e., the local detect algorithm LDETECT, the bicubic spline fit to the background map, and the map detection algorithm MDETECT have been described in Hasinger et al. (1993). The detection threshold of these algorithms has been set at a very low likelihood value, so that the resulting list of possible source positions contains several hundred spurious detections. This position list has then been fed into the 'multi-ML' crowded field detection and parameter estimation algorithm first described by Hasinger, Johnston & Verbunt (1994a). This method, which has been implemented in EXSAS, works on binned image data and fits superpositions of several PSF profiles on top of an external background to sections of the data (typically subimages of arcmin size). Best-fitting positions and normalizations are obtained by maximizing the likelihood statistic $\mathcal{L}$ (Cash 1979) or, correspondingly, by minimizing the quantity

$$\mathcal{S} = -2 \ln \mathcal{L} = -2 \sum_{i,j} (Y_{\rm mod}(i,j) - N(i,j) \ln Y_{\rm mod}(i,j).$$

$Y_{\rm mod}(i,j)$ is the sum of all model point source contributions plus the background value in the image pixel $[i,j]$, and N is the measured number of photons in pixel $[i,j]$. For *ROSAT* PSPC data the multi component PSF (Hasinger et al. 1994b; David et al. 1996) is approximated by a single Gaussian function with a width increasing with off-axis angle. The significance $\Delta\mathcal{S}$ of any of the individual point source contributions is then estimated by a likelihood ratio test between the best fit with and without the corresponding component. If $\Delta\mathcal{S}$ falls below a threshold value, the corresponding component is omitted from the next iteration and only significant components are maintained. Since $\Delta\mathcal{S}$ follows a χ^2 distribution, the errors of the best-fitting parameters (68 per cent confidence single parameter of interest) are determined by searching the parameter space for which $\Delta\mathcal{S} = \mathcal{S} - \mathcal{S}_{\rm min} = 1$. Before the next region of interest is fitted, the current PSF contributions are added to the background model.

The complete source detection and parameter estimation procedure is too complicated to validate its results and, e.g., quantify its detection efficiency analytically. We therefore performed extensive simulations of artificial *ROSAT* fields run through the same set of algorithms to study their properties. Based on these simulations we have chosen a likelihood detection threshold of $\Delta\mathcal{S} = 10$, corresponding to a 4σ detection. We emphasize, however, that our survey sensitivity limit of 3×10^{-14} erg cm^{-2} s^{-1} is substantially above the detection threshold in all fields. Observed fluxes in the 0.5–2 keV band are calculated for each source using the detected counts, the corresponding exposure time and vignetting correction, an energy-to-flux conversion factor (ECF) and a PSF-loss correction factor (PCF) determined from simulations. In order to derive the ECF, we assumed a power-law spectrum with energy index -1 and Galactic absorption, folded through the instrument response.

The source detection algorithm is optimized for point sources. Subsequent to running the automatic detection algorithm, all fields were visually inspected for clusters of point sources which could indicate that there is actually an underlying extended source present. In such cases the source flux was aggregated into a single source, whose position was taken to be the centroid of the counts. The corresponding uncertainty in the position was taken to be the radius that would include most of the counts of the merged source.

After the first pass through the detection algorithm, each source was assigned a number which was preserved through the whole of the remaining process, even though many of these sources were dropped in subsequent steps of the procedure. Internally within the RIXOS programme, sources were referred to by this number (Sid) qualified by the field number listed in Table 1 (Fid). Sources believed to be extended as described in the previous paragraph were assigned Sid numbers by adding 500 to the Sid number of the brightest component point source. All sources with Sid > 500 are in this category.

2.2 Previously catalogued sources

The NED and SIMBAD data bases were searched for known objects within 5 arcmin of the position of each RIXOS X-ray source. All the correlations were then checked manually, taking into account the RIXOS and catalogued positional errors, and consulting the relevant references in NED and SIMBAD.

When the identification was uncertain (or irrelevant for our identification programme, e.g., a radio source of unknown ID with no redshift), the RIXOS X-ray source was selected for optical spectroscopy and treated like any other source in the sample.

The X-ray sources in RIXOS with likely catalogued counterparts are flagged in the main RIXOS catalogue, Table 2, and the counterparts are listed in Table 3.

2.3 Optical identification

As a first stage in the optical identification process, the X-ray

Downloaded from https://academic.oup.com/mnras/article-abstract/311/3/456/1016504 by Estación Experimental del Zaidín user on 25 September 2018

Table 3. Catalogue identifications of RIXOS sources.

RIXOS Source	Catalogue identification
RX J001002.5+110837	BD+108B, HD560B, MS0007.4+1051
RX J012433.2+034334	[HB89] 0121+034
RX J012457.3+035347	[HB89] 0122+035
RX J020608.5+151235	IC 1777
RX J020619.1+150341	AG+14 185
RX J032754.0+023344	UGC 02748
RX J040523.4−125936	HD 25853
RX J040534.9−125842	SHK 278:[dM91] 04
RX J041612.1+011432	HD 27007
RX J071858.8+712432	87GB 071317.6+712947 (radio source)
RX J072001.6+711524	AG+71 238
RX J072014.5+713228	Zw0714.8+7140
RX J080309.3+650808	HD 65497
RX J082007.6+372840	IRAS F08168+3738
RX J082733.7+263716	87GB 082432.4+264636 (radio source)
RX J084715.7+373214	[HB89] 0844+377
RX J084907.0+373158	A708
RX J085340.3+134927	MS0850.8+1401
RX J085345.5+134948	HD 75976
RX J090926.5+424228	[HB89] 0906+429
RX J091049.4+430407	B3 0907+432 (radio source)
RX J094614.5+732034	AG+73 264
RX J095253.8+075042	[HB89] 0950+080, MS 0950.2+0804
RX J100110.2+552835	[HB89] 0957+557
RX J100120.3+555349	[HB89] 0957+561A,B
RX J100447.7+050016	HD 87392
RX J100454.8+050418	UGC 05432
RX J100953.8+510049	HD 233710
RX J105813.1+493927	[HB89] 1055+499
RX J110741.4+723235	[HB89] 1104+728
RX J112106.0+133825	[HB89] 1118+139
RX J112337.1+384140	HD 98969
RX J113655.3+295131	[HB89] 1134+301
RX J115951.8+553231	MS 1157.3+5548
RX J120108.9−033423	HD104368
RX J120403.2+280715	MS 1201.5+2824
RX J121832.6+301443	HD107054
RX J122907.4+312329	HD108693
RX J123118.4+201308	HD108984
RX J123154.9+195309	4C +20.30? (see sect. 3.2)
RX J123225.3+202316	1E 1229.9+2039, EXO122956+2039.8
RX J125612.1+472113	AG+47 995
RX J125639.4+471519	B3 1254+475 (radio source)
RX J125645.9+570726	HD238172
RX J125738.4+472759	BD+48 2069A,B
RX J131058.8+323335	87GB 130837.7+324939 (radio source)
RX J131112.2+322907	MS 1308.8+3244
RX J133740.5+480758	GJ520B
RX J133751.1+480815	GJ520A
RX J134334.1+553644	A1783
RX J141231.5+435539	IRAS14105+4409
RX J153350.9+264229	AG+26 1493, AG+26 1494
RX J153441.0+265443	AG+27 1450
RX J163239.0+781152	NGC 6217
RX J180434.6+693742	IPC180506+6937
RX J180530.7+694516	EF Dra, 1E 1806.0+6944
RX J180603.7+694024	MS 1806.5+6939
RX J232509.8+233017	HD220626

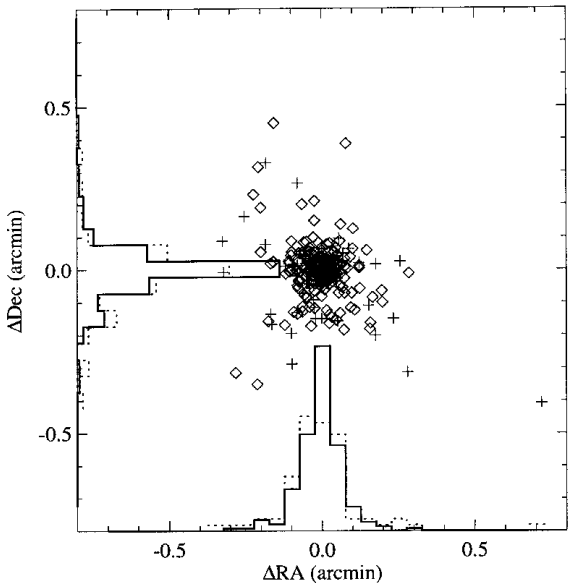

Figure 1. Positional offsets of secure point-like optical counterparts with respect to the X-ray source centroid. Diamonds are AGN, crosses are stars. The distribution of positional offsets projected on to each of the right ascension and declination axes are plotted as histograms, the solid line being AGN and the broken line stars.

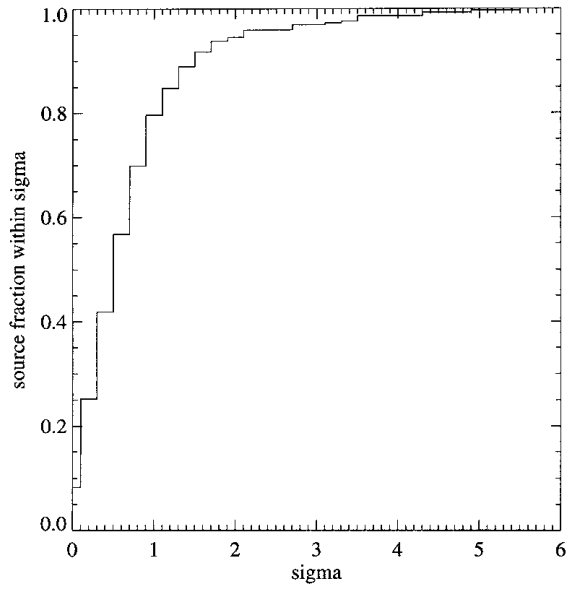

Figure 2. Cumulative distribution of positional offsets for secure point-like RIXOS sources (AGN + stars). The fraction of sources, the separation of which from the X-ray centroid is less than a given value, is plotted against the separation, expressed in units of the 1σ error radius.

source positions were superimposed on Palomar Observatory Sky Survey (POSS) images using parametrized data derived from measurements made with the Automated Plate Measuring (APM) machine at Cambridge (Lewis & Irwin 1996).

The primary means of determining the nature of each X-ray source was through optical spectroscopy. Low-resolution spectra were taken of optical targets close to the X-ray position to search for known classes of X-ray emitter. The search radius was extended until such an optical counterpart was found, or until the separation of the X-ray and optical positions became such that association was unlikely.

For well-defined point-like X-ray sources the limiting separation was generally taken to be about 30–40 arcsec for extragalactic counterparts, a number that was established at the beginning of the programme based on experience with the first identifications. For stars we allowed some extra distance to account for the possibility of proper motion, unless we had a recent image of the field.

Downloaded from https://academic.oup.com/mnras/article-abstract/311/3/456/1016504 by Estación Experimental del Zaidín user on 25 September 2018

We can verify our assumptions *post facto* by examining the distribution of optical counterpart positions from the full catalogue with respect to each X-ray centroid. Fig. 1 shows the two-dimensional distribution of offsets for AGN and stellar counterparts, classes of sources that are expected to be point-like. This diagram illustrates that the large majority of such sources are found within about 6 arcsec of the X-ray position. Fig. 2 shows similar information, but as a cumulative distribution of offsets expressed in units of the 1σ error radius of each source, derived from the X-ray source fitting algorithm.

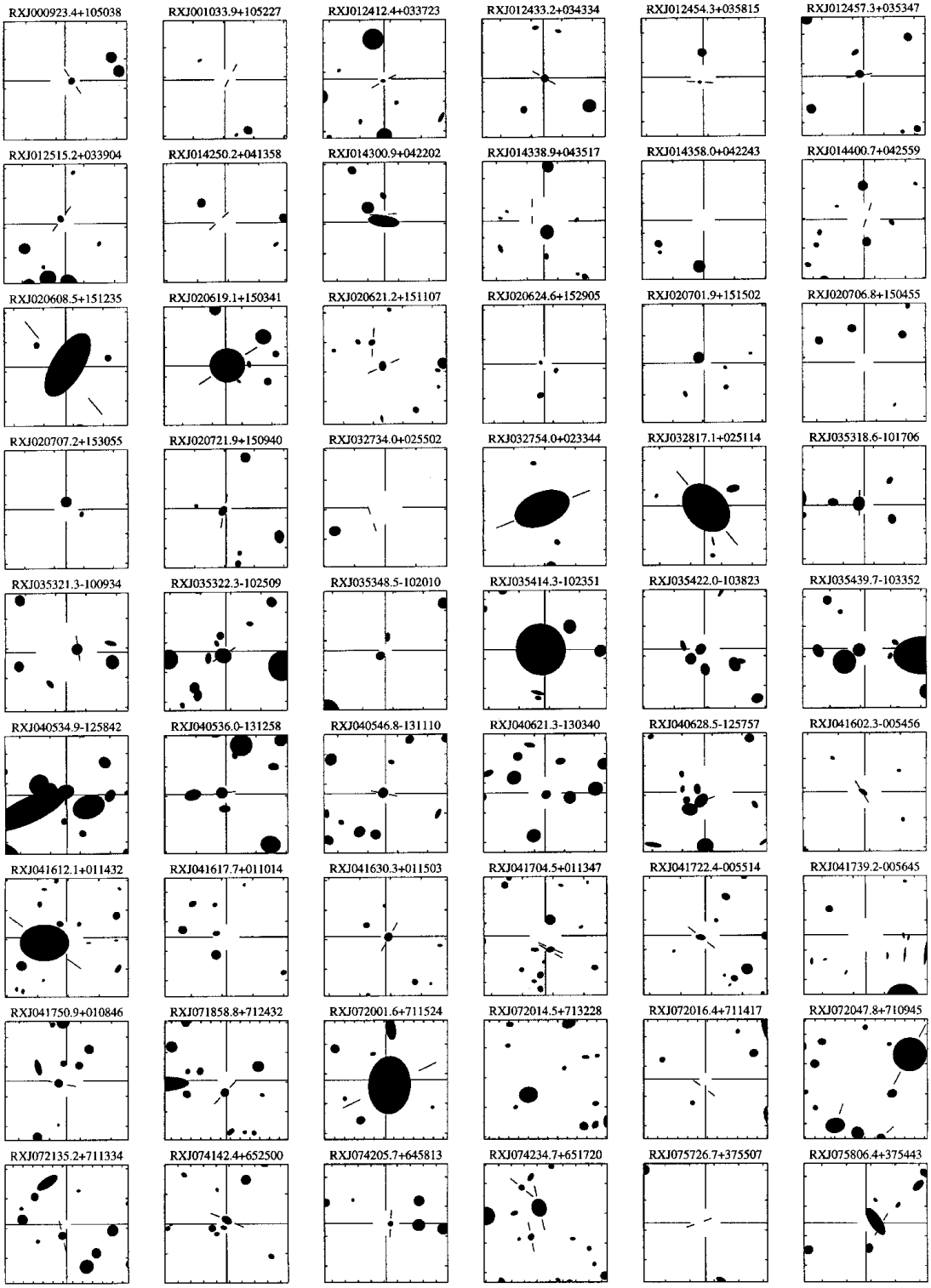

Figure 3. Optical finding charts for each RIXOS source derived from parametrized POSS-E data measured with the APM at Cambridge. Each chart shows a region of sky two arcmin on a side centred on the X-ray position. The 90 per cent confidence error circle is defined by the gaps in the 'cross hairs'. In the case of extended sources where the errors are not statistical, no cross hairs are shown. The position of optical counterparts is indicated by tick marks. For visual simplicity, no distinction is made between stellar and extended objects.

Downloaded from https://academic.oup.com/mnras/article-abstract/311/3/456/1016504 by Estación Experimental del Zaidín user on 25 September 2018

Account was also taken of the morphology of the X-ray source in setting the radius within which optical counterparts were sought, specifically whether the X-ray source was extended and whether it may be affected by source confusion. For instance, in some cases sources which are formally classified by the X-ray detection algorithm as single objects are clearly elongated in shape. This suggests that they may in fact be two sources closely separated on the sky. In these cases the area searched for optical counterparts was modified to allow for this possibility. This is important in reducing the number of potentially spurious 'blank fields' which could otherwise occur if the counterpart search was confined to the X-ray centroid of closely coincident sources.

In cases where there is more than one potential counterpart within the X-ray search radius, we endeavoured to take optical spectra of them all, irrespective of whether a plausible counterpart had already been found. In this way we were sensitive to possible

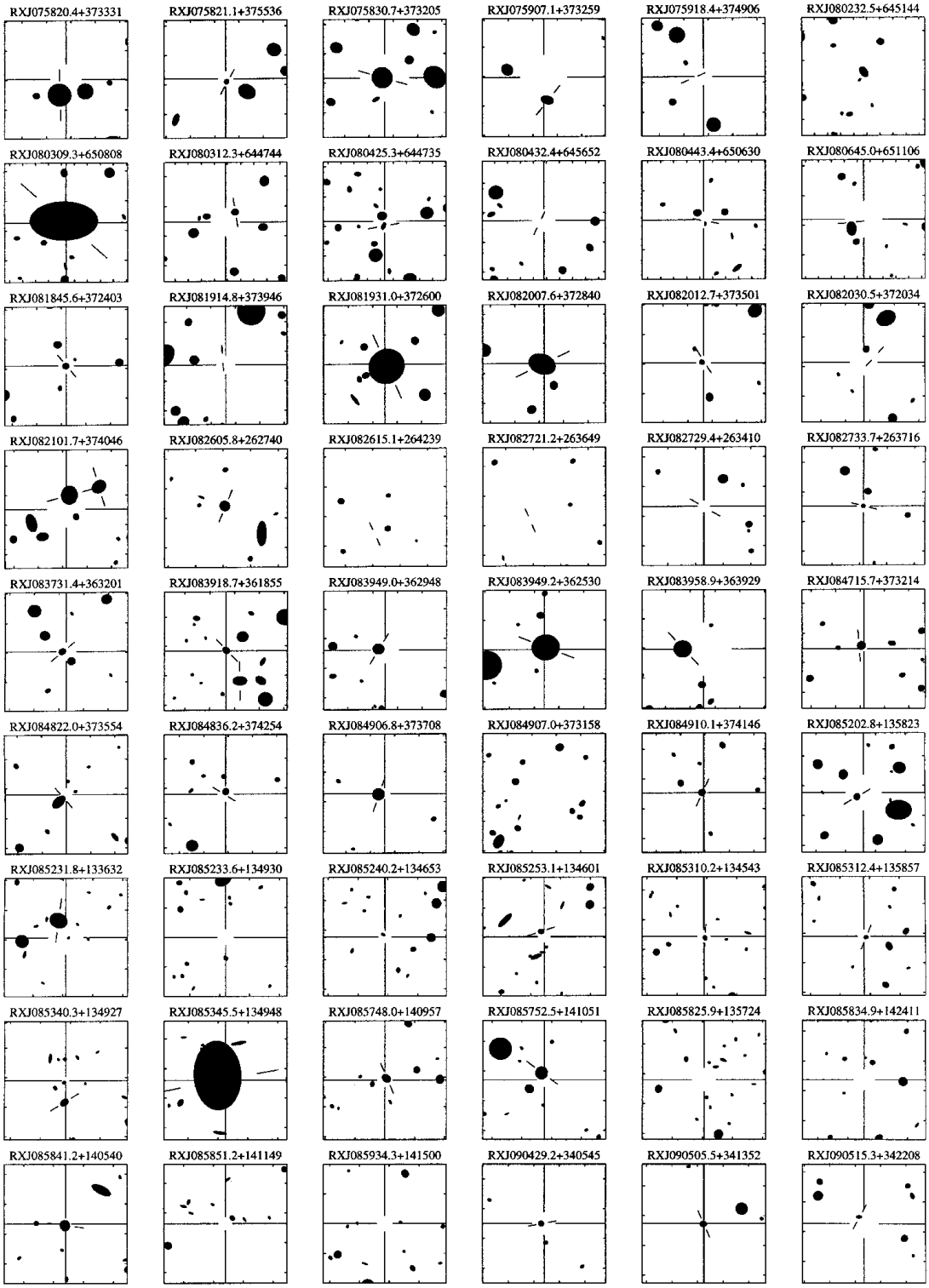

Figure 3 – *continued*

Downloaded from https://academic.oup.com/mnras/article-abstract/311/3/456/1016504 by Estación Experimental del Zaidín user on 25 September 2018

multiple counterparts such as dMe star pairs, gravitationally lensed quasars and galaxy clusters.

The low-resolution spectroscopy was supplemented by higher resolution work aimed at confirming chromospheric activity in bright stellar counterparts.

A parallel programme of optical CCD imaging was undertaken to complement the optical spectroscopy. The primary goal of this programme was to reveal optical counterparts that were below the sky survey plate limit. X-ray sources were scheduled for imaging studies such that those without obvious optical counterparts on the sky survey were given highest priority. The optical imaging programme also proved valuable in identifying or confirming the presence of faint galaxy clusters. The overall RIXOS identification work evolved responsively, such that information from the imaging

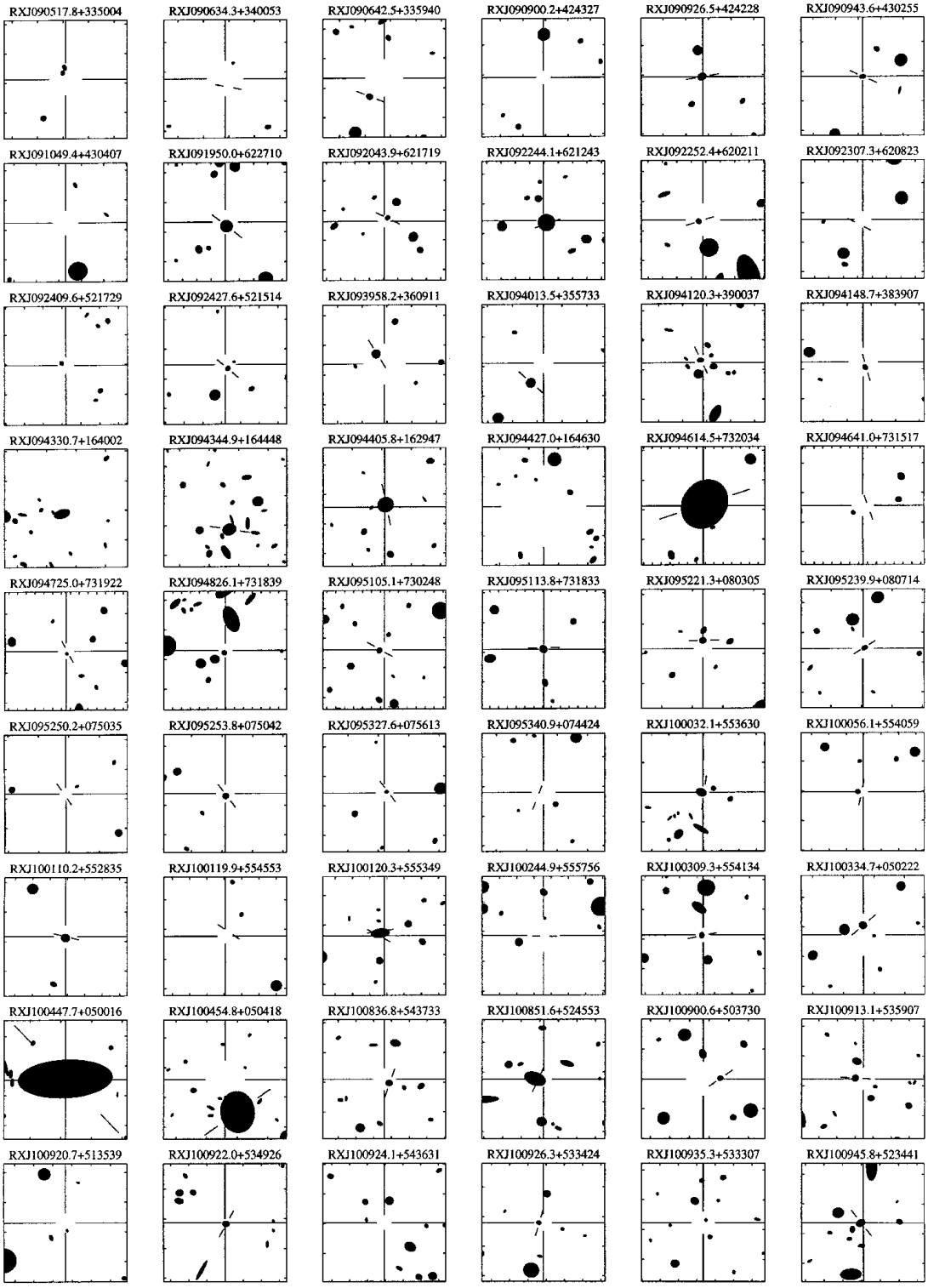

Figure 3 – *continued*

Downloaded from https://academic.oup.com/mnras/article-abstract/311/3/456/1016504 by Estación Experimental del Zaidín user on 25 September 2018

programme was fed back rapidly to the spectroscopy programme and *vice versa*. This was facilitated by a near real-time first-cut reduction of the data, the products of which were held in a data base that was available to each observer at the telescope and to personnel at their home institute who planned each observing run.

The default passband for the RIXOS imaging was the Johnson *R* filter. Additional passbands (*U*, *B*, *V* and *I*) were also used as necessary.

2.4 Instrumentation

The RIXOS optical identification work was facilitated by an award of 'International Time' on the La Palma telescopes by the Comite Científico International, the body that oversees use of Canarian astronomical telescopes. In this scheme up to 5 per cent of the total schedulable observing time is given over annually to a programme that involves collaboration between countries with

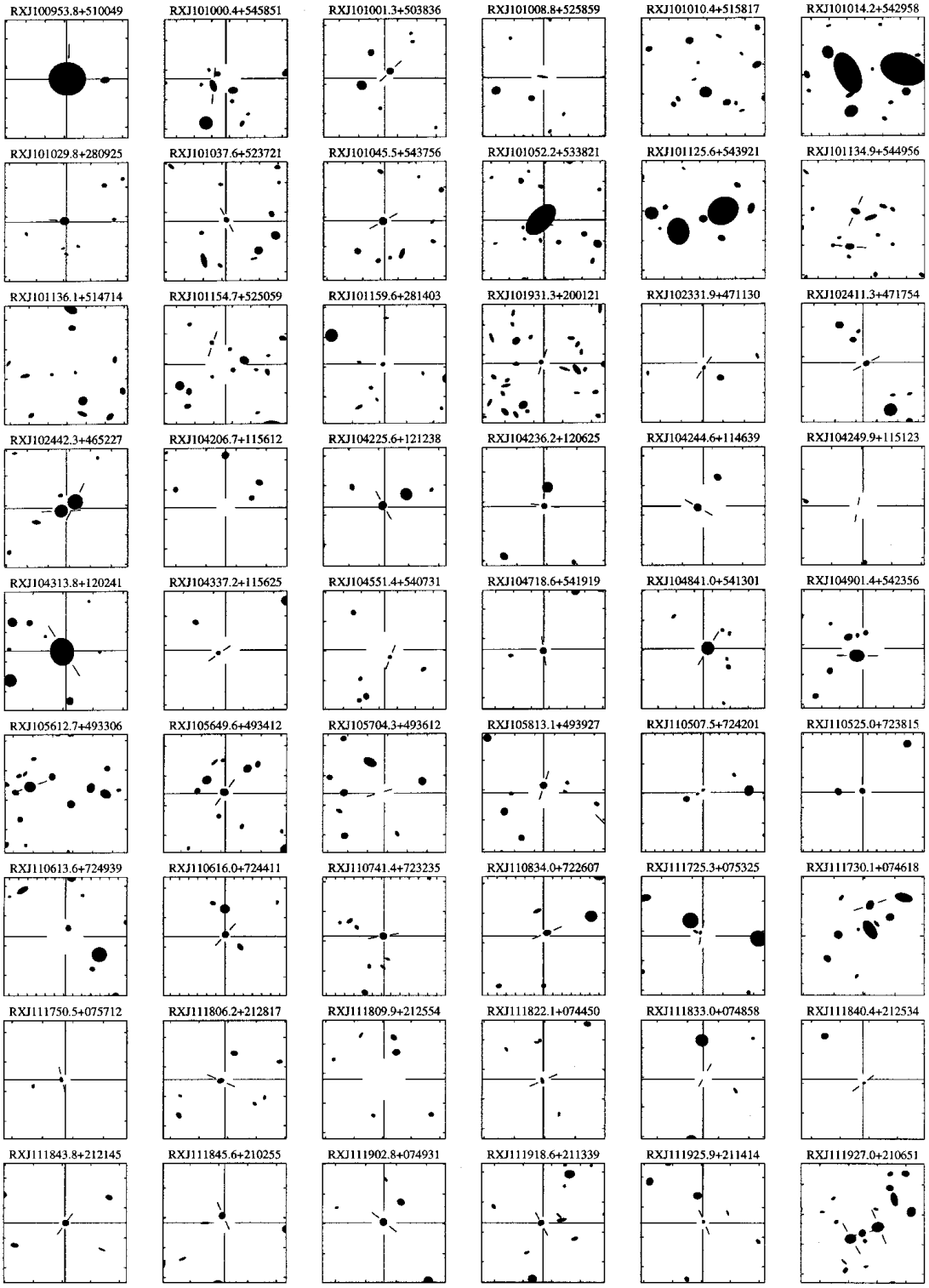

Figure 3 – *continued*

Downloaded from https://academic.oup.com/mnras/article-abstract/311/3/456/1016504 by Estación Experimental del Zaidín user on 25 September 2018

interests in the Canarian observatories. The telescopes used for RIXOS were the three that comprise the Isaac Newton Group, namely the 4.2-m William Herschel Telescope (WHT), the 2.5-m Isaac Newton Telescope (INT) and the 1.0-m Jacobus Kapteyn Telescope (JKT), as well as the 2.5-m Nordic Optical Telescope (NOT). The observational programme was carried out in several observing runs in three observing semesters in the interval 1993 February to 1995 March.

All the spectroscopy was done on either the WHT or INT, while the primary telescopes used for the imaging programme were the NOT, INT and JKT, with limited deep imaging also being conducted on the WHT.

2.4.1 *Spectroscopy*

The WHT spectroscopy utilized the twin-armed ISIS spectrograph.

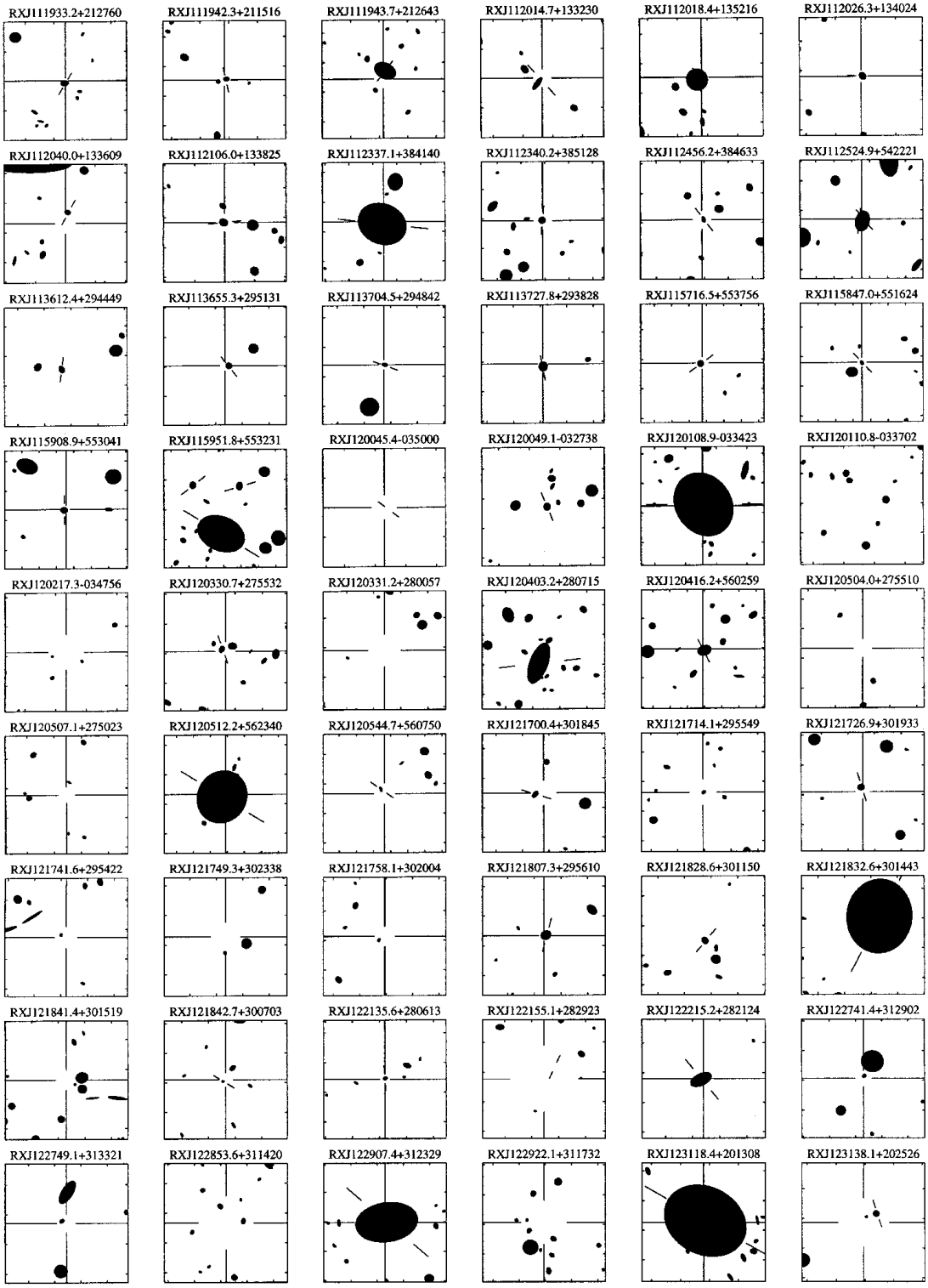

Figure 3 – *continued*

Downloaded from https://academic.oup.com/mnras/article-abstract/311/3/456/1016504 by Estación Experimental del Zaidín user on 25 September 2018

The input starlight is separated into blue and red beams by a dichroic filter, which for the RIXOS programme had a crossover wavelength of 5400 Å. Each of the two spectrograph arms was equipped with a TEK 1124 × 1124 CCD chip. In the standard configuration used in the low-resolution RIXOS work, the blue spectrograph arm was equipped with the R300B grating, which yielded spectra with a dispersion of approximately 1.5 Å pixel^{-1}. The R158R grating was used in the red arm yielding approximately 2.5 Å pixel^{-1}. The lower threshold of the blue grating was set at 3700 Å, while the upper threshold of the red grating was set at 8400 Å. This configuration provided some overlap to aid cross-calibration of the two arms.

Much of the INT spectroscopy utilized the Faint Object Spectrograph (FOS), a crossed dispersed fixed format spectrograph that

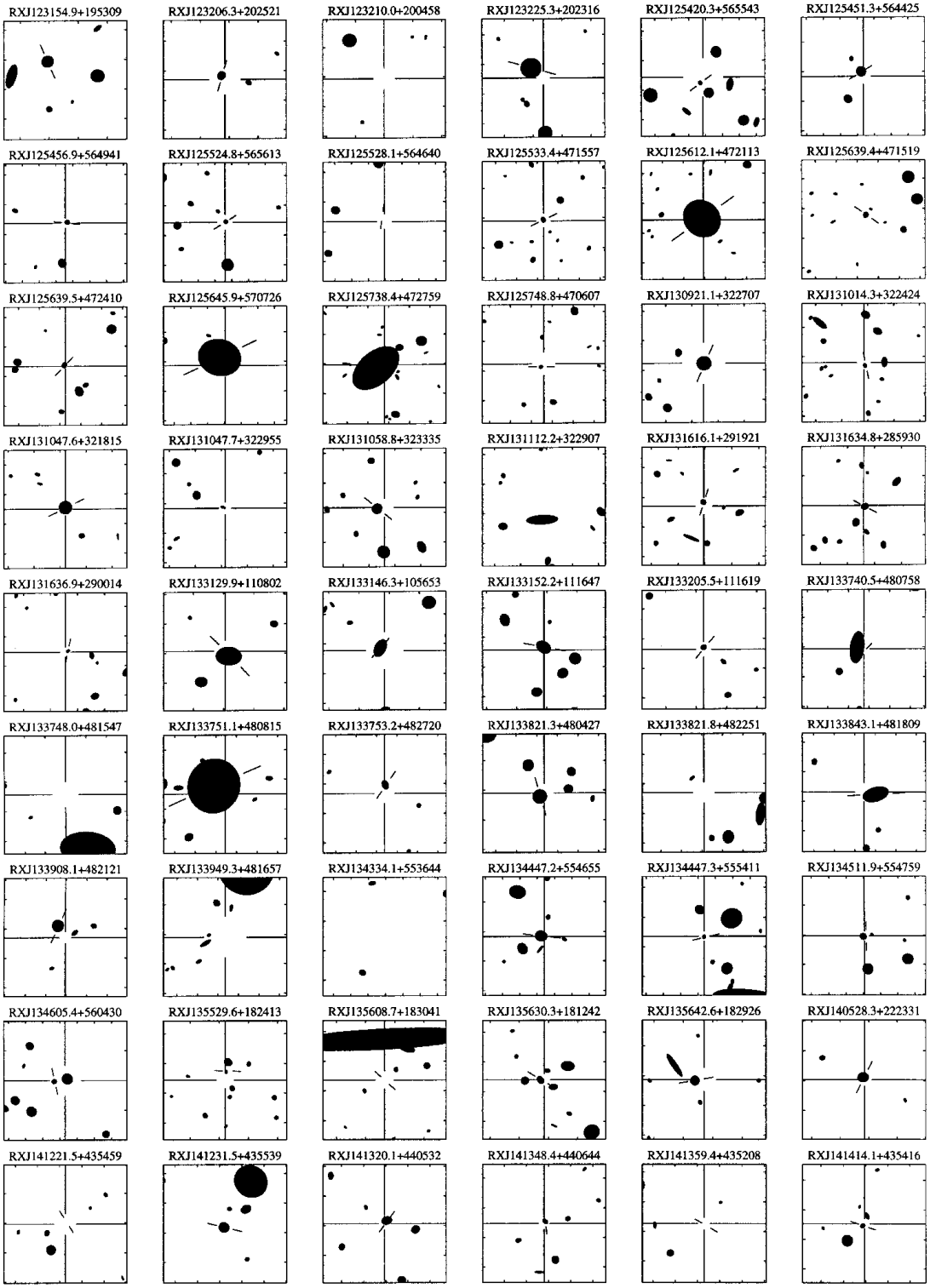

Figure 3 – *continued*

Downloaded from https://academic.oup.com/mnras/article-abstract/311/3/456/1016504 by Estación Experimental del Zaidín user on 25 September 2018

yields spectral coverage between the atmospheric cut-off and ~1 μm in two orders. Spectral resolution is 16 Å in the red (first order), and 8 Å in the blue. FOS was not available for the final RIXOS runs. Instead, we used the Intermediate Dispersion Spectrograph (IDS) with the R150V grating and a TEK 1124 × 1124 CCD chip. This gave coverage between 3600 Å and ~1 μm, but with some contamination longward of 8000 Å due to second-order light.

Some RIXOS sources have bright stars in or near their X-ray error circles, many of which have not previously been recorded as 'active'. In order to search for line emission indicative of chromospheric activity, and confirm that the star was the source of the X-ray emission, we recorded some higher resolution spectra of such stars using the IDS. These covered the Ca II H and K lines (3934 and 3963 Å) and the Hα line in separate exposures.

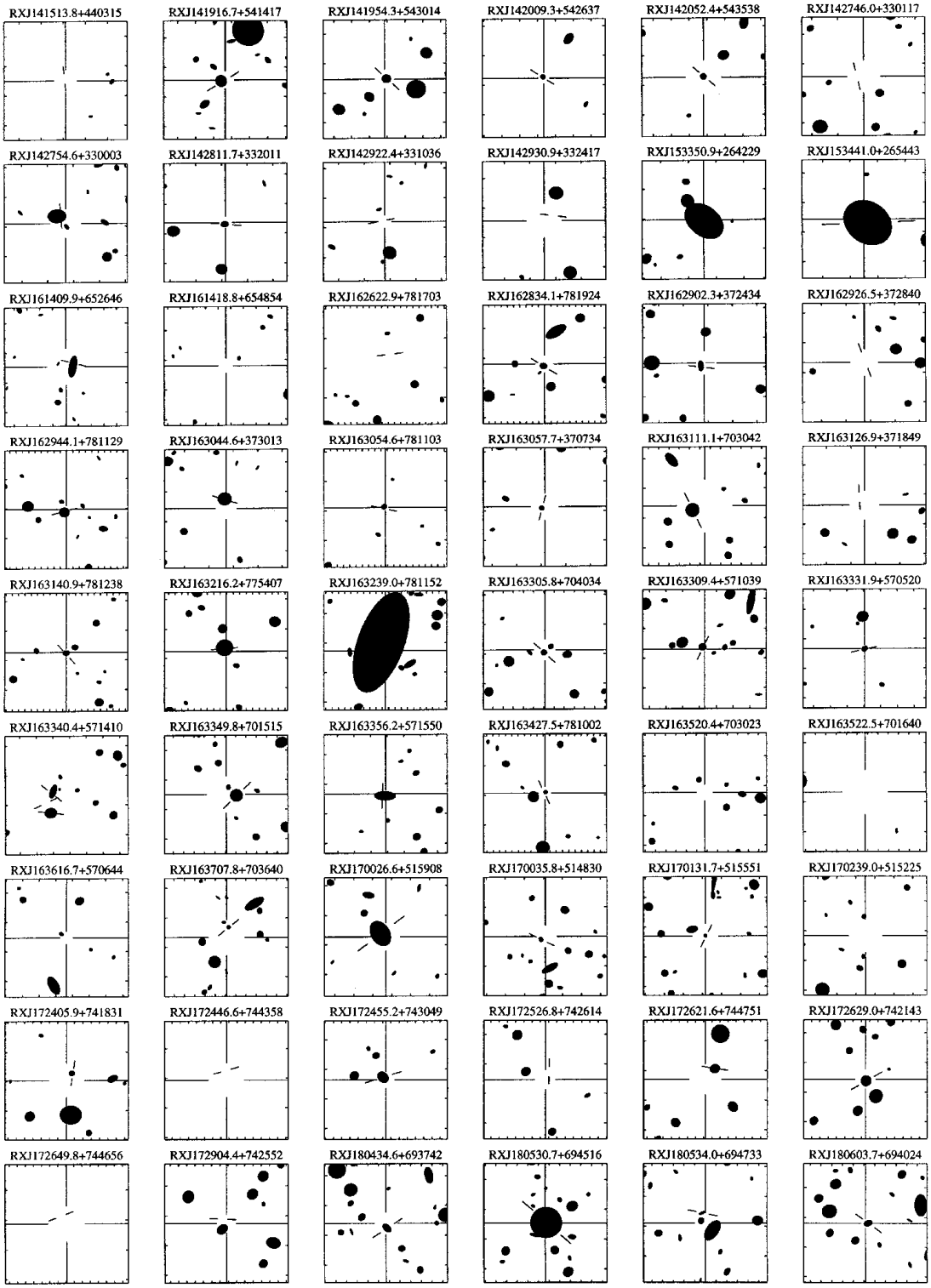

Figure 3 – *continued*

Downloaded from https://academic.oup.com/mnras/article-abstract/311/3/456/1016504 by Estación Experimental del Zaidín user on 25 September 2018

All spectroscopy of single objects was done where possible with the slit at or close to the parallactic angle to avoid colour-dependent light loss. Occasionally, to maximize observing efficiency, the spectrograph slit was orientated so as to place two (or more) nearby objects on the slit together. In such cases, however, we tried to ensure that the observations were made at low zenith distance, to minimize differential refraction effects.

2.4.2 Imaging

Several RIXOS fields were imaged in the *R* band at the beginning of the programme with the FORD CCD camera on the INT. This 2048×2048 device covers a large field of view (11 arcmin) so that the whole of the central region of the PSPC field, used for RIXOS, could be imaged in four exposures. Additionally, short exposures of the central region of each PSPC field were made under photometric conditions, overlapping the corners of each of the four main images. This allowed us to derive accurate *R* magnitudes for candidates in all the fields.

The CCD imaging instrumentation available on the NOT was evolving rapidly during the RIXOS programme. Consequently, a variety of cameras and formats were used, covering a region of sky between 1.5 and 3 arcmin^2 with a pixel size of about 0.2 arcsec. The JKT CCD camera covered a field of view of about 6 arcmin^2, with a pixel size of approximately 0.3 arcsec.

A limited number of deep exposures were obtained using a CCD camera mounted at the auxiliary focus of the WHT. This provided images of a 1-arcmin diameter region of sky which was recorded on a TEK 1024×1024 CCD chip at a spatial scale of 0.11 arcsec per pixel. Such exposures were interleaved with ISIS spectroscopy (which can be done with minimal overhead) to make deep images of selected fields during intervals of very good seeing.

3 CATALOGUE DESCRIPTION

The main RIXOS source catalogue is presented in Table 2. Column 1 contains the source name, formed from the position of the X-ray centroid. Column 2 provides the 90 per cent error in the X-ray position in arcseconds.

Columns 3 and 4 of Table 2 contain the position of the optical counterpart, except for clusters of galaxies and sources with no optical identification where the X-ray position is repeated. For point-like optical objects the positional accuracy is better than 1 arcsec. The positions are derived from astrometry of the relevant POSS plate when the object is visible on it, or otherwise from a CCD image, using stars that are recorded on both the CCD image and the POSS to define a common frame. A plate solution of six parameters was adopted for small-format CCD frames, and 12 parameters for the large format FORD CCD frames.

Columns 5 to 8 give the X-ray flux, the count rate, the total number of counts used to detect the X-ray source, and the X-ray spectral slope of the source respectively. The first number in column 5 is the X-ray flux that was used to define the catalogue (from the counts given in column 7), based on a uniform spectral energy slope of -1 and with a (small) correction for Galactic absorption (see Table 1 for the Galactic absorbing column in the line of sight to each field centre). The second number in column 5 is the flux from our fit to the X-ray spectra of the sources (see Section 2 and Mittaz et al. 1999). For those sources with the lowest number of counts the best-fitting slope and flux have very large associated errors, but the corresponding values are also given for completeness. In a few cases (e.g., P700223−126, P700208−219 and P700216−265) the *ROSAT* observation was performed with spacecraft wobble switched off. This could lead in principle to incorrect estimates of the source fluxes if an average conversion factor between counts and flux is assumed. This is due to potential obscuration of the sources by the supporting wire grid, that would be different for each position in the detector. The fitted flux given in column 4 is obtained using the exposure map of each observation, which includes the effect of the supporting wire grid, so it is possible to estimate this effect by comparing both fluxes in column 4 for the point sources. The fluxes are very similar in most of the sources in these three fields with point-like counterparts, so this effect is probably not very important.

Column 6 contains the count rate (PHA channels 52–201) of the sources, estimated from 'cleaned' data from which observing segments with high background count rate and other bad data have been removed. These count rates are also corrected for vignetting (using the exposure maps).

The best-fitting power-law slope, along with the marginalized 1 sigma error, is given in column 8. It should be noted that the appropriateness of a power-law spectral approximation is a function of source type, and this is discussed more extensively in Mittaz et al. (1999).

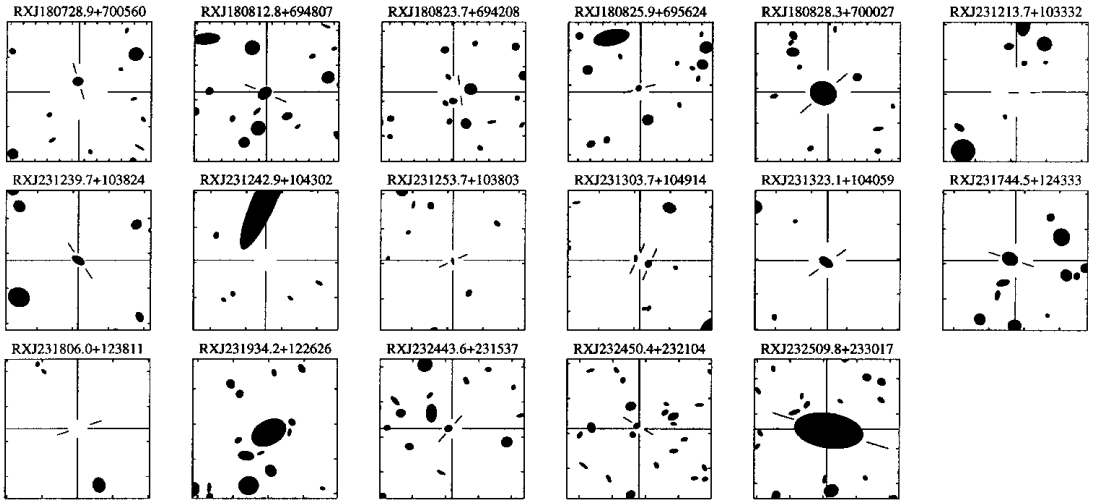

Figure 3 – *continued*

Downloaded from https://academic.oup.com/mnras/article-abstract/311/3/456/1016504 by Estación Experimental del Zaidín user on 25 September 2018

A feature of the X-ray spectral fitting algorithm is that it assumes that the X-ray source is point-like, and it applies corrections for the energy-dependent PSF of the *ROSAT* telescope accordingly. In contrast, the catalogue was defined on the basis of the integrated flux of extended sources. Thus for such sources, the spectral fit, count rate and flux estimate refer to the centroid of the source only. This means that for extended sources (which by convention have a RIXOS source number, Sid, greater than 500) there is generally a significant discrepancy between the first and second numbers in the flux column (with the first column giving a more accurate estimate of the integrated source flux).

Column 9 gives the magnitude of the optical counterpart if there is one (or the integrated magnitude of the brightest cluster galaxy for cluster candidates). These are derived from a variety of sources depending on availability, and indicated by the symbol that precedes the magnitude. We have, however, attempted to maximize uniformity by quoting a number which refers to the *R* band or the closest approximation to it. Where we have calibrated *R*-band CCD images of the source we use those. Otherwise we use values derived from the POSS E plates, or (for sources not registered on the POSS E plates) a value estimated from our slit spectroscopy folded through the standard *R*-filter response. The accuracy of these 'slit magnitudes' is discussed by Puchnarewicz et al. (1996a) and is found empirically to be within 30 per cent. For bright stars (where the parametrized POSS data are inaccurate) or previously catalogued sources which were not re-observed by us, we quote catalogued magnitudes.

In column 10 we give, for AGN counterparts, the power-law

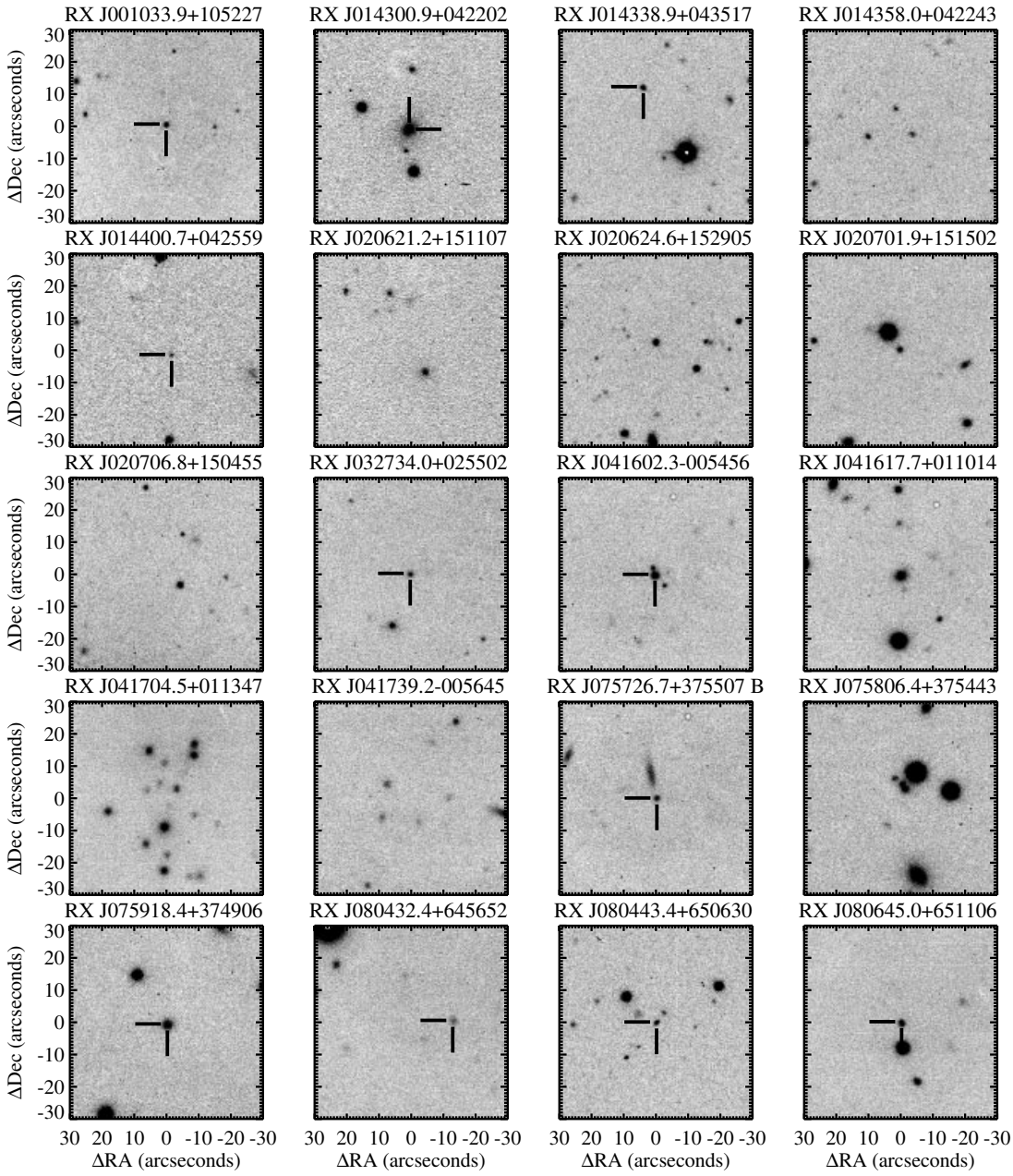

Figure 4. CCD images of selected RIXOS sources (see Table 2). A region of sky 1 arcmin on a side is shown in each image. This is generally centred close to the X-ray centroid, but in some cases the region shown is offset significantly from the centre in order to show specific features, or to establish the location of the CCD image with respect to the POSS chart by including objects in common. Optical counterparts are indicated by tick marks.

Downloaded from https://academic.oup.com/mnras/article-abstract/311/3/456/1016504 by Estación Experimental del Zaidín user on 25 September 2018

slope that best represents the optical continuum spectrum (after removing lines and other features). The fitting procedure is discussed in more detail by Puchnarewicz et al. (1996a), and its accuracy is generally limited by systematic effects to a value of about 50 per cent in the slope. No attempt was made to fit a power law to AGN whose optical spectrum exhibits a contaminating component due to the host galaxy.

Column 11 classifies the optical counterpart into one of five categories, Star, AGN, ELG, Clus or Gal (or blank for unidentified sources), while column 12 gives additional classification information where relevant. The classification 'ELG', for emission-line galaxy, is used for any individual counterpart which has unresolved emission lines at redshift greater than zero, particularly if the lines are superimposed on a galaxy-like continuum. Broad-line objects

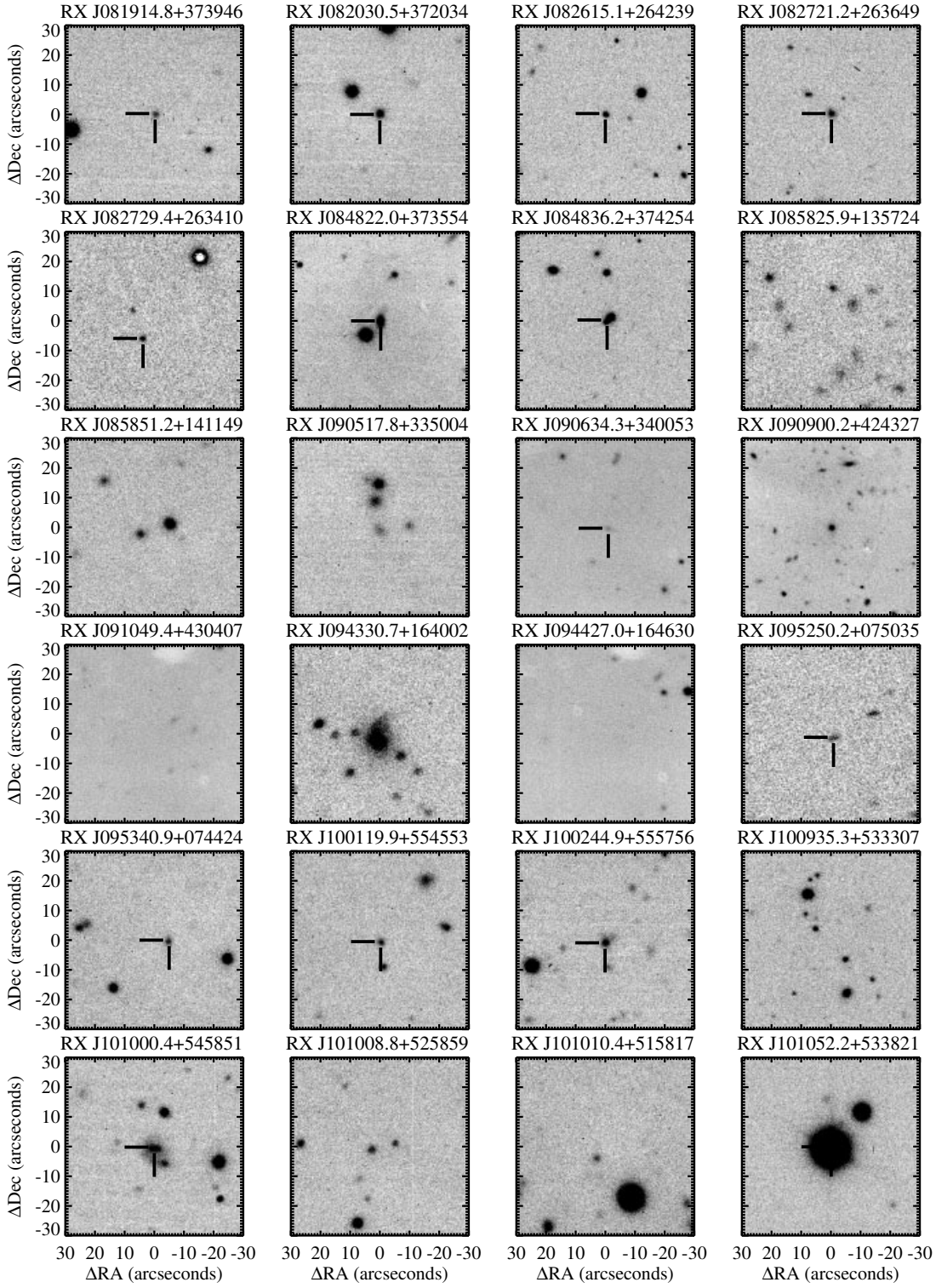

Figure 4 – *continued*

Downloaded from https://academic.oup.com/mnras/article-abstract/311/3/456/1016504 by Estación Experimental del Zaidín user on 25 September 2018

are classified as 'AGN'. Isolated galaxies without emission lines are classified as 'Gal'. The number in parentheses following the cluster classification, 'Clus', is the number of galaxies measured at the cluster redshift. A colon indicates that the identification is uncertain. In the case of the 'Star' category all objects which have not been demonstrated to have chromospheric activity (based on the detection of Ca II or Balmer emission lines in their spectrum) are formally marked as uncertain, although for bright stars the probability of chance association is very low, and the failure to detect chromospheric emission is probably due to its low equivalent width.

The redshift of extragalactic counterparts is listed in column 13. The emission lines upon which this is based are listed in column 14 for AGN and ELG counterparts. As an indicator of the spectral appearance, column 15 gives the FWHM of one of the lines,

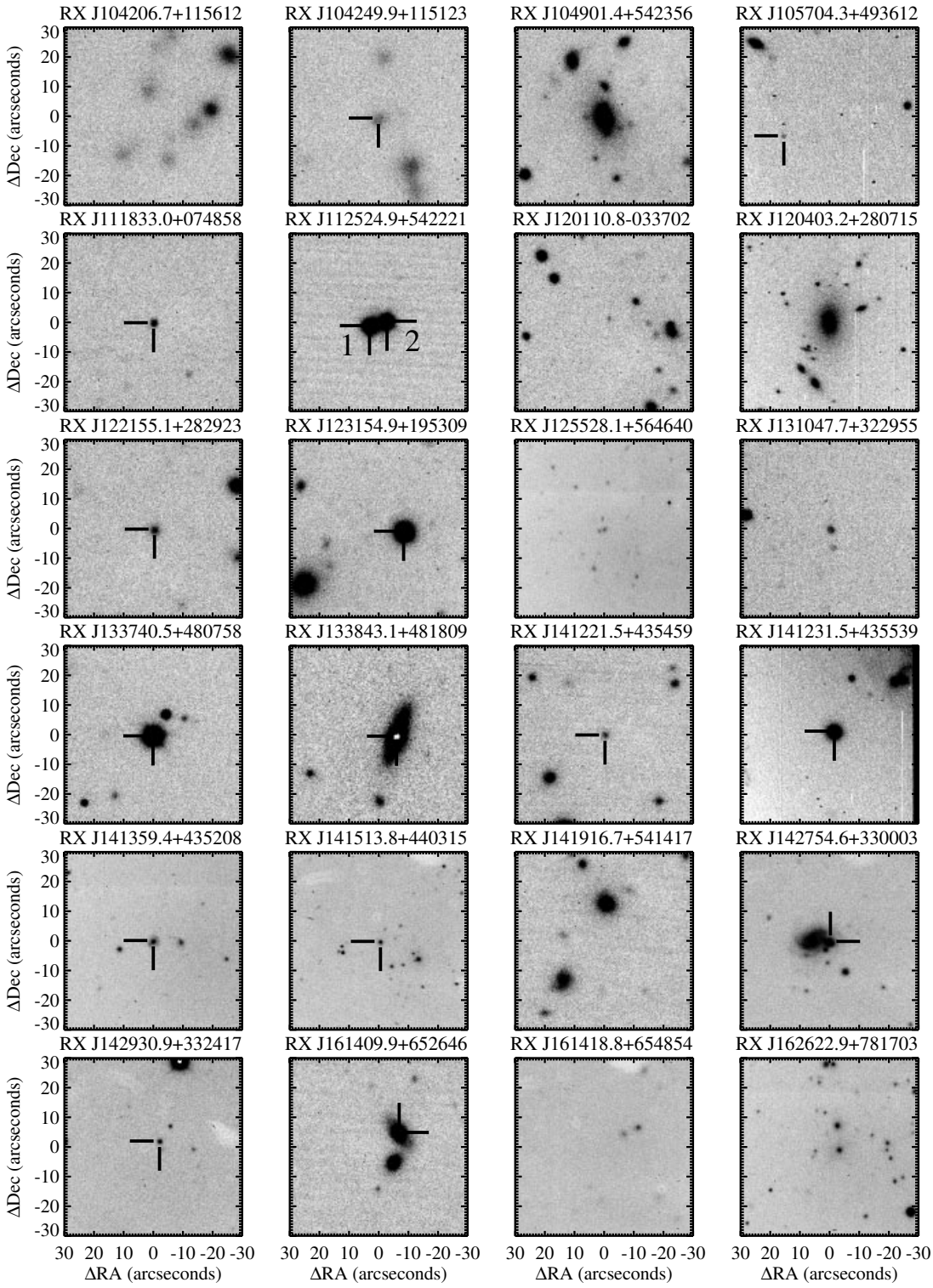

Figure 4 – *continued*

Downloaded from https://academic.oup.com/mnras/article-abstract/311/3/456/1016504 by Estación Experimental del Zaidín user on 25 September 2018

underlined in column 14, in units of 1000 km s^{-1} and rounded down to the nearest 1000 km s^{-1}. For maximum uniformity, preference is given to Hβ or Mg II when these are available and well defined.

Column 16 indicates whether ancillary information is available on the source. An 'N' indicates that there is a note on the source in Section 3.2. A 'C' marks sources which have catalogue cross-references in Table 3, whereas an 'I' means that there is a CCD image of the field (see Section 3.1).

The final column of the Table 3 (number 17) contains a cross-reference to the field number and source number as defined internally within the RIXOS programme and used in other publications to refer to RIXOS sources (Puchnarewicz et al. 1996a, 1997; Mittaz et al. 1999). The field number (Fid) is the same as that in column 1 of Table 1.

The contents of Table 3 are available on http://www.mssl.ucl.ac.uk/www_astro/rixos.html. Data on the RIXOS AGN are available in the NASA Extragalactic Data base (NED).

3.1 Images and finding charts

An optical 'finding chart' for each RIXOS source is contained in Fig. 3, based on the parametrized POSS-E data. Each chart shows a region of sky 2 arcmin square that is centred on the X-ray centroid. The 90 per cent confidence error circle is defined by the gap in the 'crosshairs', and the position of any optical counterpart or counterparts is indicated by tick marks. In the case of extended sources where the errors are not statistical, no crosshairs are shown.

Fig. 4 shows selected CCD images of RIXOS sources, specifically those where the CCD image adds to the information available from the POSS charts alone (the most obvious example being cases where the optical counterpart is not visible on the POSS). The region of sky depicted is 1 arcmin square in the case of the CCD images. This is generally centred close to the X-ray centroid, but in some cases the region shown is offset significantly from the centre in order to show specific features, or to establish the location of the CCD image with respect to the POSS chart by including objects in common.

3.2 Notes on individual sources

RX J001002.5+110837: This catalogued bright star produces a blank finding chart, so we have chosen not to plot it.
RX J014250.2+041358: A single, very broad feature at 6220 Å is identified as Mg II. There is possible C III] emission at 4200 Å, but the spectrum is noisy at this wavelength.
RX J014300.9+042202: Point-like X-ray source. The tentative ID is a $z = 0.135$ galaxy which lies about 7 arcsec north of the X-ray position (Fig. 4). The point-like optical object which is a similar

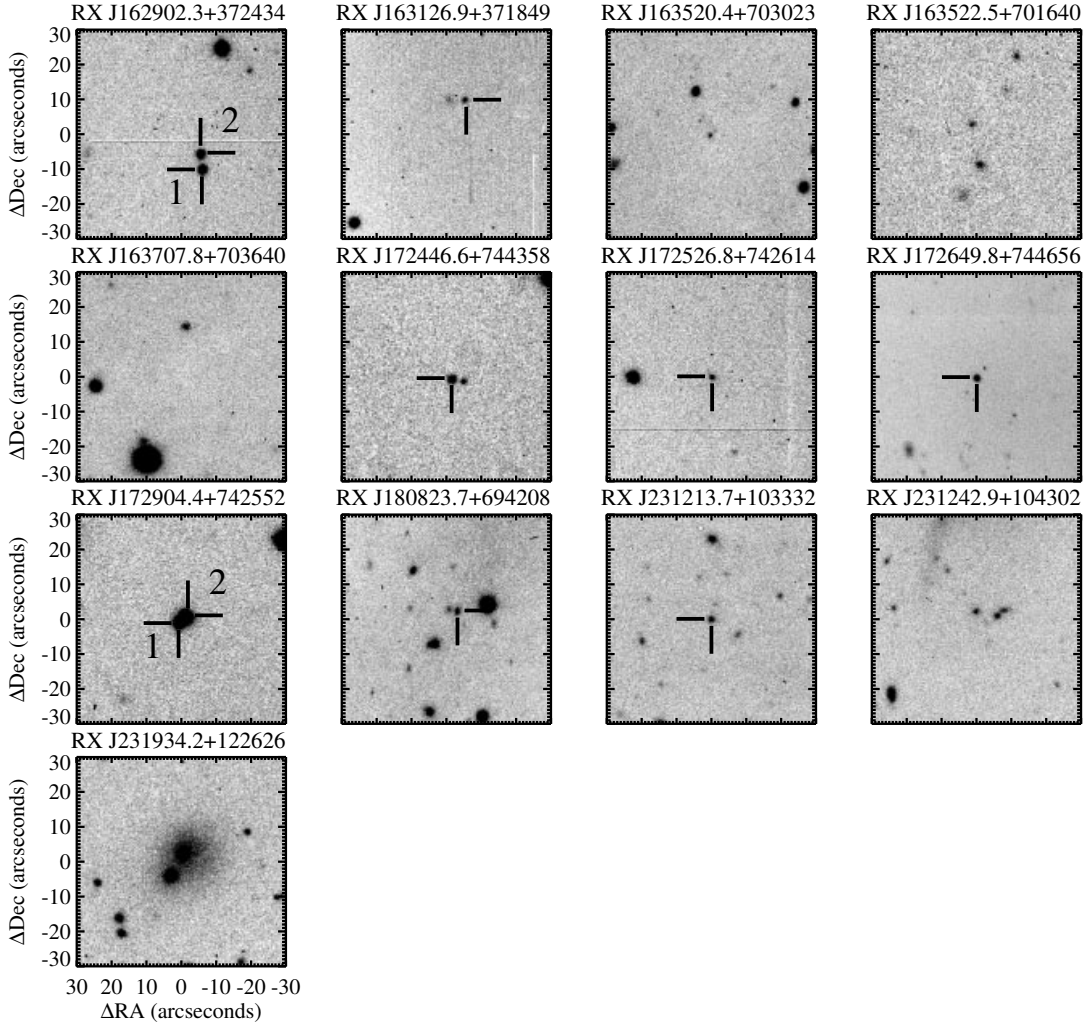

Figure 4 – *continued*

Downloaded from https://academic.oup.com/mnras/article-abstract/311/3/456/1016504 by Estación Experimental del Zaidín user on 25 September 2018

distance to the south of the X-ray position is a late-type star, as is the object of similar brightness which lies to the north-east. There is a faint optical object very close to the X-ray position, but its colours appear unremarkable on *U*, *B* and *R* CCD images.

RX J020701.9+151502: The object close to the X-ray position (Fig. 4) which lies to the south-east of the relatively bright star seen on the POSS (which is of late type) is UV bright on CCD images relative to other objects in the field and is a likely ID.

RX J020706.8+150455: A UV-bright object close to the X-ray position, the brightest object visible in the image of the field contained in Fig. 4, is the probable ID, but no spectrum is available.

RX J040546.8−131110: A point-like X-ray source. The single optical spectrum of the object centred in the error circle shows a blue continuum, with a possible emission line at 5400 Å which coincides with the join between the blue- and red-arm ISIS spectra. Classified as a possible AGN at unknown redshift.

RX J040621.3−130340: The object closest to the X-ray position appears slightly extended on an *R*-band CCD image.

RX J041612.1+011432: The tentative stellar ID is about 20 arcsec from the X-ray position.

RX J072047.8+710945: Initially considered a single extended X-ray source, this is actually two. There is a star with a flux of 4.7×10^{-14} erg cm^{-2} s^{-1} to the north-west of the X-ray position, and a $z = 0.23$ cluster of galaxies with a flux of 2.1×10^{-13} erg cm^{-2} s^{-1} (0.5–2.0 keV) which is centred to the south-east of the catalogued X-ray source. This cluster is in turn about one Abell radius north of the cluster A 574.

RX J085340.3+134927: A likely ID is the Seyfert 2 galaxy which lies towards the edge of a relatively large X-ray error circle. However, there is also an Hα emission-line galaxy at the same redshift in the error circle [RA(2000) $08^{h}\ 53^{m}\ 41\overset{s}{.}02$, Dec.(2000) $+13°\ 49'\ 19\overset{''}{.}2$], together with several other fainter objects which have not been observed spectroscopically. It is thus also possible that we are seeing compact cluster emission, although there is no evidence that the X-ray emission is extended. This is also an EMSS source, where the ID is listed as the Sy 2.

RX J085345.5+134948: The bright A-type star is itself an unlikely ID. The correct ID is probably a faint companion, or an unrelated line-of-sight object.

RX J085825.9+135724: An overdensity of galaxies on the CCD image in the vicinity of the X-ray source (Fig. 4) suggests probable cluster emission, but no spectroscopy is available.

RX J090517.8+335004: Complex X-ray source, with the two main components separated by ∼40 arcsec and aligned approximately north–south. There are four (or five?) counterparts within the X-ray error circle. The northernmost is a star, while the nature of the others is unknown. This is a potential compact galaxy group.

RX J091049.4+430407: There is a radio source less than an arcmin from the X-ray position. However, the X-ray image is complex and is probably of two X-ray sources separated by ∼30 arcsec, aligned with a position angle of approximately 140°. A deep WHT *R*-band image of the X-ray position is blank.

RX J094427.0+164630: Extended diffuse X-ray source, possible cluster candidate, but no spectroscopy done.

RX J100120.3+555349: Gravitationally lensed quasar [HB89] 0957+561 (Hewitt & Burbidge 1989). Considered as a single X-ray source.

RX J100454.8+050418: Diffuse X-ray emission, probably associated with the galaxy that is listed as the optical counterpart.

RX J100851.6+524553: Suggested ID is the brighter (more westerly) of a close stellar pair.

RX J101010.4+515817: Apparently diffuse X-ray source which is either a collection of faint point sources (all individually below our survey limit) or a low surface brightness extended object. There is no obvious optical counterpart.

RX J101052.2+533821: This is a K4 star. It has a fainter M companion 11 arcsec to the north and 11 arcsec to the west.

RX J101125.6+543921: This is a complex X-ray source with at least two components. There are a number of possible optical counterparts, these being a pair of stars approximately 40 arcsec to the north-west of the X-ray centroid (not resolved on the parametrized POSS chart), a galaxy at $z = 0.044$ approximately 1 arcmin to the south-east of the X-ray centroid, and a fainter Hα emission-line galaxy which is close to the centre of the X-ray error circle. All may contribute flux, although the centroid of the X-ray emission favours the two galaxies.

RX J101136.1+514714: Diffuse X-ray source.

RX J102442.3+465227: Close stellar pair. The shape of the X-ray contours suggests that this is actually two X-ray sources, one corresponding to each star.

RX J111730.1+074618: The most probable ID is a cluster of galaxies at redshift 0.16; however, there is also a 17th magnitude $z = 0.136$ H II region galaxy about 30 arcsec north of the X-ray centre (PA ∼ 350°).

RX J111809.9+212554: Probably at least two X-ray sources with a separation of approximately 1 arcmin at a PA of 135°. The catalogued X-ray position is the centroid of the emission. The object to the north-west of the X-ray centroid is an M star.

RX J112018.4+135216: Close pair of stars.

RX J112524.9+542221: This is a pair of optically active M stars; thus we have considered this to be two X-ray sources.

RX J120049.1−032738: We believe this to be a cluster based on the X-ray image, which is very diffuse. The estimated diameter is 2 arcmin. We have probable redshifts for three galaxies, two at $z = 0.39$ and the other at $z = 0.28$. Thus, if this is a cluster, the redshift is ambiguous.

RX J120110.8−033702: The X-ray source is extended with a flattened morphology. The pair of objects about 30 arcsec to the north-east of the X-ray centroid are both stars. The object to the west is double, one component of which is a galaxy at redshift 0.211. There are other plausible galaxies in the optical image of similar magnitude, so this remains a cluster candidate.

RX J120330.7+275532: The galaxy to the west of the suggested ID exhibits narrow Hα/[N II] emission at a redshift of 0.142.

RX J121828.6+301150: Diffuse X-ray emission which may be a cluster at $z \sim 0.36$ (based on one galaxy, closest to the X-ray centroid) with a probable point source embedded. The point source may be an M star 20 arcsec to the south-west of the X-ray centroid, but the estimated X-ray flux of the star in isolation would place it below the RIXOS3 threshold.

RX J122135.6+280613: Lyman forest absorption plus Lyman edge detected.

RX J123138.1+202526: The object closest to the X-ray position on the POSS E chart is not detected in our CCD images and is probably not real. Thus the M5 star is the closest object to the X-ray position and is a probable ID.

RX J123154.9+195309: The X-ray source is elongated with PA ∼45°, with the emission concentrated to the north-east. Two optical objects have been observed: the one 30 arcsec to the west of the X-ray centroid is a star, while the object 20 arcsec to the north-east is an AGN at $z = 0.142$ with broad Hα emission. There is probably significant X-ray emission from the AGN, but the extended emission could be from a cluster of galaxies at unknown redshift. The X-ray source is formally coincident with the radio

Downloaded from https://academic.oup.com/mnras/article-abstract/311/3/456/1016504 by Estación Experimental del Zaidín user on 25 September 2018

source 4C +20.30. However, the 4C source has a large positional uncertainty. The NVSS shows a source (NVSS J123153.2+194947) with a consistent radio spectral index which is likely to be the origin of the emission recorded in the 4C catalogue. The NVSS source is, however, several arcmin from the RIXOS X-ray source, and thus it is unlikely that the radio and X-ray sources are related.

RX J125738.4+472759: Visual binary system. However, the X-ray contours favour the G8 star as the X-ray candidate, so we have considered this as a single X-ray source.

RX J131058.8+323335: A variable optical and radio source discussed by Machalski & Engels (1994).

RX J133146.3+105653: The star has a visual companion, about 2 mag fainter than it and located to the south-east.

RX J141231.5+435539: The majority of the X-ray emission is centred on the indicated Sy2 galaxy (also catalogued as IRAS14105+4409). However, there is also a close pair of Hα emission-line galaxies ($z = 0.13$) about 30 arcsec to the north-west of the X-ray centroid, and visible at the edge of the CCD image in Fig. 4.

RX J142754.6+330003: The AGN is seen through the disk of a $z \sim 0.1$ foreground galaxy whose nucleus lies about 7 arcsec to the east of the AGN.

RX J161418.8+654854: A point-like X-ray source. There are no obvious optical counterparts in the X-ray error circle, even in the deep WHT image. A possible genuine blank field.

RX J162902.3+372434: Double quasar. Again, we have considered this to be a single physical X-ray source.

RX J163616.7+570644: A *ROSAT* HRI image reveals a point-like X-ray source at a position consistent with that of the POSS object close to the PSPC position. The PSPC and HRI fluxes are consistent with one another.

RX J172904.4+742552: A close pair of optically active M stars. We have counted this as two different physical X-ray sources.

RX J180603.7+694024: This is close to an EMSS source which is identified as a $z = 0.461$ AGN in Stocke et al. (1991). However, this AGN is inconsistent with the RIXOS position (it is the object at PA $\sim 15°$ just within the northern edge of our POSS finding chart) and is also outside the EMSS error circle. The suggested RIXOS ID (a $z = 0.321$ Seyfert galaxy) is close to the centre of the RIXOS error circle and is also consistent with the EMSS position. A spectrum of the RIXOS ID taken on the Keck telescope by Hasinger (unpublished) reveals broad Hα.

RX J180823.7+694208: A point-like X-ray source. The suggested counterpart is a blue object which may have narrow Hα and [O III] emission lines, although the spectrum is of poor quality. The redshift is 0.17 if these line identifications are correct. The object ~20 arcsec to the west of this is a late-type star which shows no evidence of activity. The object ~20 arcsec to the south-east of the candidate is a galaxy at a redshift of 0.41.

RX J231303.7+104914: The error circle of this X-ray source contains two AGN at different redshifts (1.333 and 0.715). This has been treated as two different X-ray sources.

4 SURVEY STATISTICS

As noted previously, 82 *ROSAT* fields were used in the optical work on the RIXOS survey. In 64 of these fields, all X-ray sources brighter than the survey flux limit of 3×10^{-14} erg cm^{-2} s^{-1} were examined during the spectroscopy programme (although not all were successfully identified). Work on the remaining 18 fields is complete to a higher flux level of $\sim 8 \times 10^{-14}$ erg cm^{-2} s^{-1}, but only partially complete below this. We refer to the 64 fields that have been searched down to 3×10^{-14} erg cm^{-2} s^{-1} as the RIXOS3 subsample, and the remaining 18 fields as the RIXOS8 subsample. The area surveyed in each *ROSAT* pointing is about 0.25 deg^2. Thus RIXOS3 covers a sky area of 15.77 deg^2, with the RIXOS8 subsample adding a further 4.44 deg^2, to a total area of 20.21 deg^2.

The RIXOS survey as a whole contains 401 X-ray sources brighter than 3×10^{-14} erg cm^{-2} s^{-1}, of which 296 are in RIXOS3 fields, and 105 are in RIXOS8 fields. Fig. 3 provides finding charts for the 396 X-ray sources originally detected in these fields (except for RX J001002.5 + 110837; see Section 3.2). In the course of the survey, five of these sources were found to be actually two X-ray sources very close together (RX J072047.8+710945, RX J102442.3+465227, RX J112524.9+542221, RX J172904.4+742552 and RX J231303.7+104914; see Section 3.2), taking the total number of different X-ray sources to 401, as quoted above. We have included in Table 2 one line for each one of these two counterparts. Furthermore, two of the X-ray sources

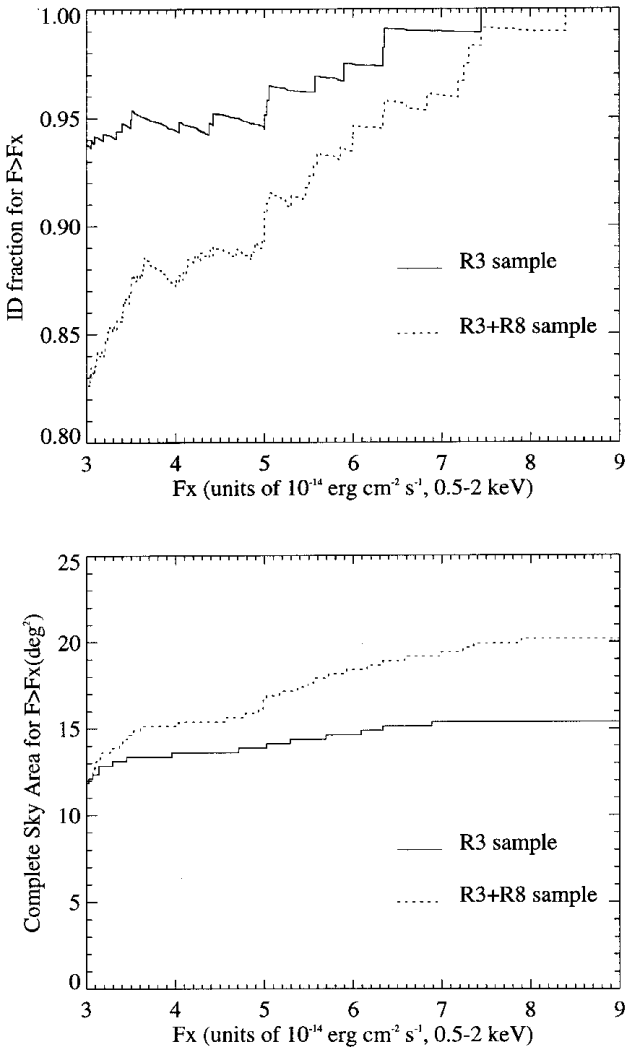

Figure 5. Upper: the identified fraction of RIXOS sources above a give flux threshold. Data are plotted for the RIXOS3 sample alone, and for the combined RIXOS3 and RIXOS8 sample. Lower: the sky area over which identifications are complete as a function of flux threshold. Again separate curves are plotted for the RIXOS3 sample alone, and for the combined RIXOS3 and RIXOS8 sample.

Downloaded from https://academic.oup.com/mnras/article-abstract/311/3/456/1016504 by Estación Experimental del Zaidín user on 25 September 2018

found in this survey corresponded to double quasars (RX J100120.3+555349 and RX J162902.3+372434). We have given in Table 2 the optical data for both members of each pair, but we have chosen to consider each one of these pairs a single physical X-ray source. Finally, we have also included a line for each one of the two stars that are near the position of RX J125738.4+472759, although we believe that only one of them is the real counterpart (see Section 3.2). In total, the 396 originally detected X-ray positions, plus the eight X-ray sources with two entries make the total of 404 lines in Table 2.

In the upper panel of Fig. 5 we plot the fraction of sources brighter than a given flux that have been identified for the RIXOS3 fields alone, and for the full survey (RIXOS3+RIXOS8). It is seen that 94 per cent of sources with fluxes greater than 3×10^{-14} erg cm^{-2} s^{-1} have been identified in RIXOS3. In the combined sample the corresponding number is 83 per cent.

We can also describe the completeness of the survey based on the brightest source in each field that remains unidentified. This can occur either because we failed to confirm a counterpart (generally the case in RIXOS3) or because the source was not worked on in the spectroscopic programme (as is the case for a number of sources in RIXOS8). We can thus plot the effective area of sky that is completely identified above a given X-ray flux as a function of flux, shown in the lower panel of Fig. 5.

The optical (R) magnitude of point-like optical counterparts is plotted against their 0.5–2.0 keV X-ray flux in Fig. 6. The faintest AGN counterparts have $R \sim 22$ at the survey flux limit. The well-defined upper boundary of optical magnitude versus X-ray flux for AGN presumably reflects the limited range of X-ray to optical flux ratio in this class of object.

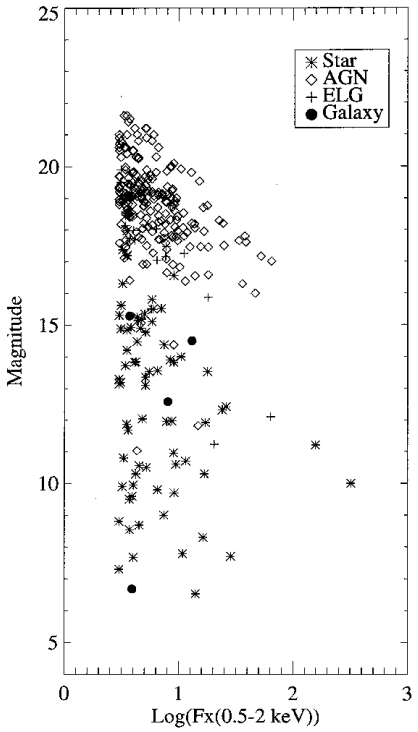

Figure 6. Optical (R) magnitude versus the logarithm of the 0.5–2.0 keV X-ray flux for various classes of identified RIXOS sources. The X-ray flux is expressed in units of 10^{-14} erg cm^{-2} s^{-1}.

5 NUMBER COUNTS

The integrated $\log N$–$\log S$ curves [$N(>S)$] are shown in Fig. 7, for both the RIXOS3 sample (upper panel) and all RIXOS sources above a flux of 3×10^{-14} erg cm^{-2} s^{-1} (lower panel). A single power-law fits well the total differential $\log N$–$\log S$ curves, yielding a slope of 2.6 ± 0.3. Previous studies of the 0.5–2 keV $N(>S)$ curve with *ROSAT* used a broken power-law model for fitting, finding a break below our flux limit ($\sim$2–3 $\times 10^{-14}$ erg cm^{-2} s^{-1}). Our single power-law slope is hence directly comparable to the power-law slope above the break in those studies. Our sample partially overlaps with that of Hasinger et al. (1993), so it is hardly surprising that the slope above the break of their broken power-law fit is compatible with ours (2.72 ± 0.27). Branduardi-Raymont et al. (1994) used a different sample (but again containing some fields also used in RIXOS), obtained from the United Kingdom Deep and Medium Surveys (Carballo et al. 1995; McHardy et al. 1998). The slope of the 'bright branch' of their $N(>S)$ fit is very similar to ours ($2.64^{+1.19}_{-0.52}$), though with larger uncertainties due to their lower number of sources.

The $N(>S)$ curves for the different types of sources in both samples are also included in Fig. 7. It is clear from that figure that AGN dominate the source counts below a flux of

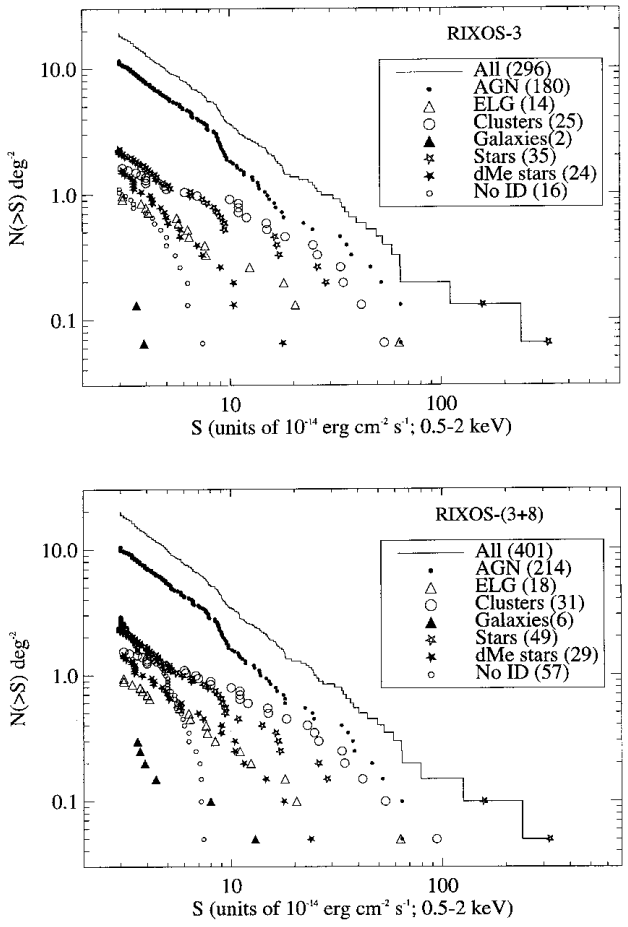

Figure 7. Log N–Log S distributions for various classes of sources in the RIXOS survey. The upper plot shows results from the RIXOS3 sample alone, while the lower plot shows data from the total sample, which includes both RIXOS3 and RIXOS8 fields. The number of objects in each category is listed within parentheses in the legend.

Downloaded from https://academic.oup.com/mnras/article-abstract/311/3/456/1016504 by Estación Experimental del Zaidín user on 25 September 2018

$\sim 10^{-13}$ erg cm^{-2} s^{-1}, making up about 50 per cent of the total number of sources. Comparing the $N(>S)$ of our clusters with that of Rosati et al. (1998), we find approximately a factor of 2 less clusters at our flux limit than they do (we find ~ 1.2 deg^{-2}, while they find ~ 2.4 deg^{-2}). This is probably because our detection algorithm was optimized for the detection of point sources (or at least unresolved sources down to the angular resolution of *ROSAT*), and the visual inspection of 'clusters' of point sources only picked up very bright nearby extended clusters, so we very likely missed an important fraction of distant fainter clusters. Nevertheless, the slope of our best fit to the RIXOS3 cluster sample (2.1 ± 0.9) is similar to theirs (~ 2), albeit with a large uncertainty.

Stars and clusters have similar densities at our flux limit. The less abundant types of sources are 'normal' galaxies and ELGs. The total number of both types of sources are at the level or below the number of unidentified sources, making definitive statements about their global properties difficult from RIXOS-sized samples, as emphasized by Page et al. (1997a). As expected, the fraction of unidentified sources increases strongly at the faintest flux levels, where the faintness of the optical counterparts and the presumably worse position determinations from X-rays conspire to make a definitive identification more difficult.

6 SUMMARY AND CONCLUSIONS

This paper presents the RIXOS catalogue, a medium-sensitivity, flux-limited survey of X-ray sources detected in *ROSAT* PSPC fields, together with optical identifications to a high level of completeness. The scientific content of the survey has been explored in a number of papers which make use of RIXOS catalogue data. In an early study Castander et al. (1995) discussed the implications for the evolution of X-ray-selected galaxy clusters (although the relatively crude manual selection of extended sources used in RIXOS has since been superseded by superior techniques; see Burke et al. 1997 and Scharf et al. 1997). The evolution of the X-ray luminosity function of AGN has been considered in detail using a combination of RIXOS and *Einstein* Extended Medium Survey data in Page et al. (1996), work that was extended to include data from a *ROSAT* deep survey in Page et al. (1997b). The evolution of narrow-emission-line galaxies has also been discussed, in Page et al. (1997a). The X-ray and optical continuum properties of RIXOS AGN have been analysed in Puchnarewicz et al. (1996a), while AGN with a very red optical continuum are discussed further in Puchnarewicz & Mason (1998). This work is extended to include the optical and UV emission-line properties in Puchnarewicz et al. (1997). The X-ray spectral properties of RIXOS sources, including sources in RIXOS fields fainter than the formal survey flux limit, are considered in Mittaz et al. (1999). The clustering of RIXOS AGN has been studied by Carrera et al. (1998). One individual RIXOS source of interest is discussed in Puchnarewicz, Mason & Carrera (1996b).

There may be minor differences between the data used in the above publications and those reported in the present catalogue, due to additional information or improved quality control. In general, the information presented in the present work supersedes that in earlier papers.

ACKNOWLEDGMENTS

The RIXOS project has been made possible by the award of International Time on the La Palma telescopes by the Comité Científico Internacional. This research has made use of data obtained from the Leicester Data Archive Service (LEDAS), and we especially thank Steve Sembay for his kind assistance. We thank the Royal Society for a grant to purchase equipment essential to the RIXOS project. FJC, XB, RC and JIGS thank the DGES for financial support, under project PB95-0122. The INT, JKT and WHT are operated on the island of La Palma by the Isaac Newton Group in the Spanish Observatorio del Roque de los Muchachos of the Instituto de Astrofísica de Canarias. The NOT is operated by the Nordic Optical Telescope Scientific Association in the Spanish Observatorio del Roque de los Muchachos. This research has made use of the NASA/IPAC Extragalactic Data base (NED), which is operated by the Jet Propulsion Laboratory, California Institute of Technology, under contract with the National Aeronautics and Space Administration. It also made use of the Lyon-Meudon Extragalactic Data base (LEDA) maintained at CRAL, Lyon, France.

REFERENCES

Boyle B. J., McMahon R. G., Wilkes B. J., Elvis M., 1995, MNRAS, 272, 462
Branduardi-Raymont G. et al., 1994, MNRAS, 270, 947
Burke D. J., Collins C. A., Sharples R. M., Romer A. K., Holden B. P., Nichol R. C., 1997, ApJ, 488, L83
Carballo R., Warwick R. S., Barcons X., González Serrano J. I., Barber C. R., Martínez-González E., Pérez-Fournon J.Burgos, 1995, MNRAS, 277, 1312
Carrera F. J., Barcons X., Fabian A. C., Hasinger G., Mason K. O., McMahon R. G., Mittaz J. P. D., Page M. J., 1998, MNRAS, 299, 229
Cash W., 1979, ApJ, 228, 939
Castander F. J. et al., 1995, Nat, 377, 39
David F. R. et al., 1996, in Briel U. et al., eds, The *ROSAT* Users Handbook
Hasinger G., Burg R., Giacconi R., Hartner G., Schmidt M., Trümper J., Zamorani G., 1993, A&A, 275, 1
Hasinger G., Johnston H., Verbunt P., 1994a, A&A, 288, 466
Hasinger G. et al., 1994b, Legacy, 4, 40, MPE/OGIP Calibration Memo CAL/ROS/93-015
Hasinger G., Burg R., Giacconi R., Schmidt M., Trümper J., Zamorani G., 1998, A&A, 329, 482
Hewitt A., Burbidge G., 1989, ApJS, 69, 1
Lewis G., Irwin M., 1996, Spectrum, Newsletter of the Royal Observatories, 12, p. 22
Machalski J., Engels D., 1994, MNRAS, 266, 69P
McHardy I. M. et al., 1998, MNRAS, 295, 641
Mittaz J. P. D. et al., 1999, MNRAS, 308, 233
Page M. J. et al., 1996, MNRAS, 281, 579
Page M. J., Mason K. O., McHardy I. M., Jones L. R., Carrera F. J., 1997a, MNRAS, 289, 693
Page M. J., Mason K. O., McHardy I. M., Jones L. R., Carrera F. J., 1997b, MNRAS, 291, 324
Puchnarewicz E. M., Mason K. O., 1998, MNRAS, 293, 243
Puchnarewicz E. M. et al., 1996a, MNRAS, 281, 1243
Puchnarewicz E. M., Mason K. O., Carrera F. J., 1996b, MNRAS, 283, 1311
Puchnarewicz E. M. et al., 1997, MNRAS, 291, 177
Rosati P., Della Ceca R., Norman C., Giacconi R., 1998, ApJ, 492, L21
Scharf C. A., Jones L. R., Ebeling H., Perlman E., Malkan M., Wegner G., 1997, ApJ, 477, 79
Shanks T., Georgantopoulos I., Stewart G. C., Pounds K. A., Boyle B. J., Griffiths R. E., 1991, Nat, 353, 315
Stark A. A., Gammie C. F., Wilson R. W., Bally J., Linke R. A., Heiles C., Hurwitz M., 1992, ApJS, 79, 77
Stocke J. T. et al., 1991, ApJS, 76, 813
Trümper J., 1983, Adv. Space Res., 4, 242
Voges W. et al., 1999, A&A, 349, 389
Zimmermann H. U. et al., 1994, MPE Report, 257

This paper has been produced using the Royal Astronomical Society/ Blackwell Science TEX macros.

Downloaded from https://academic.oup.com/mnras/article-abstract/311/3/456/1016504 by Estación Experimental del Zaidín user on 25 September 2018